Chapter 4:
$^{40}Ar/^{39}Ar$ geochronology of adularia from the hydrothermal systems in the Seongsan district, South Korea

4.1 INTRODUCTION

This chapter presents the results of $^{40}Ar/^{39}Ar$ dating of adularia from the Eunsan, Moisan and Chunsan systems. Previous geochronological work has focussed on alunite and sericite from the high-sulfidation systems at Seongsan and Ogmaesan (Kim & Nagao, 1992), with the low-sulfidation style alteration at Eunsan, Moisan and Chunsan undated until now.

Field relationships outlined in the previous Chapter indicate that the low-sulfidation adularia-bearing alteration is later than the high-sulfidation alteration across the Seongsan district. However, prior to the dating presented here, it was not known just how much later the low-sulfidation alteration was or whether it is part of the same overall metallogenic event as the high-sulfidation alteration. Furthermore, the age data presented here will determine the timing of the switch between earlier wrenching and later extensional stress regimes in the district.

4.1.1 Previous geochronological work in the Seongsan district

Kim & Nagao (1992) $^{40}K/^{40}Ar$ dated a variety of rocks regionally and alunite and sericite from the Ogmaesan and Seongsan high-sulfidation clay mines. Their results showed that the basement Sani granite located ca. 8km north of the field area has an age of 144.8±1.9Ma, basalt within the Hwawon Formation has an age of 103.4±2.5Ma, andesite within the Uhangri Formation has an age of 95.4±2.9Ma, a least-altered sample of Hwangsan Tuff ca. 10km from the Seongsan district has an age of 86.4±1.8Ma to 84.5±1.3Ma, and locally, altered Hwangsan Tuff has an age of 83.1±1.6Ma. Samples of alunite have apparent ages of 81.4±1.0 to 80.8±1.0Ma from Ogmaesan and 80.9±1.2 to 80.8±0.9Ma from Seongsan. Samples of hydrothermal sericite have apparent ages of 80.2±1.1 to 79.0±1.2Ma from Ogmaesan and 79.7±1.0 to 78.1±1.1Ma from Seongsan. The AVdb debris flow breccia unit that unconformably overlies the Hwangsan Tuff has an age of 74.2±1.7Ma to 72.5±1.3Ma.

Field relationships and dating cited above suggest that the Ic_2 complexes of the Seongsan district are probably the same age as the Bulguksa Series granitoids, which include the Jiyoungsan granite (81.5±4.0Ma), the Weolchulsan granite (81.2±4.0Ma and 77.0±1.2Ma), the Weolgangdu porphyry (77.9±3.8 and 75.0±2.8Ma), and the Jangseong granite porphyry (71.8±3.6Ma).

All of these age data are presented along with age data of adularia from the low-sulfidation systems in Figure 4-2.

4.2 NEW $^{40}Ar/^{39}Ar$ GEOCHRONOLOGICAL DATA ON THE EPITHERMAL SYSTEMS OF THE SEONGSAN DISTRICT

4.2.1 Geochronology methods

4.2.1.1 Introduction

Adularia was chosen for dating as it is the key K-bearing mineral indicative of near-neutral hydrothermal fluid circulation and low-sulfidation hydrothermal alteration. Illite was avoided as it was difficult to be absolutely certain that all illite in a particular sample was directly related to the low-sulfidation event, rather than earlier propylitic or high-sulfidation alteration (Chapter 3, Table 3-3). However, using adularia for dating has some limitations. Its crystal state is disordered, which can give rise to Ar leakage and potentially erroneous age dates (Dong & Morrison, 1995). This potential problem was minimised by thorough thin section and XRD investigation of potential samples. Only samples with predominantly pristine rhombic euhedral adularia crystals were dated. Rhombic adularia is the least disordered of all the crystalline forms of adularia, and hence has the least potential to leak Ar and least likely to give erroneous ages (Dong & Morrison, 1995). If the dates are erroneous, they tend to be younger than actual ages, therefore at least constraining a minimum age of the sample.

4.2.1.2 Geochronology sample selection and paragenesis

Three samples of crystalline adularia infill vein material from Au-Ag mineralised intervals at the Eunsan, Moisan and Chunsan low-sulfidation systems were submitted for $^{40}Ar/^{39}Ar$ stepwise age-dating. Following detailed thin section petrography, samples of selected drill core slabs from Eunsan (EN006 72m), Moisan (MS008 148m) and Chunsan (CH003 115m), along with detailed thin section photographs of the adularia, were sent to Dr W. J. Dunlap who undertook final sample preparation, mineral separation, irradiation and analysis. Dr W. J. Dunlap commented that the adularia crystal shape and size were very suitable for age dating (pers. comm. March 2004). These samples are paragenetically associated with the most strongly Au-Ag mineralised zones associated with adularia alteration, representative of the low-sulfidation systems (Chapter 3, Table 3-3). Furthermore, these adularia samples also have complimentary oxygen and hydrogen isotope data on paragenetically equivalent associated quartz infill (Chapter 5).

4.2.1.3 Geochronology final sample preparation and analysis

The Ar and He Thermochronology and Geochronology, Director's Unit, Research School of Earth Sciences (RSES), Australian National University, conducted all $^{40}Ar/^{39}Ar$ final sample preparation and age determinations for this study. Dr W. J. Dunlap (Fellow) of RSES provided details of final sample preparation and the analytical methodology used.

The GA1550 Biotite standard was used, which is the in-house standard developed at the RSES. Two very in-depth studies involving this standard are 1: Renne et al. (1998) and 2: Spell & McDougall (2003). For purposes of this study, Spell & McDougall has been used with 98.5Ma as the standard age. Moreover, most agree that this standard is accurate to better than 0.3% for determining the J value of irradiation.

The concentrates from mineral separation were weighed and wrapped in aluminium foil. Samples were then sealed in an outer aluminium canister. The inner packaging components consisted of a pure silica glass tube with a cadmium liner (0.2mm thick) between the glass and outer canister. The fluence monitor was packed in the canister at regular intervals. The canister was then irradiated for 192 hours in the HIFAR reactor at Lucas Heights, New South Wales. The canister was inverted three times during the irradiation, to reduce the neutron fluence gradient across the container.

After irradiation and a cooling off period, samples were repacked in tin (Sn) foil. The biotite standard and samples from this study were loaded onto an extraction line connected to a VG 3600 gas source mass spectrometer with a resolution of ca. 600. Samples were heated in a series of steps for variable durations (see Appendix 5-4 for times and temperatures of each step). Data was reduced using the Macintosh program "Noble", developed at the Research School of Earth Sciences, Canberra, Australia. Correction factors to account for K-, Cl-, and Ca-derived Ar isotopes are: $(^{36}Ar/^{37}Ar)_{Ca} = 3.5 \times 10^{-4}$; $(^{39}Ar/^{37}Ar)_{Ca} = 7.86 \times 10^{-4}$; $(^{40}Ar/^{39}Ar)_{K} = 2.7 \times 10^{-2}$, $(^{38}Ar/^{39}Ar)_{K} = 0.136$; $(^{38}Ar)_{Cl}/(^{39}Ar)_{K} = 8.0$.

Blanks and backgrounds were generally atmospheric, and/or insignificant in terms of fraction of gas analysed. Air standards were used to determine mass fractionation, which is known within about 0.2%, and was assumed not to vary on the time scale of sample analysis.

4.2.2 Geochronology results

Step-wise $^{40}Ar/^{39}Ar$ data show that Chunsan adularia has an apparent age of 78.1±0.3Ma; Eunsan adularia has an apparent age of 77.9±0.3Ma; and Moisan adularia has an apparent age of 77.4±0.5Ma (see Appendix 4 for raw data). The step-wise data are individually presented within Figure 4-1 and show that the samples have well-defined plateau ages. These age data are presented in Figure 4-2, where they are compared with previous dating to highlight relationships across the Seongsan district.

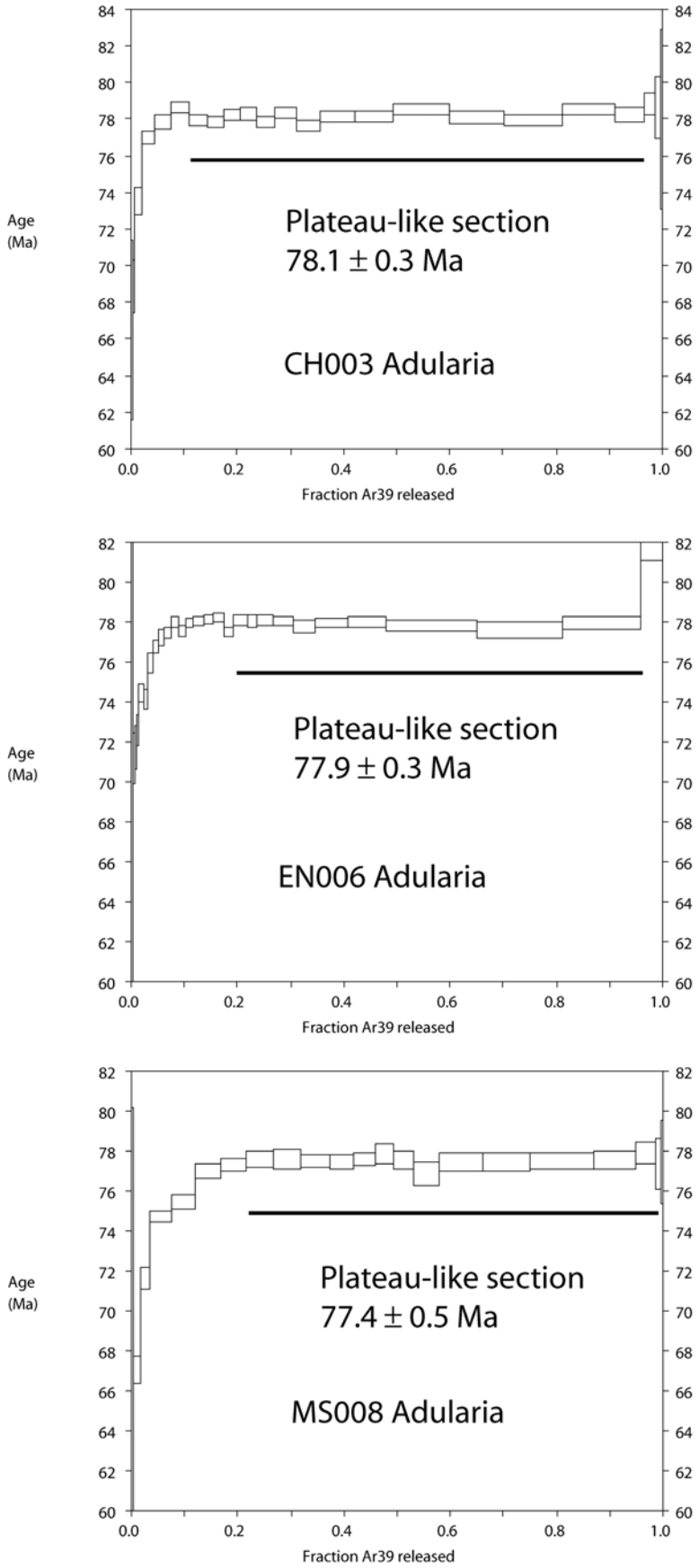

Fig. 4-1 Step-wise $^{40}Ar/^{39}Ar$ apparent plateau age data (this study) on adularia from the low-sulfidation systems of the Seongsan district (Chunsan system CH003 115m; Eunsan system EN006 72m; Moisan system MS008 148m). Adularia from each sample show well-defined apparent plateau ages between 78.4 and 76.9Ma (77.7±0.8Ma).

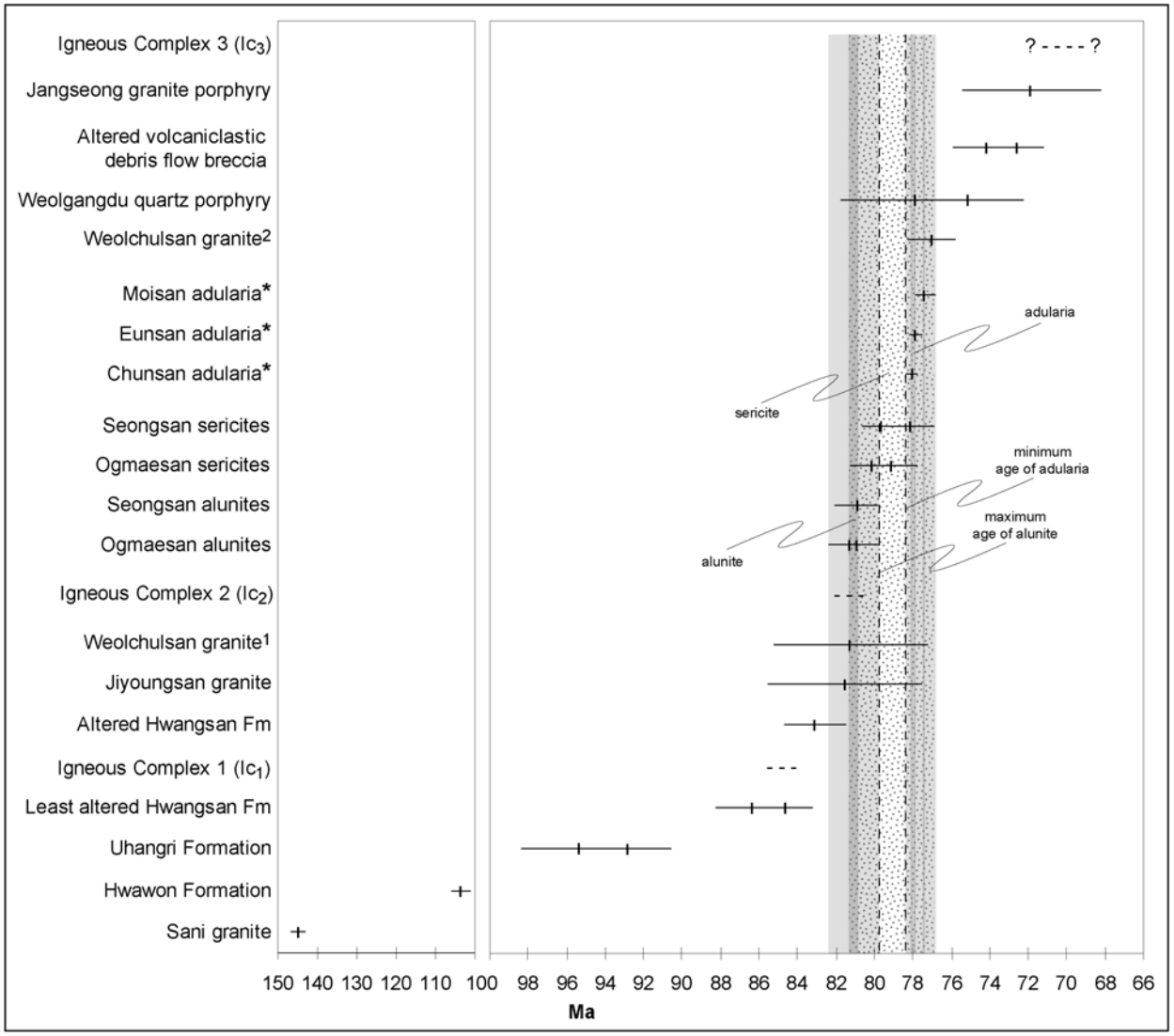

Fig. 4-2 New step-wise $^{40}Ar/^{39}Ar$ apparent plateau age data for the low-sulfidation systems (* - this study) with previous $^{40}K/^{40}Ar$ apparent age data for various rocks and alteration in the district and surrounding region (Kim & Nagao, 1992). In addition, field relationships constrain the ages of igneous complexes within the Seongsan district. Adularia ages are consistently younger than those of alunite from nearby high-sulfidation systems consistent with field relationships (Chapter 3). Dark grey areas highlight age range whereas the light grey areas highlight analytical error of age range. Stippled area represents age range of sericite samples.

4.2.3 Interpretation of geochronological data

4.2.3.1 Lengths of hydrothermal activity

Cathles et al. (1997) show that hydrothermal activity should be closely tied (ca. 0.1Ma) to specific episodes of intrusion and that the length of hydrothermal activity will be in the order of 0.1Ma. This timeframe of ca. 0.1Ma for ore-forming hydrothermal activity has been suggested for a number of systems, such as Porgera (Ronacher et al., 2002) and Round Mountain (Henry et al., 1997). Much longer timeframes for active hydrothermal activity of up to 0.8Ma from a single intrusion have been modelled numerically under certain geological conditions (Cathles et al., 1997). However, field evidence shows that even within districts that comprise multiple co-magmatic events, e.g. the Potrerillos district, Chile (Marsh et al., 1997) where igneous events were essentially continuous over ca. 8Ma, individual ore-forming hydrothermal systems still appear to show a close temporal link to individual intrusions and are short-lived (ca. 0.1Ma).

4.2.3.2 Apparent ages versus actual ages of formation

Alunite apparent ages from Kim & Nagao (1992) show a discrete range of 82.4 to 79.7Ma. Adularia apparent plateau ages show a discrete range of 78.4 to 76.9Ma. Sericite apparent ages from Kim & Nagao (1992) show a broad range of 81.3 to 77.0Ma, which overlap considerably with alunite and adularia apparent ages. However, actual ages of formation are dependent on the apparent age of the sample, the closure temperature of the material dated and the thermal history of the area (McInnes et al., 2005; McDougall & Harrison, 1999).

Closure temperatures for alunite have been calculated to be 280±20ºC (Love et al., 1998). Closure temperatures for illite have not been measured directly but have been estimated at 190±30ºC (Kesler et al., 2004). Closure temperatures for K-feldspar (adularia) have been estimated at 150±30ºC (Harrison & McDougall, 1980). The thermal history of the Seongsan district has not been directly determined. However, paragenetic relationships between igneous and hydrothermal events place some constrains on the thermal history of the district. The earliest hydrothermal event recognised in the district was propylitic alteration and then by advanced argillic, which was overprinted by phyllic-adularia alteration (Chapter 3). The thermal gradient of the district would have been increasing through propylitic alteration, and then peaking around advanced argillic alteration, then cooling at an unknown rate until the onset of phyllic-adularia alteration, which may have locally increased the thermal gradient, then cooling to background levels. More detailed constrains on temperatures and pressures of formation are examined in Chapter 5.

Alunite closure temperature is 280±20ºC. Alunite would have formed close to the thermal peak of the district. Phase relationships (Hemley, et al., 1980) indicate a likely temperature of

formation similar to the closure temperature (see Chapter 5) and therefore, the apparent ages would approximate actual alunite ages of formation. This is reflected by their tight age range.

It is unknown whether the sericite dated by Kim & Nagao (1992) is related to earlier propylitic alteration, advanced argillic alteration, overprinting phyllic-adularia alteration or some mixture of all three. Illite that may have formed during early propylitic alteration would not have passed through its closure temperature (190±30ºC) until after the peak thermal event of advanced argillic alteration, thereby producing an apparent age that does not reflect the actual age of formation. Therefore, due to the lower closure temperature of illite compared to alunite, the sericite that were dated by Kim & Nagao (1992) have significant potential to have been re-set by the thermal peak in the district, and could actually represent early propylitic sericite, which would pre-date alunite formation, and/or sericite associated with advanced argillic alteration and/or sericite from phyllic-adularia alteration. Detailed examination of the age data suggest that possibly one sericite apparent age could be associated with phyllic-adularia alteration as the apparent age is identical to an apparent plateau age of adularia from Chunsan (78.1Ma). However, without detailed sericite sample paragenesis and knowledge of the thermal history of the district, the sericite actual age of formation remains speculative. The broad spread of sericite apparent ages implies that the samples dated comprise mixed origins of sericite, possibly including a mix of propylitic, advanced argillic and phyllic altered samples.

Adularia closure temperature is 150±30ºC. This allows the possibility that the actual age of adularia formation could be older than the apparent plateau ages as the temperature of formation would likely have been higher than the closure temperature (Chapter 5). Estimations of cooling rates for epithermal systems are difficult to find. Love et al. (1998) calculated cooling rates of 50ºC/Ma for the Mount Skukum district in the Yukon Territory, Canada. This area shares distinctly similar geology and alteration to the Seongsan district, comprising shallow level epithermal barren advanced argillic alteration overprinted by phyllic-adularia alteration and associated adularia-Au-Ag mineralisation, which show an apparent age difference of around 1.5Ma. This cooling rate was calculated for the alunite alteration, which formed broad alteration zones from magmatic fluids. Section 4.2.3.3 shows that the advanced argillic alteration at Seongsan spans a period of 2.7Ma. Therefore, it is not appropriate to use this for calculations of cooling rates for adularia within vein systems. McInnes et al. (2005) calculated cooling rates for several magmatic-hydrothermal systems and show that these types of systems can cool much more rapidly, in the order of 1,000's to 10,000's of ºC/Ma. This appears to be more geologically valid for vein systems. Closure temperatures would be reached at the end of the hydrothermal system, which is generally in the order of 0.1Ma (Section 4.2.3.1). Then, using cooling rates from McInnes et al. (2005), closure temperatures would be reached in less

than 0.01Ma, which is an order of magnitude less than the error in the $^{40}Ar/^{39}Ar$ age data, therefore the apparent ages of the adularia likely approximate actual ages of formation.

4.2.3.3 Comparison of high- and low-sulfidation age data: implications for the timing and length of each hydrothermal system

The age data in Figure 4-2 show that the host rocks of the district span a period of 88.2 to 81.5Ma. Alunite-bearing advanced argillic alteration formed from 82.4 to 79.7Ma, implying a strong genetic link to magmatic processes that formed the host rocks. The length of high-sulfidation alteration spans a period of 2.7Ma, although this range is probably a function of sample selection and dating technique by Kim & Nagao (1992).

Based on detailed paragenetic studies (Chapter 3), the phyllic-adularia assemblages clearly overprint advanced argillic alteration. The age data presented show that apparent plateau age data from adularia are ca. 2Ma younger than the apparent age of alunite. By utilising a consideration of closure temperatures and the likely thermal history of the district as determined from detailed paragenetic studies (Chapter 3), the apparent age data for alunite and adularia are inferred to approximate actual ages of formation. The age difference between alunite and adularia formation could have been closer due to potential Ar loss. However the relatively flat plateaus and only minor trailing left hand edges of the adularia age spectra (ca. 0.0 to 0.15 fraction of Ar released) suggest that potential Ar loss was minor (Harrison & McDougall, 1980; McDougall & Harrison, 1999). The sericite apparent ages from Kim & Nagao (1992) are inferred to have been re-set and/or comprise mixtures of different aged sericite. Therefore, the hydrothermal systems of the Seongsan district that formed the high-sulfidation advanced argillic systems and the overprinting low-sulfidation phyllic-adularia systems formed at least 1.3Ma apart, suggesting that there were two discrete hydrothermal events, rather than one evolving hydrothermal event. However, they could be considered two distinct parts of a broader long-lived cycle of crustal convergence, subduction, volcanism and associated hydrothermal activity.

4.2.3.4 Correlation of low-sulfidation age data with igneous events

Examination of Figure 4-2 shows that adularia from Chunsan, Eunsan and Moisan formed at the same time as various igneous events in the surrounding region, including the Weolchulsan granite[2] and Weolgangdu quartz porphyry. The significance of this is that although these igneous events were not manifested locally, the processes that led to their development may also have led to the development of the low-sulfidation systems within the Seongsan district. This will be explored further in Chapter 6. The widespread rhyodacitic intrusive plugs (Ic_2) that are the most obvious intrusive rocks in the Seongsan district (Appendix 6) were emplaced prior to alunite-bearing high-sulfidation alteration (82.4 to 79.7Ma), indicating that these intrusive rocks

predate low-sulfidation hydrothermal activity by between 1.3 to 5.5Ma. Dating also indicates that adularia from Eunsan, Moisan and Chunsan predates formation of the unconformable AVdb unit and Ic_3 by between 1.0 to 5.7Ma.

4.3 SUMMARY OF RESULTS FOR THIS CHAPTER

This Chapter documented the results of geochronological analyses performed on geologically well-constrained samples of adularia from the low-sulfidation Au-Ag vein systems of the district. It also compares this new data with previous age data on the high-sulfidation clay/sulfate systems. Results show that the change from advanced argillic alunite-bearing alteration to adularia-phyllic alteration (based on apparent age data) was within ca. 2Ma of each other. Estimates on the actual age of formation of alunite and adularia were conducted and showed that apparent ages approximate actual ages. This suggests that the epithermal systems of the district formed from two discrete hydrothermal systems rather than one evolving hydrothermal system that would be expected to show a <0.5Ma gap between them. The apparent and estimated actual age ranges also confirm that the high-sulfidation systems formed first, followed by the low-sulfidation systems, consistent with cross cutting field relationships.

Chapter 5:
An investigation into the origins and characteristics of fluids in the epithermal systems of the Seongsan district, South Korea

5.1 INTRODUCTION

This chapter presents the results of numerous geochemical analyses performed on paragenetically well-constrained samples from both the high- and low-sulfidation systems in the Seongsan district. This work was undertaken to determine geochemical conditions under which alteration and mineralisation formed at each of the epithermal systems in the district, and gain further insight into the hydrothermal fluid evolution of the district. Geochemical analyses presented here include fluid inclusion analyses, an examination of mineral phase relationships (Sections 5.2 & 5.3) and oxygen, hydrogen and sulfur isotope analyses (Sections 5.4 & 5.5). Some trace metal data for each system is also presented to further highlight the geochemical signature of each system (Section 5.6).

This information is used to examine how the high- and low-sulfidation systems may or may not relate to each other. It has already been established that the low-sulfidation systems are slightly younger than the high-sulfidation systems (Chapter 4), with the former occurring during extension and the latter during wrenching (Chapter 2). Mineral phase relationships and stable isotope analyses characterise the fluids associated with high-sulfidation advanced argillic alteration and low-sulfidation quartz-adularia-Au-Ag veins.

5.2 MICROTHERMOMETRIC ANALYSIS OF FLUID INCLUSIONS

Much time and effort was expended attempting to find primary fluid inclusions that formed during alteration and veining in the Seongsan district. Analysis of paragenetically well-constrained fluid conclusions has the potential to provide direct evidence of the hydrothermal fluid chemistry, phase states and the pressure and temperature conditions during each stage of alteration and mineralisation. Secondary fluid inclusions formed after cessation of hydrothermal activity are also common along healed fractures in many systems, and need to be distinguished from primary inclusions directly associated with hydrothermal activity.

5.2.1 Previous microthermometric fluid inclusion work in the Seongsan district

Koh (1996) examined fluid inclusions from drusy quartz within a ‘quartz’ alteration zone within the Seongsan high-sulfidation system of unclear paragenesis (Fig. 1-18). Koh (1996) recognised four types of inclusions: liquid-rich, two-phase (majority of observed inclusions); gas-rich, two-phase (very small minority); liquid-rich and CO_2 bearing two-phase (minority); and gas-rich and CO_2 bearing two-phase (minority). Homogenisation temperatures range from 127 to 361ºC with a mean of 210ºC, salinities range from 0.4 to 7.9 wt% NaCl eq. with a mean value of 3.9 wt%. Koh (1996) concludes that the low homogenisation temperature and salinity

indicate the Seongsan high-sulfidation system is an epithermal system formed from meteoric water.

5.2.2 Sample selection for fluid inclusion microthermometry

Most stages of alteration and mineralisation within the Seongsan district contain quartz, but few of these stages contain quartz that hosts workable fluid inclusions. Of the 200+ thin section samples investigated that represented all alteration types from each system, only 11 contained fluid inclusions of a workable size. Doubly polished thick-section plates were made of these 11 samples. Despite detailed examination of these 11 plates, only five contained fluid inclusions of a workable size. The majority of these fluid inclusions are very small (ca. 3-5μm) pseudo-secondary or secondary liquid-rich and liquid-vapor inclusions. Primary, pseudo-secondary, secondary, necked and decrepitated inclusions were distinguished using the criteria of Roedder (1984) and Shepherd et al. (1985).

Three samples containing workable fluid inclusions were obtained from Eunsan (EN ●*092*, EN006 72m and EN006 81m), and one sample each from Chunsan (CH003 115m) and Moisan (MS006 51.6m). Additional fluid inclusion data obtained by Koh (1996) from Seongsan is also used. No workable fluid inclusions were found from Ogmaesan.

Fluid inclusions in EN ●*092* are hosted by crystalline quartz infill from 'quartz-only' veins (Fig. 5-1E). These veins pre-date the main-stage of Au-Ag mineralisation at Eunsan. Fluid inclusions in EN006 72m and 81m are hosted by crystalline calcite and quartz infill from quartz-adularia±calcite veins (Fig. 5-1B & C). This calcite and quartz represents late-stage infill precipitated during the main-stage of Au-Ag mineralisation at Eunsan.

Fluid inclusions in CH003 115m are hosted by crystalline quartz infill from quartz-adularia-pyrite veins (Fig. 5-1A). This infill formed synchronous with the main-stage of adularia alteration and Au-Ag mineralisation at Chunsan.

Fluid inclusions in MS006 51.6m are hosted by crystalline quartz infill from quartz-calcite veins (Fig. 5-1F). These veins formed synchronous with the main-stage of adularia and siliceous alteration and Au-Ag mineralisation at Moisan.

5.2.3 Fluid inclusion morphology, classification and paragenesis

Quartz, and to a lesser extent calcite, host the majority of the fluid inclusions. Despite detailed examination, inclusions of a workable size are not common. Unworkable inclusions are necked, decrepitated or are too small to be analysed (typically <3μm) (Roedder, 1984; Shepherd et al.,

1985). Inclusions typically occur either as planar or radiating trails, variable arrays or less commonly as clusters. No primary fluid inclusions of a workable size were observed. Secondary inclusions are mostly single-phase liquid only inclusions ca. <5 to 10μm in size. Larger (ca. 20 to 30μm) two-phase liquid-rich inclusions are less common. Many inclusions showed evidence for necking and decrepitation, and as such were unsuitable for analysis. Solid phases other than ice and clathrate were not observed in the inclusions. Due to the lack of primary fluid inclusions, no direct analysis of fluid inclusion gases was attempted.

Secondary and pseudo-secondary fluid inclusions from this study and Koh (1996) were classified on the basis of liquid to vapour ratios (L:V) and whether CO_2 is present as follows (Table 5-1):

1: liquid only single phase inclusions
2a: liquid-rich two phase inclusions
2b: gas-rich two phase inclusions
3a: liquid-rich and CO_2 bearing two phase inclusions
3b: gas-rich and CO_2 bearing two phase inclusions

Group 1 are single phase inclusions. Group 2 are two phase inclusions, split into either '2a' – liquid-rich or '2b' – gas-rich types. Group 3 are two phase inclusions with CO_2, split into either '3a' – liquid-rich or '3b' – gas-rich types. The vein minerals, fluid inclusion host mineral, mineral and fluid inclusion paragenesis and fluid inclusion morphologies are summarised in Table 5-2.

5.2.4 Fluid inclusion microthermometric results

Thermometric measurements on fluid inclusions were made using a Linkam heating-freezing stage, calibrated with synthetic fluid inclusion standards. Freezing and heating data from this study are reproducible to ±0.1ºC and ±2ºC respectively.

Heating and freezing measurements were made on pseudo-secondary and secondary two-phase liquid-rich fluid inclusions in quartz and calcite. Freezing runs were conducted initially, and then heating runs. The smallest inclusions were analysed first to reduce heating-induced decrepitation. Measurements from five samples from Eunsan, Moisan and Chunsan of final ice and clathrate melting temperatures were determined for 22 inclusions. Measurements of homogenisation temperatures were made on 40 inclusions. The microthermometric results are summarised in Table 5-3. Appendix 4 contains the raw data.

Initial freezing experiments were conducted below –180°C to determine whether CH_4, N_2, CO_2 or H_2O were the dominant fluid and/or gas phase present, based on the eutectic temperatures for these systems. Due to a lack of any solids forming at eutectic temperatures indicative of ice and potential clathrate, it was determined that the systems appeared to be H_2O-NaCl with rare occurrences of H_2O-CO_2-NaCl.

Final melting temperatures (Tm) are plotted in Figure 5-2 and range from -1.5 to +5.6ºC (this study); and -3.6 to +9.2ºC (Koh, 1996). The data shows a bimodal distribution reflecting final melting temperatures of ice and clathrate respectively. The final ice melting temperatures from type 2a inclusions show a range from -0.2ºC to -3.6ºC. The final ice melting temperatures determined during this study range from -0.3ºC to -1.5ºC, with a distinct cluster between 0 and -1.0ºC.

Clathrate formation was not observed in fluid inclusions from Eunsan or Chunsan. Ice-clathrate phase relations indicate that dissolved CO_2 can reduce the final ice melting temperatures by up to -1.48ºC without any clathrate formation (Hedenquist & Henley, 1985). The presence of dissolved CO_2 rather than salts could account for depressed final ice melting temperatures. Therefore, the calculated salinities for Eunsan and Chunsan are a maximum.

Inclusions from Moisan have final melting temperatures between +1.6 and +5.6ºC. Only one solid phase appears to be present when frozen, however initial melting temperatures below 0ºC suggest that both ice and clathrate were present, but did not form distinct phases. Due to the limited number and size of the workable inclusions, this relationship could not be examined further at Moisan. Melting temperatures above 0ºC imply the presence of one or more clathrate phases even though these cannot be distinguished from ice when the inclusion is frozen.

Homogenisation temperatures (Th) are plotted in Figure 5-3 and range from 120 to 193ºC and cluster at 160 to 170ºC. Homogenisation temperature from Koh (1996) range from 127 to 361ºC.

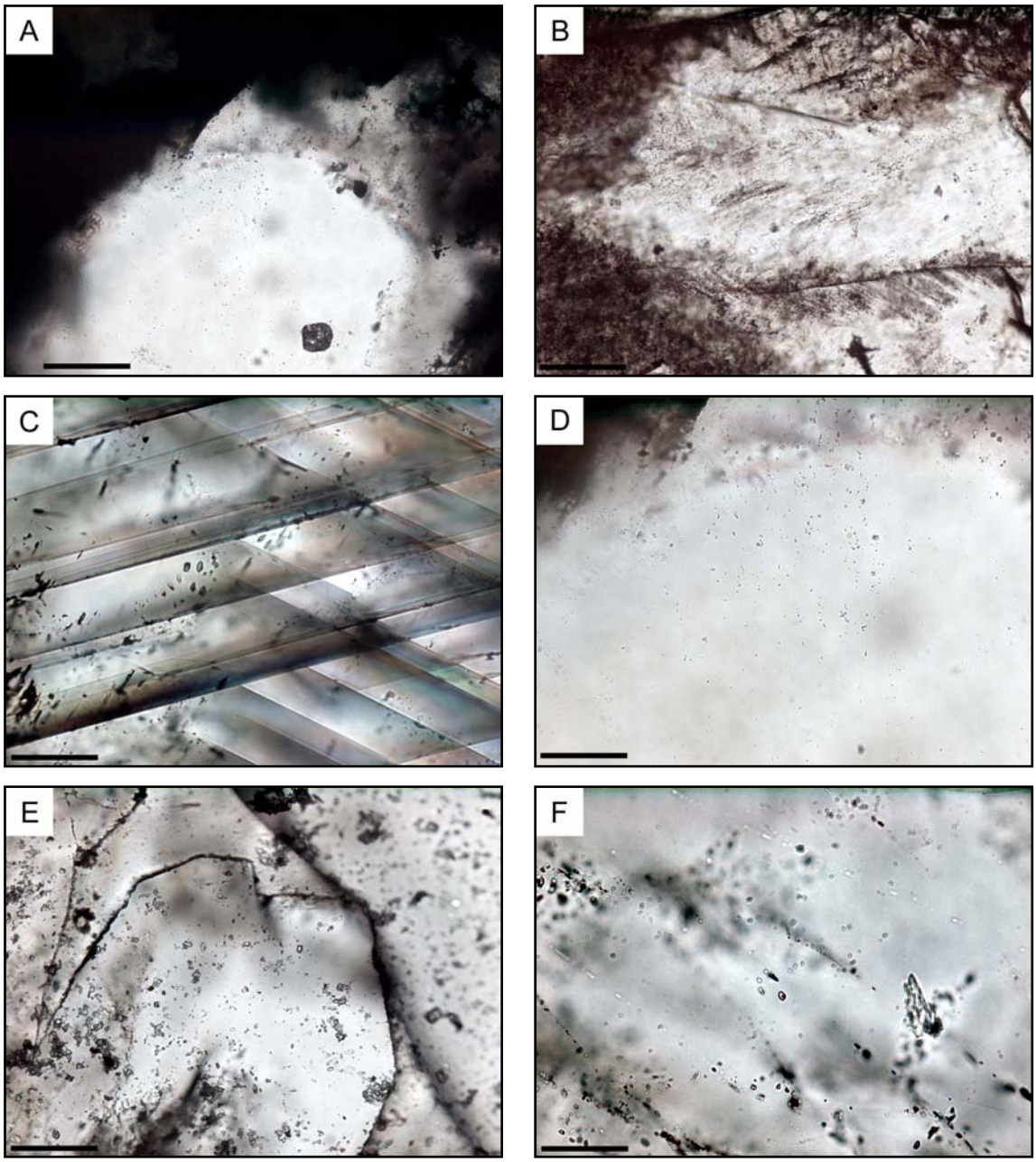

Fig. 5-1 Fluid inclusions from Eunsan, Moisan and Chunsan. This Figure highlights how small most fluid inclusions are. '**A**': sample CH003 115m (scale bar = 0.1mm) fluid inclusions in quartz as minute, pseudo-secondary to secondary inclusions in variably radiating trails. '**B**': sample EN006 81m (scale bar = 0.2mm) fluid inclusions in quartz as minute, pseudo-secondary to secondary inclusions in densely packed arrays. '**C**': sample EN006 72m (scale bar = 0.05mm) fluid inclusions in calcite as minute, pseudo-secondary to secondary inclusions typically in variably oriented trails. '**D**': sample CH003 115m (scale bar = 0.05mm) minute liquid-only (**type 1**) and liquid-rich (**type 2a**) fluid inclusions. '**E**': sample EN •*092* (scale bar = 0.1mm) typically liquid-rich (**type 2a**) and lesser gas-rich (**type 2b**) fluid inclusions. Note the irregular and necked nature of the fluid inclusions. '**F**': sample MS006 51.6m (scale bar = 0.05mm) **type 3a** fluid inclusions with no CO_2 phase evident at room temperature, but heating-freezing experiments show the presence of clathrate.

FI types (schematic)	typical size (µm)	liquid : vapour (L:V)	composition	identified this study	identified Koh (1996)	combined classification
	<5µm	L	H_2O	1		1
	<10µm	L>V	H_20	2	I	2a
	<10µm	V>L	H_20	3	II	2b
	10µm	L>V	$H_20 + CO_2$	4	IIIa	3a*
	20-30µm	V>L	$H_2O + CO_2$		IIIb	3b

Table 5-1 Fluid inclusion types, morphological summaries and classification, based on inclusions from this study and Koh (1996). * - fluid inclusion types 3a (both this study and Koh, 1996) generally do not show a CO_2 phase at room temperature, therefore can only be distinguished from type 2a fluid inclusions during microthermometric analysis. If CO_2 is found to be present, then the fluid inclusion can be categorised as type 3a as opposed to type 2a.

samples	vein minerals	FI host mineral	min. ^ parag.	FI # parag.	FI composition	dominant FI type ~	L:V
this study:							
EN •*092*	qtz	qtz	sil	PS / S	H_2O	2a/2b	L>>V
EN006 72m	qtz+adu+cal	cal	adu	PS / S	H_2O	2a	L>>V
EN006 81m	qtz+adu+cal	qtz	adu	PS / S	H_2O	2a	L>>V
CH003 115m	qtz+adu+py	qtz	adu	PS / S	H_2O	2a	L>>V
MS006 51.6m	qtz+cal	qtz	sil	PS / S	H_2O - CO_2	3a	L>>V
Koh (1996):	FI type						
SS deposit	2a	qtz	sil	unknown	H_2O		L>V
	2b	qtz	sil	unknown	H_2O		V>L
	3a	qtz	sil	unknown	H_2O - CO_2		L>V
	3b	qtz	sil	unknown	H_2O - CO_2		V>L
SS data combined:		qtz	sil	unknown	H_2O - CO_2		mixed

Table 5-2 Fluid inclusion samples. ^ = mineral paragenesis. # = fluid inclusion paragenesis – pseudo-secondary to secondary (PS/S). Pseudo-secondary to secondary fluid inclusions formed from a fluid trapped later than that which produced the mineral hosting the fluid inclusions. ~ = dominant fluid inclusion type – represents the dominant fluid inclusion type, as defined in Section 5.2.2.2 (see also Table 5-3). L:V = liquid to vapour ratio. qtz = quartz; cal = calcite; adu = adularia; sil = siliceous.

For type 2a inclusions, salinity was estimated using equation (1) (Bodnar, 1993). For type 3a inclusions, salinity was estimated using equation (2) (Chen, 1972):

$$W = (-1.78 \times Tm) - (0.0442 \times Tm^2) - (0.000557 \times Tm^3) \quad (1)$$

where: W = wt% NaCl equiv.
Tm = final ice melting temperature

$$W = +0.00098241 \times (10\text{-}Tm) \times (Tm^2 + 45.385T + 1588.75) \quad (2)$$

where: W = wt% NaCl equiv.
Tm = final clathrate melting temperature

The calculated salinity ranges for Eunsan and Chunsan are 0.5 to 2.6wt% NaCl equiv. (Table 5-3, Fig. 5-4). The calculated salinity range for Moisan is 8.1 to 13.7wt% NaCl equiv. (Table 5-3, Fig. 5-4). Equation 2 was used to calculate the salinity ranges for Moisan since final melting temperatures >0ºC implies the presence of clathrates.

The calculated salinity range for Moisan is based on observations of final melting temperatures >0ºC, interpreted as clathrate, therefore used equation (2). Final melting temperatures >0ºC under conditions of medium salinity are expected with the presence of clathrate.

Homogenisation temperature versus salinity was plotted to determine fluid processes such as boiling or mixing as highlighted by Shepherd et al. (1985) (Fig. 5-4). The data highlights differences in the character of pseudo-secondary and secondary inclusions from Eunsan, Moisan and Chunsan systems.

samples	vein minerals	FI host mineral	min. ^ parag.	FI # parag.	FI composition	dominant FI type ~	L:V	T_h range (ºC)	n=	av. T_h (ºC)	T_m range (ºC)	n=	av. T_m (ºC)	NaCl wt.% equiv.	NaCl wt.% av.
this study:															
EN •*092*	qtz	qtz	sil	PS / S	H_2O	2a/2b	L>>V	138 to 154	4	147	-0.6	1	-0.6	1.1	1.1
EN006 72m	qtz+adu+cal	cal	adu	PS / S	H_2O	2a	L>>V	147 to 171	9	163	-0.7 to -0.3	6	-0.4	0.5 to 1.2	0.7
EN006 81m	qtz+adu+cal	qtz	adu	PS / S	H_2O	2a	L>>V	154 to 193	13	166	-0.5 to -0.3	5	-0.4	0.5 to 0.9	0.7
CH003 115m	qtz+adu+py	qtz	adu	PS / S	H_2O	2a	L>>V	130 to 152	10	142	-1.5 to -0.4	5	-0.9	0.7 to 2.6	1.6
MS006 51.6m	qtz+cal	qtz	sil	PS / S	H_2O - CO_2	3a	L>>V	120 to 134	4	127	+1.6 to +5.6	*5	+3.6	8.1 to 13.7	11.0
Koh (1996):	FI type														
SS deposit	2a	qtz	sil	unknown	H_2O		L>V	127 to 361	38	213	-3.6 to -0.2	20	-2.0	0.4 to 5.9	3.4
	2b	qtz	sil	unknown	H_2O		V>L	168	1	168	-	0	-	-	-
	3a	qtz	sil	unknown	H_2O - CO_2		L>V	223	1	223	+5.7 to +9.2	*7	+7.6	1.6 to 7.9	4.7
	3b	qtz	sil	unknown	H_2O - CO_2		V>L	325 to 331	2	328	+7.3 to +8.2	*5	+7.6	3.6 to 5.2	4.7
SS data combined:		qtz	sil	unknown	H_2O - CO_2		mixed	127 to 361	42	210	-0.2 to +9.2	32	+1.6**	0.4 to 7.9	3.9

Table 5-3 Summary fluid inclusion heating and freezing data from this study and from Koh (1996). ^, # and ~ as per description in Table 5-2. L:V = liquid to vapour ratio. * - highlights Tm data corresponding to final melting temperatures for clathrate. ** - highlights data that is an average of both final ice and clathrate melting temperatures, as such is misleading to average Tm, as data is bimodal.

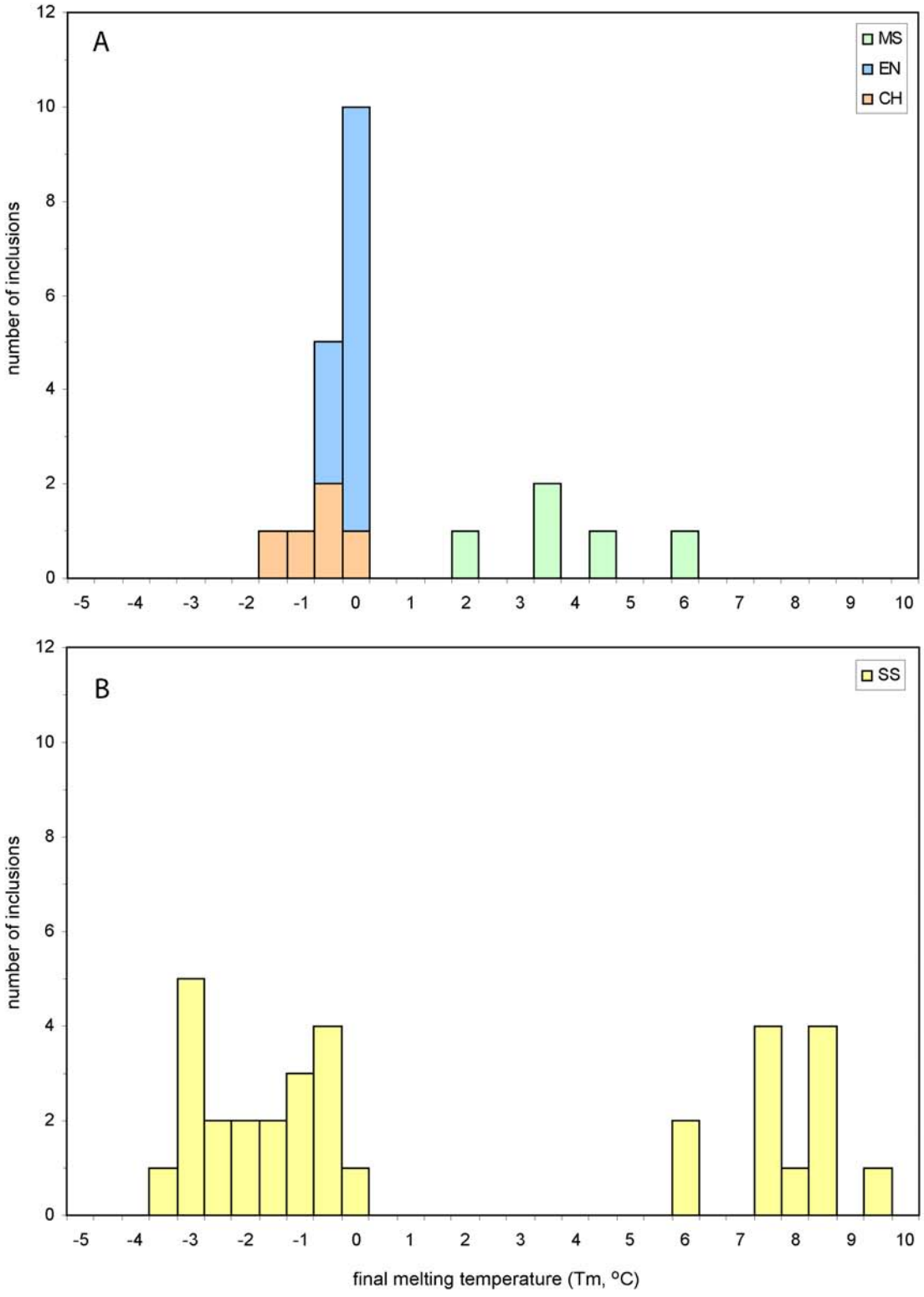

Fig. 5-2 Histogram of final melting temperatures (combined ice (<0ºC) and clathrate (>0ºC)). '**A**': data from this study, highlighting the distinctive character of secondary inclusions from Moisan compared to Eunsan and Chunsan; '**B**': data for the Seongsan deposit from Koh (1996), highlighting the distinctive character of fluid inclusions from Seongsan compared to Eunsan, Moisan and Chunsan.

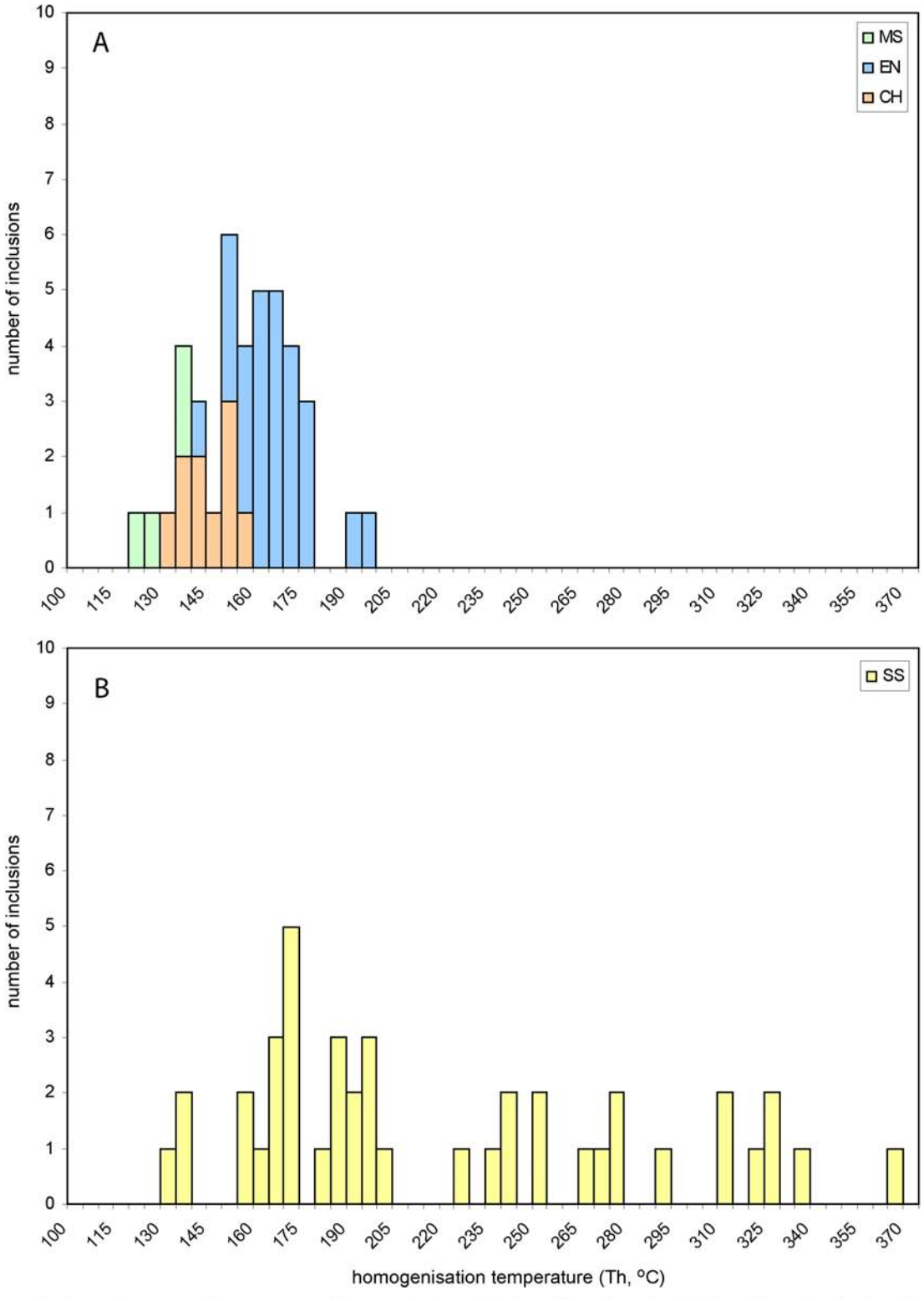

Fig. 5-3 Histogram of homogenisation temperature. '**A**': data from this study, highlighting the low but fairly continuous range of homogenisation temperatures from Moisan, Chunsan and Eunsan; '**B**': data for the Seongsan deposit from Koh (1996).

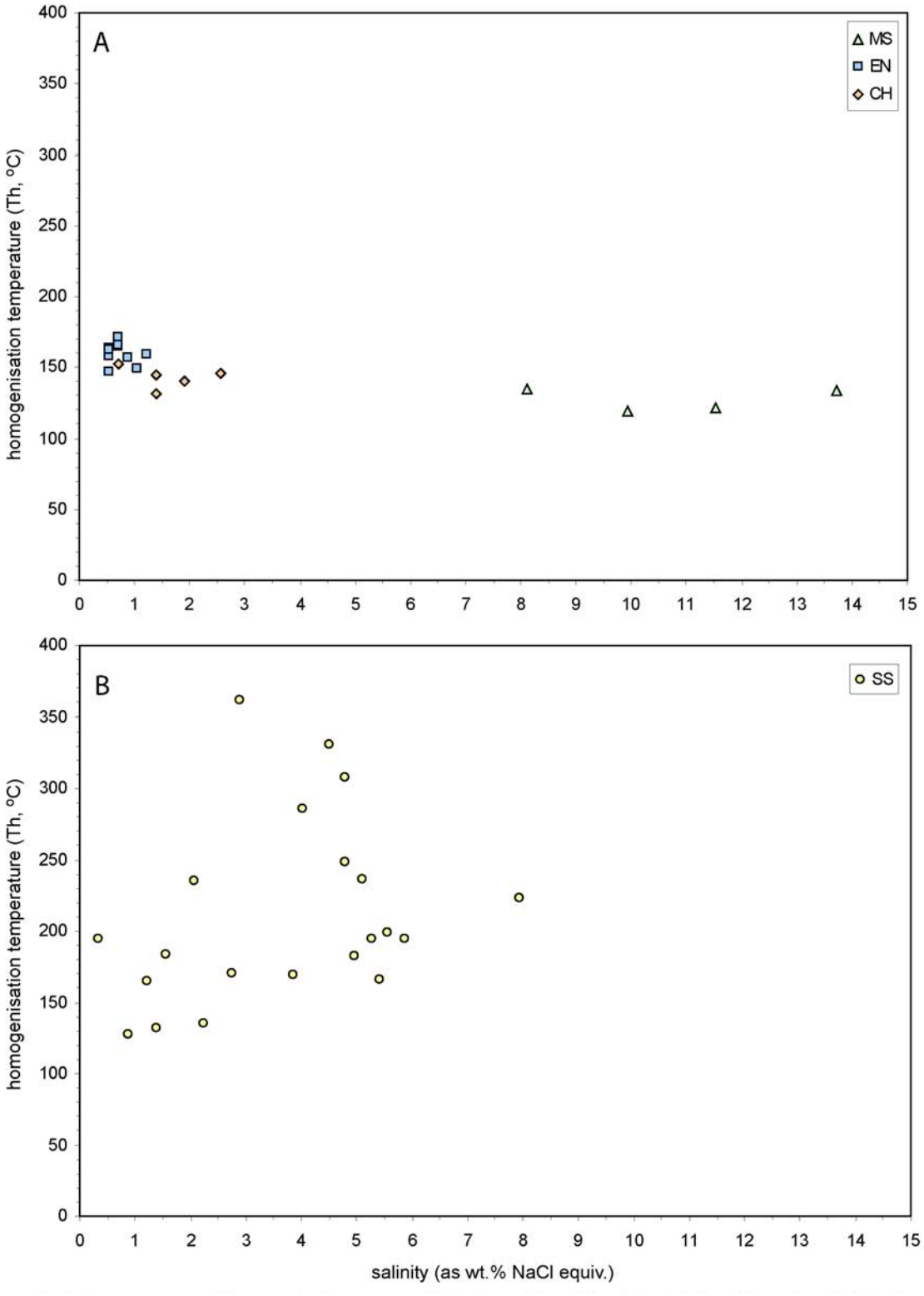

Fig. 5-4 Homogenisation temperature versus salinity plot. '**A**': data from this study, showing the more saline character of fluid inclusions from Moisan compared to those from Eunsan and Chunsan; '**B**': data for the Seongsan deposit from Koh (1996), which shows a greater spread of salinities than Eunsan, Chunsan and Moisan.

5.2.5 Interpretation of the microthermometric results

Due to the lack of primary fluid inclusions within the Seongsan district, this method of investigation has provided little information on the temperature and pressure of fluids responsible for alteration and mineralisation, or the composition of primary fluids in either the high- or low-sulfidation systems.

Homogenisation temperature data show a broad range. Data from this study only show a range between 120 to 193ºC. As these predominantly represent pseudo-secondary to secondary type 2a inclusions (liquid-rich two phase), these are not representative of primary fluids, but they do represent minimum secondary fluid trapping temperatures.

The lack of workable fluid inclusions is expected given the fine-grained nature of the high-sulfidation alteration. Similarly, within the low-sulfidation systems, mineralisation is typically associated with chalcedonic quartz, and few workable fluid inclusions directly associated with mineralisation are therefore present. The reason for the lack of workable fluid inclusions in material from the Seongsan system obtained during this study compared with those samples obtained by Koh (1996) is not understood. Samples used during this study encompassed all types of alteration and styles of mineralisation. However, Koh (1996) had access to underground mine exposures of quartz-rich zones that may have been more conducive to hosting workable fluid inclusions. The fluid inclusion data set obtained from this study is small and does not represent the primary hydrothermal fluids of the district.

5.3 GEOCHEMICAL CONDITIONS OF FORMATION: IMPLICATIONS FROM MINERAL STABILITIES

This section examines the geochemical conditions under which alteration and mineralisation formed.

5.3.1 Previous constraints on the temperature during alteration in the Seongsan district

Kim & Kusakabe (1993) undertook an oxygen and hydrogen isotope study of hydrothermally altered minerals from Seongsan and Ogmaesan. By using co-existing quartz-kaolinite mineral pairs, they determined that the advanced argillic alteration at Seongsan formed between 224 and 281ºC and at Ogmaesan between 175 and 250ºC.

At Moisan, the basal spacings of illite (Leach, 2000) implies a temperature of formation around 200ºC, with some samples showing higher crystallinity suggesting temperatures of formation up to 250ºC (Corlett, 1999). At Chunsan, the basal spacings of illite (Leach, 2000) implies a temperature of formation around 200 to 230ºC.

5.3.2 Alteration conditions: implications from mineral stabilities

5.3.2.1 Advanced argillic alteration assemblages

Advanced argillic alteration assemblages within the Seongsan district are simple with only two or three minerals generally present. These simple high variance assemblages provide few constraints on the conditions under which alteration took place.

A pressure-temperate (P-T) plot for the system Al_2O_3-SiO_2-H_2O is shown in Figure 5-5. The positions of reactions in the P-T diagram are largely dependant on temperature (Fig. 5-5), with changes in pressure of several Kb resulting in reaction temperatures only changing by a few degrees at most. Epithermal systems are generally regarded to have formed at less than 1Kb pressure, however, if these systems were close to surface and fluid dominated, the pressure could have been as low as 0.1Kb. Due to a lack of fluid inclusions, an estimate has to be made for the pressure of hydrothermal activity at Seongsan and Ogmaesan. By using a range of estimated pressures, we can see only a minimal difference in the calculated temperature. A significant difference in temperature would only result if the pressure was less than 0.05Kb.

Maximum limits for the temperature of hydrothermal activity at Seongsan and Ogmaesan can be constrained by comparison of mineral assemblages with calculated mineral stability ranges. Advanced argillic alteration at Seongsan and Ogmaesan typically contain quartz, kaolinite, dickite and alunite, with a distinct absence of pyrophyllite. For a quartz-saturated system, the

temperature of the dehydration reaction kaolinite to pyrophyllite ranges from 273±10ºC (calculated at 1Kb; Hemley et al., 1980) to 260ºC (estimated graphically from Fig. 5-5 at 0.1Kb). For a quartz-under-saturated system, the same reaction ranges from 300±10ºC (calculated at 1Kb; Hemley et al., 1980) to 288ºC (estimated graphically from Fig. 5-5 at 0.1Kb). The broader advanced argillic 1, 2 and 3 altered zones at Seongsan and Ogmaesan are quartz-saturated, whereas the core zones of vuggy silica are quartz-under-saturated.

If a pressure of ca. 0.3Kb is assumed, the lack of pyrophyllite in both Seongsan and Ogmaesan implies an alteration formation temperature less than ca. 262ºC for the broader zones of quartz-bearing advanced argillic alteration. Leached vuggy core zones at Seongsan have been affected by quartz under-saturated fluids whose temperature may have been as great as ca. 292ºC. As no pyrophyllite has been observed, this temperature has not been reached, therefore 280ºC is estimated as the maximum temperature reached at Seongsan. A maximum temperature of formation of 250ºC is estimated for Ogmaesan. This estimation is based on the lower intensity of alteration development at Ogmaesan compared to Seongsan. These maximum temperatures are similar to maximum temperatures obtained from isotope analysis of co-existing mineral-pairs by Kim & Kusakabe (1993) (see: Previous work, Section 5.3.1).

These temperatures are higher than those obtained from fluid inclusion analysis, although this is to be expected as the fluid inclusions are pseudo-secondary or secondary. Mineralogical phase relations therefore provide a better estimate of the temperature of alteration than fluid inclusion analysis in this case.

Figure 5-6 shows the stability fields of the quartz-kaolinite and quartz-dickite advanced argillic assemblages. As no pyrophyllite has been observed within the Seongsan district, this suggests that silica concentrations and/or temperatures were not sufficiently high to allow pyrophyllite formation. Furthermore, no diaspore, andalusite or corundum have been observed within the district, suggesting that the system remained below 300ºC and probably at quartz saturation. Localised quartz-under-saturated conditions may have existed, but were not sufficiently under-saturated enough for diaspore formation. Figure 5-7 examines alunite stabilities and shows that high H_2SO_4 concentrations are required for alunite to form, but a lower ratio of K_2SO_4 to H_2SO_4 is required otherwise muscovite or K-feldspar will form (Fig. 5-7).

5.3.2.2 Phyllic-adularia alteration assemblages

Illite crystallinity can be used to further constrain the temperature of alteration formation at Eunsan, Moisan and Chunsan. Previous XRD studies of Moisan and Chunsan (Section 5.2.1) imply temperatures of formation around 250ºC and 200 to 230ºC respectively.

XRD analysis of clays at Eunsan was conducted during this study (Chapter 3, Appendix 5). A sharpening of the XRD peaks with depth indicating a more ordered crystal structure implies an increase in temperature of formation with increasing depth (Appendix 5). The lack of illite/smectite and the presence of illite indicate a temperature of formation of at least 230ºC (Reyes, 1990).

Figure 5-7 shows that high K_2SO_4 and low H_2SO_4 concentrations are required before adularia will form. If the K_2SO_4 concentration falls too low, then muscovite will form, whereas if the H_2SO_4 concentration increases, then alunite will form (Fig. 5-7).

Based on the above, Eunsan, Moisan and Chunsan are inferred to have formed at ca. 230ºC. These temperatures will be used in subsequent isotope calculations.

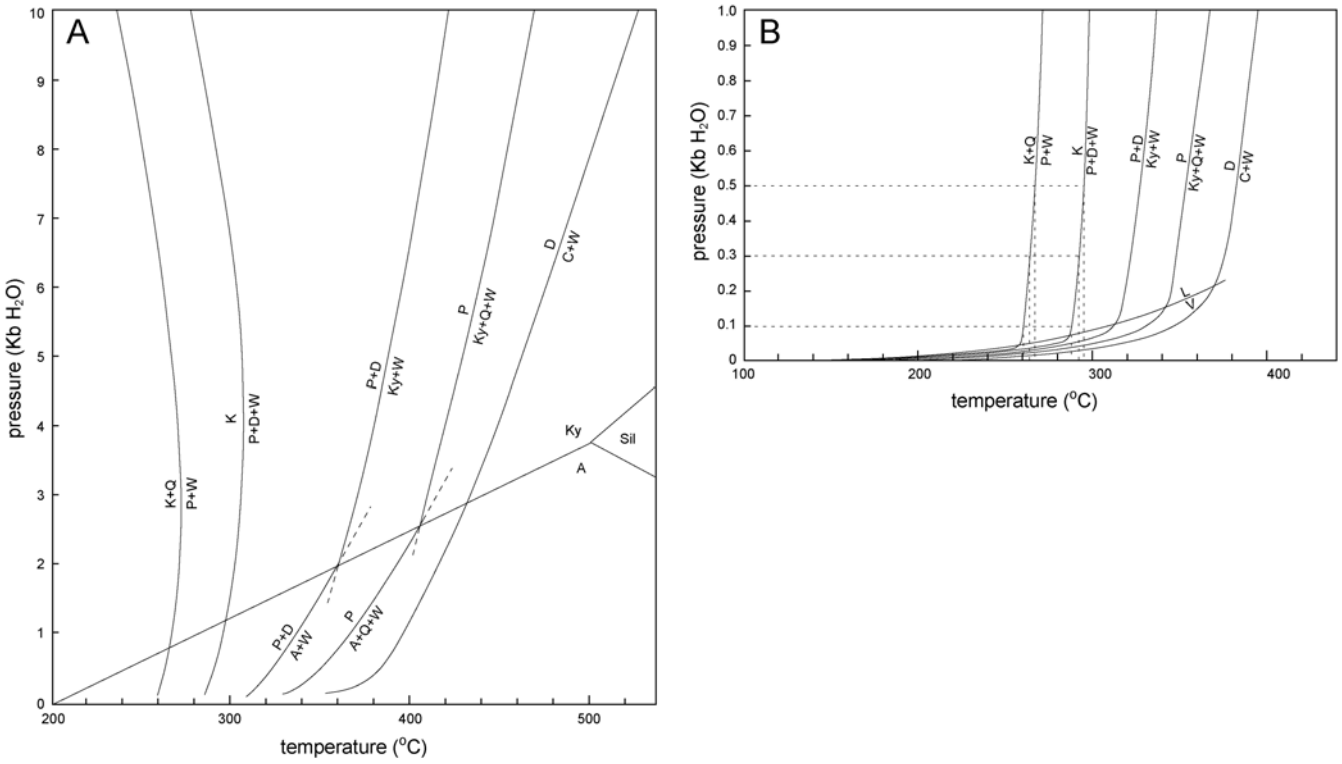

Fig. 5-5 '**A**': Calculated pressure-temperature curves in the system Al_2O_3-SiO_2-H_2O based on 1Kb stability relationships and thermodynamic data (Hemley et al., 1980). Calculated temperature dehydration reactions for kaolinite at 1Kb are 273±10ºC for kaolinite-pyrophyllite-quartz (quartz saturated) and 300±10ºC for kaolinite-pyrophyllite-diaspore (quartz under-saturated). '**B**': Calculated pressure-temperature curves in the system Al_2O_3-SiO_2-H_2O at low water pressures based on 1Kb stability relationships and derived thermodynamic data. Dashed lines show temperatures from chosen pressures. For quartz saturated system: 0.1Kb = ca. 260ºC, 0.3Kb = ca. 264ºC, 0.5Kb = ca. 267ºC; for quartz under-saturated system: 0.1Kb = ca. 288ºC, 0.3Kb = ca. 292ºC, 0.5Kb = ca. 295ºC.

Ky=kyanite; A=andalusite; Sil=sillimanite; K=kaolinite; P=pyrophyllite; D=diaspore; C=corundum; Q=quartz; W=water.

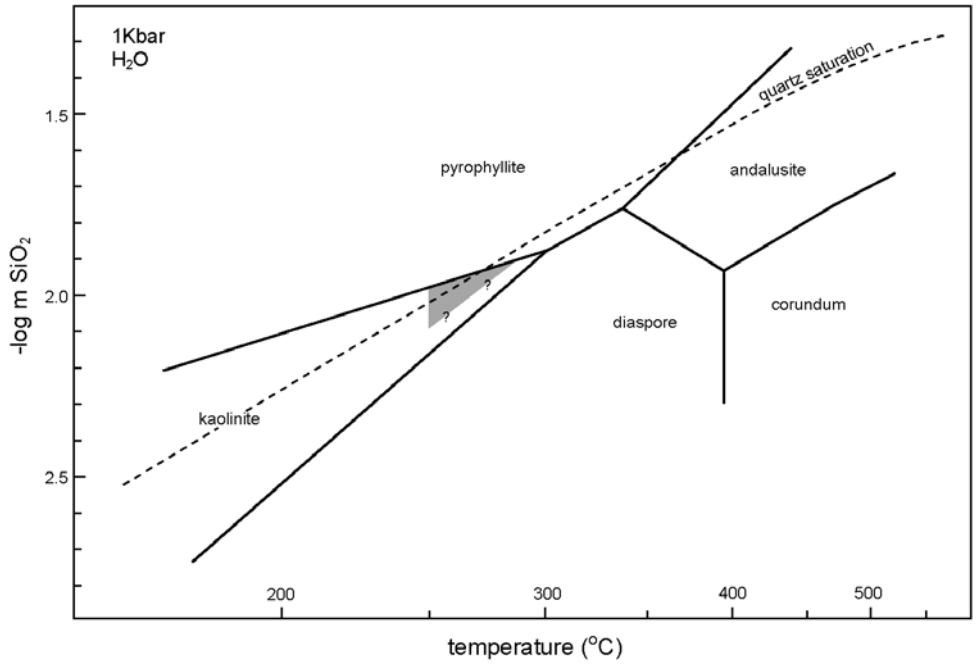

Fig. 5-6 Mineral stability relationships in the system Al_2O_3-SiO_2-H_2O at 1Kb H_2O after Hemley et al. (1980). The lack of diaspore, pyrophyllite, corundum and andalusite constrain the temperature of formation of advanced argillic alteration to ca. <280ºC. Grey shaded area represents the inferred stability fields for advanced argillic 1 and 2 alteration (quartz-kaolinite/dickite).

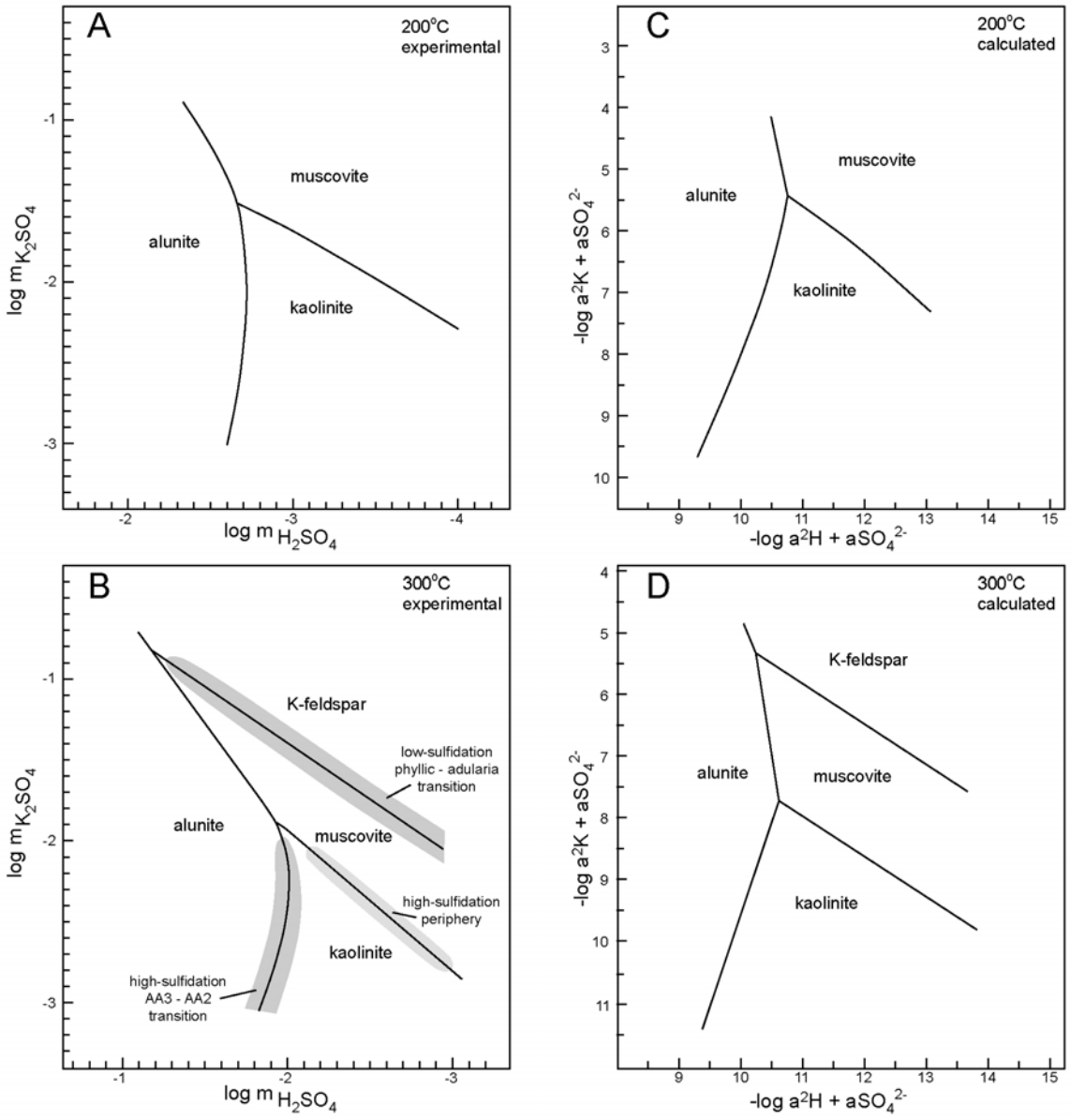

Fig. 5-7 Mineral stability relationships in the system K_20-Al_2O_3-SiO_2-H_2O-SO_3. '**A**' and '**B**' are experimentally determined at 200ºC and 300ºC; '**C**' and '**D**' are calculated at 200ºC and 300ºC. Quartz is present and total pressure is 1Kbar. Figures and thermodynamic data from Hemley et al. (1969). The shaded areas in 'B' represent stability ranges for transitional alteration zones as labelled. These shaded areas highlight that the high- and low-sulfidation alteration assemblages formed under distinctly different conditions.

5.3.3 Sulfate-sulfide mineral stabilities: further constraints on conditions of formation

The fields of key alteration minerals that characterise the advanced argillic altered systems (alunite) and the phyllic-adularia altered systems (adularia) and related sulfide minerals are distinctly different showing that these systems form under distinctly different fluid conditions (Fig. 5-8). The advanced argillic altered systems formed under oxidised, acidic, SO_4-dominant conditions, consistent with acid-sulfate epithermal systems elsewhere. The phyllic-adularia altered systems formed under reduced, near-neutral pH, H_2S-dominant conditions, consistent with adularia-sericite epithermal systems elsewhere. Under advanced argillic alteration conditions at Seongsan and Ogmaesan, Au would be transported as a chloride complex and therefore dilution, cooling and/or a pH increase would lead to Au deposition (e.g. cooling by mixing with groundwater). Under phyllic-adularia alteration conditions at Eunsan, Moisan and Chunsan, Au would be transported as a hydrosulfide complex and therefore boiling or mixing induced oxidation would lead to Au deposition, but not changes in temperature, salinity or pH (Cooke & Simmons, 2000).

Stability fields for the different high- and low-sulfidation assemblages can be defined by taking the ranges of log fO_2 from Figure 5-8 and plotting them in Figure 5-9, while ranges of log fS_2 can be constrained using the sulfide minerals (Fig. 5-9). The advanced argillic altered systems show log fO_2 around -32, which in Figure 5-9 corresponds to a log fS_2 minimum of ca. -8.5. The phyllic-adularia altered systems are stable at log fO_2 range of -37.5 to -40, which in Figure 5-9 corresponds to a log fS_2 range of -10 to -12.5.

By utilizing the log fS_2 values determined in Figure 5-9 and integrating these results into Figure 1-7, constrained by sulfide mineralogy, the following inferences are made regarding the sulfidation-state of ore-forming fluids. Sulfides associated with advanced argillic alteration at Seongsan and Ogmaesan formed under high-sulfidation state condition. Sub-economic Au-Ag-bearing sulfides at Seongsan are characterised by an intermediate-sulfidation state. No Au-Ag mineralisation was observed at Ogmaesan, so the intermediate-sulfidation fluid appears to have been absent here. Sulfides associated with Au-Ag mineralisation within the phyllic-adularia altered systems of Eunsan, Moisan and Chunsan formed predominantly under intermediate- to low-sulfidation conditions, typically associated with adularia. Au-Ag mineralisation at Chunsan also formed under low- to intermediate-sulfidation fluid conditions despite significant input of an earlier high-sulfidation fluid.

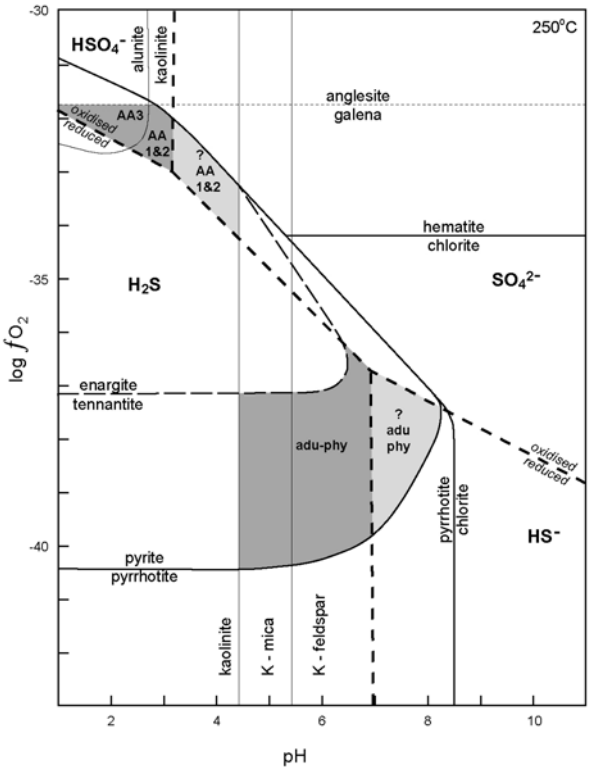

Fig. 5-8 Log fO_2 versus pH diagram at 250ºC and log ΣS = -1.7 (which approximates the Seongsan system, see Fig. 5-14). Figure and thermodynamic data from Heald et al. (1987). Dark grey shaded areas represent the maximum range of likely stability fields for advanced argillic altered systems (top left: Seongsan and Ogmaesan) and phyllic-adularia altered systems (lower centre: Eunsan, Moisan and Chunsan). Light grey shaded areas represent possible but less likely stability fields. AA1&2 = advanced argillic 1 and 2 alteration assemblages; AA3 = advanced argillic 3 alteration assemblage; adu-phy = adularia-phyllic alteration. AA1&2 and AA3 are separated by the alunite-kaolinite stability boundary. Sulfur isotope studies (Section 5.5) show that Seongsan and Ogmaesan are SO_4-dominant and that Eunsan, Moisan and Chunsan are H_2S-dominant. See main text for discussion.

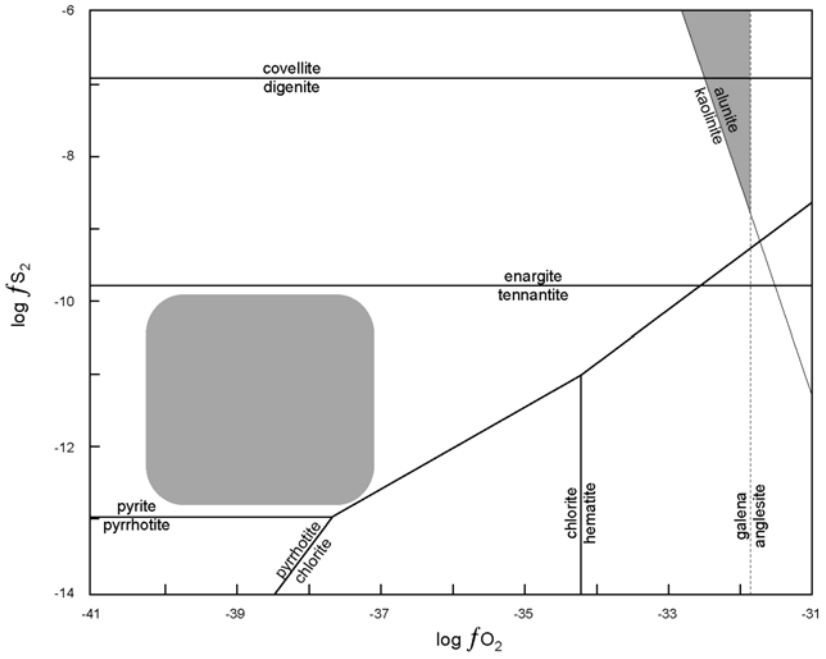

Fig. 5-9 Log fO_2 versus log fS_2 pH diagram at 250ºC. The log fO_2 is constrained from Figure 5-8. Figure and thermodynamic data from Heald et al. (1987). Grey shaded areas represent inferred stability fields for advanced argillic altered systems (top right: Seongsan and Ogmaesan) and phyllic-adularia altered systems (lower centre left: Eunsan, Moisan and Chunsan). The Au-Ag bearing sulfides at Seongsan are geochemically similar to those found within Eunsan, Moisan and Chunsan, highlighting that distinctly different fluids formed the advanced argillic alteration and Au-Ag mineralisation at Seongsan.

5.4 OXYGEN & HYDROGEN ISOTOPE CONSTRAINTS ON FLUID ORIGINS AND CHARACTERISTICS

Oxygen and hydrogen isotope studies have been undertaken to help clarify relationships, if any, between the high- and low-sulfidation systems of the Seongsan district. Some mineral pairs are also used to further constrain temperature estimates.

5.4.1 Previous oxygen and hydrogen isotopic work in the Seongsan district

Kim & Kusakabe (1993) undertook an oxygen and hydrogen isotope study of hydrothermally altered minerals from Seongsan and Ogmaesan. By using co-existing quartz-kaolinite mineral pairs, they determined that the advanced argillic alteration at Seongsan formed between 224 and 281ºC and Ogmaesan formed between 175 and 250ºC. Furthermore, they infer that the alteration kaolinite and alunite are of a hypogene origin. Koh & Chang (1997) also undertook oxygen and hydrogen isotope work on the Seongsan clay-sulfate deposits.

5.4.2 Oxygen and hydrogen isotope methods

Samples were selected from the full range of alteration and vein assemblages in the district. Both weakly altered material with relic original texture and strongly altered material adjacent to infill veins were included in the sample suite so that the affects of a range of fluid to rock ratios on the isotopic character of the rocks could be ascertained (Fig. 5-10). Samples are listed in Table 5-4 where they are grouped into five categories: 1. ‘least altered’, 2. ‘high-sulfidation – altered wall rocks’, 3. high-sulfidation – vein quartz’, 4. ‘low-sulfidation – altered wall rocks’, and 5. ‘low-sulfidation – vein quartz’. The lithology, alteration assemblage and paragenetic stage of each sample are also shown in Table 5-4 (see also: Chapter 3, Table 3-3).

Samples selected were off-cuts of diamond drill core from each of the prospects except for Ogmaesan where the lack of diamond drill core required the use of surface rock samples. These were generally large samples that were cut to obtain fresh unweathered material. Due to the very fine-grained nature of the alteration, it was almost impossible to obtain mineral separates, hence whole rock samples were used. Quartz and dickite separates were however obtained from vein material (Table 5-4). Thin sections were examined to determine the relative abundances of each mineral and their paragenetic relationships so that the whole-rock isotope value could be used to calculate inferred isotopic compositions of the formation water.

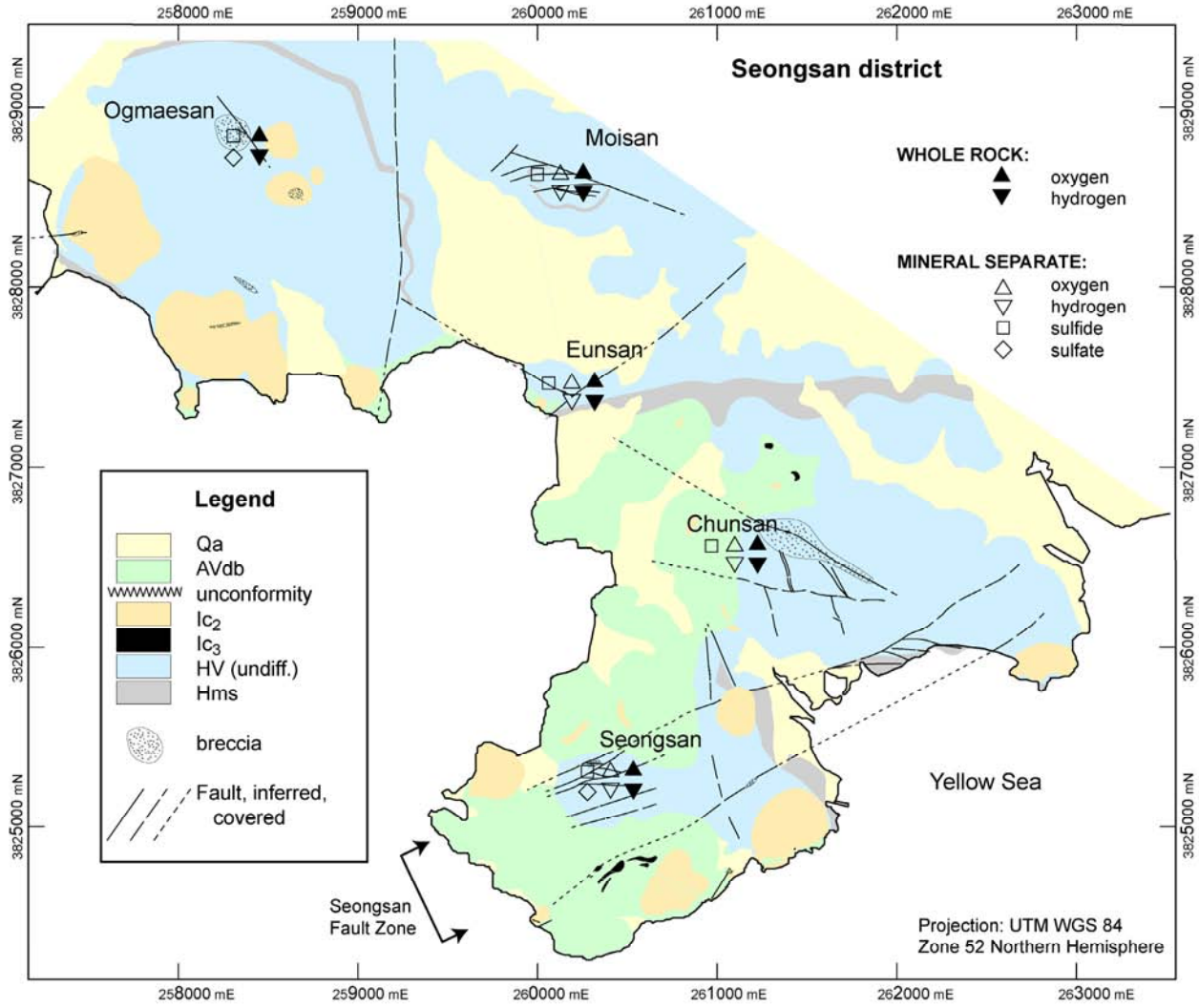

Fig. 5-10 Oxygen, hydrogen and sulfur isotope analyses undertaken at each prospect.

Samples were crushed and milled to a very fine powder. Final aliquots of ca. 10g of sample material were sent to Dr J. Miller at the University of Cape Town for analysis. Dr J. Miller undertook final sample preparation and oxygen and hydrogen isotope analysis at the Department of Geological Sciences, University of Cape Town, and provided details of final sample preparation and analytical methodology used.

Oxygen isotope analysis

Oxygen isotope ratios were determined by conventional fluorination methods (Clayton & Mayeda, 1963) using ClF_3 as the oxidising reagent (Borthwick & Harmon, 1982). Samples were reacted overnight at 550ºC. After conversion to CO_2, isotope ratios were determined on a Finnigan MAT 252 mass spectrometer housed in the department of Archaeology at UCT.

All oxygen isotope data are reported in δ notation in per mil units (‰), as:

$$\delta^{18}O = (R_{sample}/R_{standard} - 1) \times 1000 \quad (3)$$

where: R is the isotopic $^{18}O/^{16}O$ ratio.

A quartz standard (MQ) calibrated against NBS-28 was analysed in duplicate with each run of eight samples and used to convert the raw data to the V-SMOW scale using the value of 9.64% for NBS-28 recommended by Coplen et al. (1983). The average observed difference between MQ duplicates during the course of this work was 0.09‰ (n = 8).

Calculation of fluid oxygen isotopic values

The following mineral-water fractionation factors (1000 *ln* α) were used to calculate the $\delta^{18}O$ isotopic composition of the fluid assumed to be in isotopic equilibrium with the mineral:

quartz-water: $$1000\ ln\ \alpha = 3.38 \times (10^6 / T^2) - 3.40 \quad (4)$$

albite-water: $$1000\ ln\ \alpha = 2.39 \times (10^6 / T^2) - 2.51 \quad (5)$$

illite-water: $$1000\ ln\ \alpha = 2.43 \times (10^6 / T^2) - 4.80 \quad (6)$$

muscovite-water: $$1000\ ln\ \alpha = 2.38 \times (10^6 / T^2) - 3.89 \quad (7)$$

kaolinite-water: $$1000\ ln\ \alpha = 2.05 \times (10^6 / T^2) - 3.85 \quad (8)$$

alunite(SO_4)-water: $1000\ ln\ \alpha = 3.09 \times (10^6 / T^2) - 2.94$ (9)

alunite(OH)-water: $1000\ ln\ \alpha = 2.28 \times (10^6 / T^2) - 3.90$ (10)

K-feldspar(adularia)-water: $1000\ ln\ \alpha = 2.91 \times (10^6 / T^2) - 3.41$ (11)

where: T is temperature in Kelvin (= ºC + 273.15)

Equation (4) from Clayton et al. (1972; temperature range 200-500ºC); equation (5) from Matsuhisa et al. (1979; 400-500ºC); equation (6) from Eslinger & Savin (1973; 160-270ºC); equation (7) from O'Neil & Taylor (1969; 400-650ºC); equation (8) from Kulla & Anderson (1978; 175-325ºC); equation (9) from Stoffregen et al. (1994; 250-450ºC); equation (10) from Stoffregen et al. (1994; 250-450ºC); equation (11) from O'Neil & Taylor (1969; 350-800ºC).

The following relationship was used to calculate the isotopic composition of formation fluid from the isotopic composition of the mineral (Campbell & Larson, 1998):

$$1000\ ln\ \alpha_{\text{mineral-water}} = \delta^{18}O_{\text{mineral}} - \delta^{18}O_{\text{water}} \quad (12)$$

Temperature estimates from mineral pairs using oxygen isotope geothermometry

The temperature dependence of the fractionation factor makes it possible to use $\delta^{18}O$ as a geothermometer. This is done by solving simultaneous fractionation factor equations for mineral pairs. However, to use this method, several assumptions must hold true: the mineral pairs must have been co-deposited in isotopic equilibrium with each other hence forming at the same temperature from the same fluid, and they must have retained their original isotopic composition with minimal later re-equilibration or alteration (Campbell & Larson, 1998).

Co-existing quartz and dickite from a quartz-pyrite-dickite vein at Seongsan have been sampled and used for oxygen isotope geothermometry.

By combining equations (4) and (8), we get:

$$1000\ ln\ \alpha_{\text{dickite-quartz}} = (2.05 - 3.38) \times (10^6 / T^2) + (-3.85 - -3.40) \quad (13)$$

which approximates as (see equation (12)):

$$\delta^{18}O_{\text{dickite}} - \delta^{18}O_{\text{quartz}} = -1.33 \times (10^6 / T^2) - 0.45 \quad (14)$$

where the following relationship is true (Campbell & Larson, 1998):

$$\delta^{18}O_{dickite} - \delta^{18}O_{quartz} = \Delta^{18}O_{dickite\text{-}quartz} \quad (15)$$

hence:

$$\Delta^{18}O_{dickite\text{-}quartz} = -1.33 \times (10^6 / T^2) - 0.45 \quad (16)$$

therefore, solving for T:

$$T = \sqrt{\ [\ (-1.33 \times 10^6) / (\Delta^{18}O_{dickite\text{-}quartz} + 0.45)\ ]} \quad (17)$$

where: T is temperature in Kelvin (= ºC + 273.15)

Hydrogen isotope analysis

Hydrogen isotopes (^1H = Deuterium, D) were analysed following the method of Venneman & O'Neil (1993). Up to 100mg of sample powder was placed in 9mm quartz tubes that had been degassed at 800°C for 3 hours. The quartz tubes and sample powder were then placed in an oven at 110°C for a minimum of 24 hours. The samples were further degassed on a vacuum line at 200°C before pyrolysis. The resultant H_2O was frozen directly into a glass reaction tube containing Zn metal filings, while any H_2 gas produced was passed through a Cu furnace to oxidise the H_2 to H_2O which was then frozen into the same reaction tube. The reaction tube was then placed in a furnace at 450°C for 45 minutes and the resultant H_2 gas analysed directly on a Finnigan MAT 252 mass spectrometer housed in the Department of Archaeology at UCT.

All hydrogen isotope data are reported in δ notation in per mil units (‰), as:

$$\delta D = (R_{sample}/R_{standard} - 1) \times 1000 \quad (18)$$

where: R is the isotopic $^2H/^1H$ ratio.

An internal water standard (CTMP, δD = -9‰) was used to calibrate data to the SMOW scale and data were normalised so VSLAP was -428‰ on the SMOW scale (Coplen, 1993).

Calculation of fluid hydrogen isotopic values

The following mineral-water fractionation factors are used to calculate the δD isotopic composition of the fluid assumed to be in isotopic equilibrium with the mineral:

chlorite-water: $$1000\ ln\ \alpha = -5.47 \times (10^6 / T^2) - 26.27 \quad (19)$$

muscovite-water: $$1000\ ln\ \alpha = -22.1 \times (10^6 / T^2) + 19.1 \quad (20)$$

kaolinite-water: $1000\ ln\ \alpha = -2.2 \times (10^6 / T^2) - 7.7$ (21)

alunite-water: interpolation between 250ºC and 450ºC where $1000\ ln\ \alpha$ = -6 and -9 respectively (22)

where: T is temperature in Kelvin (= ºC + 273.15)

Equation (19) from Taylor (1979); equation (20) from Suzuoki & Epstein (1976; 450-800ºC); equation (21) from Gilg & Sheppard (1996; 0-330ºC); equation (22) from Stoffregen et al. (1994; 250-450ºC).

The following relationship was used to calculate the isotopic composition of formation fluid from the isotopic composition of the mineral (as per equation (12); Campbell & Larson, 1998):

$$1000\ ln\ \alpha_{\text{mineral-water}} = \delta D_{\text{mineral}} - \delta D_{\text{water}} \quad (23)$$

Determination of appropriate fractionation equations

Appropriate fractionation equations were chosen based on extensive thin section analysis and XRD data to accurately determine mineral assemblages. Where multiple minerals are present, such as in whole rock analyses, mineral proportions were visually estimated using detailed thin section petrography. Propylitic alteration is dominated by an albitisation event, hence isotopic calculations use albite-water fractionation factor equation (5) for $\delta^{18}O_{water}$ and chlorite-water fractionation factor equation (19) for δD_{water}. Remaining alteration types use appropriate fractionation factor equations (e.g. phyllic alteration uses illite-water equation (6) for $\delta^{18}O_{water}$). Where samples show multiple mineral assemblages, $\delta^{18}O_{water}$ and δD_{water} were calculated by solving simultaneous fractionation equations at a given temperature.

The fractionation factors have been determined experimentally within given temperature ranges, some of which do not cover the inferred temperature range under which the sampled material formed. These extrapolated calculated results should be used with caution.

5.4.3 Oxygen and hydrogen isotope results

$\delta^{18}O_{water}$ and δD_{water} were calculated from equations (12: $\delta^{18}O$) and (23: δD) using $\delta^{18}O_{mineral}$ and $\delta D_{mineral}$ results and fractionation factors as calculated from equations (4 to 11: $\delta^{18}O$) and (18 to 22: δD) using temperature constraints as discussed within Section 5.2. Temperature constraints assume isotopic equilibrium existed between the fluid and the mineral of formation. Results have been summarised within Table 5-4, plotted within Figure 5-11 and are interpreted within the following section.

	sample	lithology	alteration	min. ^ parag.	R	M	whole rock/mineral analysis		calculated $\delta^{18}O_{water}$ composition				calculated δD_{water} composition			
							$\delta^{18}O$ (‰)	δD (‰)	200ºC	230ºC	250ºC	280ºC	200ºC	230ºC	250ºC	280ºC
Least altered	EN001 174m	HVl	100% prop		R		6.3	-82	-1.87	-0.63	-0.32	1.00	-31	-34	-36	-38
	EN002 150m	Hms	100% prop		R		5.5	-101	-2.67	-1.43	-1.12	0.20	-50	-53	-55	-57
	EN002 156m	HVa	90% prop, 10% phy		R		4.4	-83	-3.56	-2.32	-1.97	-0.68	-29	-33	-35	-38
	EN010 104m	HV	90% prop, 10% phy		R		4.9	-87	-3.06	-1.82	-1.47	-0.18	-33	-37	-39	-42
	EN002 143m	HVs	95% prop, 5% adu		R		4.0	-79	-4.20	-2.99	-2.65	-1.34	-28	-31	-33	-35
HS altered wall rocks	SS002 12m	Ic_2	100% dick		R		10.14	-81	4.88	5.94	6.55	7.34	-63	-65	-65	-66
	SS002 135m	Ic_2	100% dick		R		8.2	-69	2.94	4.00	4.61	5.40	-51	-53	-53	-54
	SS002 148m	Ic_2	100% dick		R		7.2	-67	1.94	3.00	3.61	4.40	-49	-51	-51	-52
	SS001 169m	Ic_2	100% dick		R		6.93	-75	1.67	2.73	3.34	4.13	-57	-59	-59	-60
	SS001 295m	Ic_2	60% dick, 40% phy		R		5.3	-67	-0.28	0.86	1.51	2.36	-25	-30	-33	-37
	SS001 298m	Ic_2	50% dick, 50% phy		R		4.6	-77	-1.05	0.10	0.77	1.63	-28	-35	-38	-43
	OG 51	HV	85% qtz, 15% alu		R		7.6	-32	-3.97	-2.25	-1.26	0.02	-27	-26	-26	-26
	OG 59.1	HV	90% alu, 10% kao		R		10.0	-151	-0.30	1.24	2.13	3.28	-145	-144	-144	-144
	OG 40	HV	80% dick, 20% alu		R		9.2	-55	2.82	3.99	4.66	5.53	-40	-41	-41	-42
	OG 42b	HV	100% kao		R		9.0	-151	3.74	4.80	5.41	6.20	-133	-135	-135	-136
vein qtz	SS002 135m a	qtz	100% qtz	sil (p-a)		M	10.0	-93	-1.70	0.05	1.05	2.35		-93		
	SS002 135m e1	qtz	100% qtz	sil (p-a)		M	10.06	-89	-1.64	0.11	1.11	2.41		-89		
	SS002 135m e2	qtz	100% qtz	sil (p-a)		M	9.63	-94	-2.07	-0.32	0.68	1.98		-94		
	SS002 135m g	qtz	100% qtz	sil (p-a)		M	9.84	-68	-1.86	-0.11	0.89	2.19		-68		
	SS002 148m	qtz	100% qtz	sil (aa)		M	8.2	-78	-3.50	-1.75	-0.75	0.55		-78		
	SS002 148m	dick	100% dick	sil (aa) / AA2		M	8.4	-108	3.14	4.20	4.81	5.60	-90	-92	-92	-93

Table 5-4 (continued on next page…)

	sample	lithology	alteration	min. ^ parag.	R	M	whole rock/mineral analysis		calculated $\delta^{18}O_{water}$ composition				calculated δD_{water} composition			
							$\delta^{18}O$ (‰)	δD (‰)	200ºC	230ºC	250ºC	280ºC	200ºC	230ºC	250ºC	280ºC
LS																
altered wall rocks	CH003 90m	HVp	95% qtz, 5% phy		R		9.22	-80	-2.20	-0.47	0.51	1.80	0	-12	-18	-27
	CH003 145m a	Hms	98% qtz, 2% phy		R		8.97	-101	-2.62	-0.88	0.12	1.41	-21	-33	-39	-48
	CH003 145m b	HVo	98% qtz, 2% phy		R		7.26	-103	-4.33	-2.59	-1.59	-0.30	-23	-35	-41	-50
	CH002 207m	HVa-l	85% phy, 15% adu		R		7.14	-66	0.56	1.85	2.59	3.56	14	2	-4	-13
	CH006 93m	HVa	90% phy, 10% arg		R		10	-97	4.03	5.26	5.97	6.89	-24	-34	-40	-48
	EN010 171m	HV	100% phy		R		5.24	-79	-0.81	0.44	1.16	2.10	1	-11	-17	-26
	EN004 133m	HVf	95% adu, 5% phy		R		4.7	-100	-4.71	-3.22	-2.36	-1.25	-20	-32	-38	-47
	MS001 109m	HV	100% phy		R		4.7	-73	-1.35	-0.10	0.62	1.56	7	-5	-11	-20
	MS006 51m	HV	100% phy		R		4.32	-73	-1.73	-0.48	0.24	1.18	7	-5	-11	-20
vein qtz	CH003 115m	qtz	100% qtz	adu		M	3.53	-71	-8.17	-6.42	-5.42	-4.12			-71	
	CH006 33m	qtz	100% qtz	sil (p-a)		M	7.28	-100	-4.42	-2.67	-1.67	-0.37			-100	
	●*092* (EN)	qtz	100% qtz	sil (p-a)		M	5.11	-93	-6.59	-4.84	-3.84	-2.54			-93	
	EN006 72m	qtz	100% qtz	adu		M	2.9	-89	-8.80	-7.05	-6.05	-4.75			-89	
	EN006 81m	qtz	100% qtz	adu		M	7.1	-91	-4.60	-2.85	-1.85	-0.55			-91	
	●*082* (MS)	qtz	100% qtz	sil (p-a)		M	5.9	-87	-5.80	-4.05	-3.05	-1.75			-87	
	MS006 51m v	qtz	100% qtz	sil (p-a)		M	4.4	-99	-7.30	-5.55	-4.55	-3.25			-99	
	MS007 76m	qtz	100% qtz	adu		M	4.67	-94	-7.03	-5.28	-4.28	-2.98			-94	
	MS008 148m	qtz	100% qtz	adu		M	3.8	-90	-7.90	-6.15	-5.15	-3.85			-90	

Table 5-4 (…continued from previous page) Oxygen and hydrogen isotope data for samples from the Seongsan district. SS = Seongsan; OG = Ogmaesan; EN = Eunsan; MS = Moisan and CH = Chunsan. Calculated $\delta^{18}O_{water}$ and δD_{water} results highlighted in grey are at the preferred temperatures based on the mineral assemblages; and these data are used in Figures 5-11 & 5-12. ^ as per description in Table 5-2. R = rock sample, M = mineral separate. HS = high-sulfidation, LS = low-sulfidation. Alteration types: prop = propylitic; adu = adularia; phy = phyllic; dick = dickite; qtz = siliceous±silicic; sil (p-a) = siliceous (phyllic-adularia related); sil (aa) = siliceous (advanced argillic related); alu = alunite; kao = kaolinite. OG 51 +157mRL; OG 59.1 +130mRL; OG 40 +85mRL; OG 42b +82mRL.

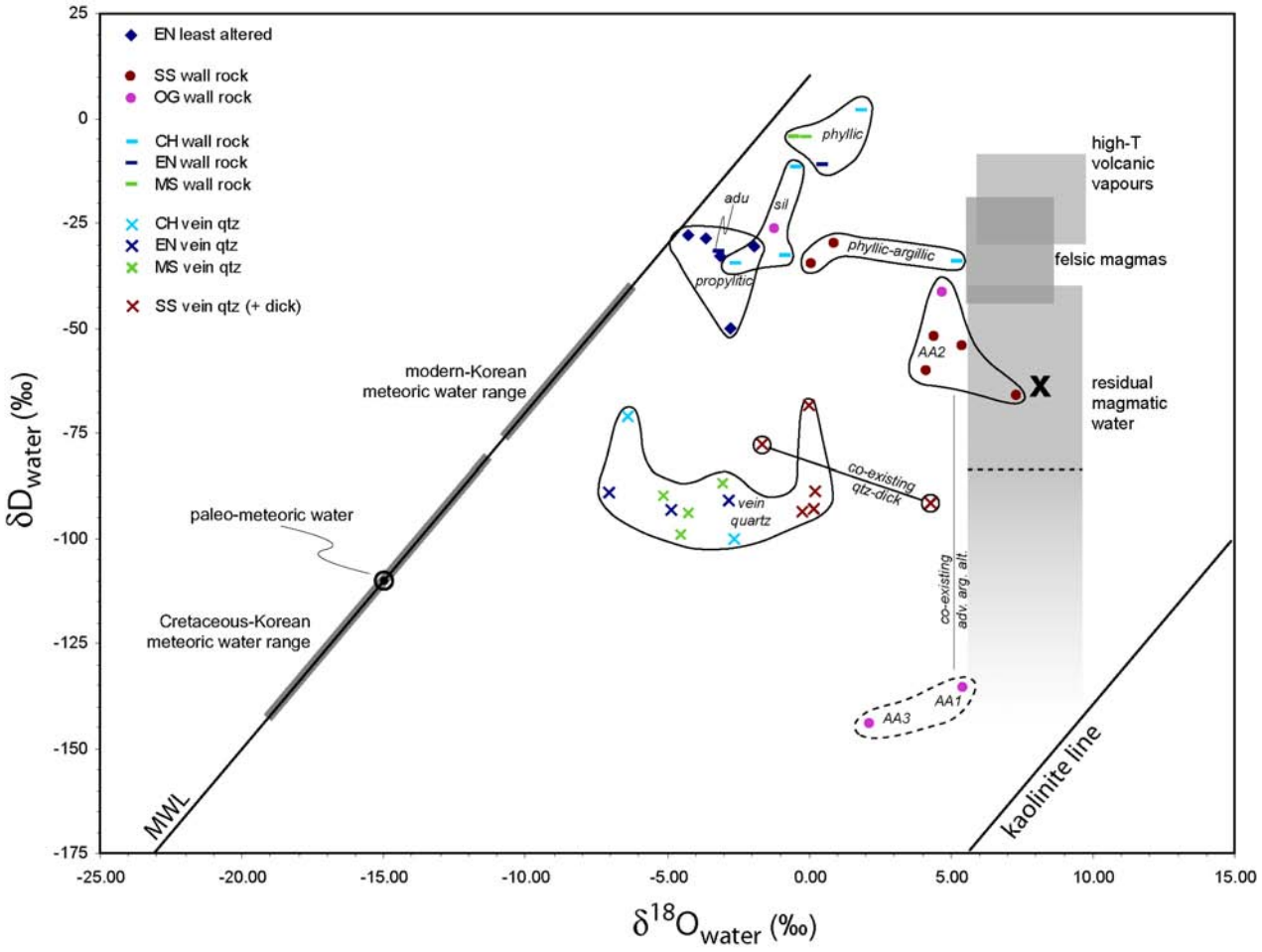

Fig. 5-11 $\delta^{18}O_{water}$ and δD_{water} results for samples analysed during this study (Table 5-4). Ranges of residual magmatic water remaining in intrusion after degassing and crystallisation (Taylor, 1974), composition of water initially dissolved in felsic melts (Taylor, 1992), and low-salinity vapour discharges from high-temperature volcanic fumaroles (Giggenbach, 1992) are shown in grey and discussed further in the main text. '**X**' = hypothetical fresh granodiorite/dacite (from Criss & Taylor, 1986). Remaining data (labelled) are plotted according to sample type. AA1, 2, 3 = advanced argillic 1, 2, 3; qtz = siliceous altered; adu = adularia altered.

EN=Eunsan; CH=Chunsan; MS=Moisan; OG=Ogmaesan; SS=Seongsan. SMOW=standard meteoric ocean water. MWL = modern-day meteoric water line; note that the paleo-meteoric water line may have varied by as much as ±5‰ in $\delta^{18}O$ (Ohmoto, 1986). Cretaceous-Korean meteoric water range (δD = -81 to -143‰) and modern-Korean meteoric water range (groundwaters: δD = -42 to -73‰; hotsprings: δD = -39 to -77‰) from Shelton et al. (1988). See main text for interpretation, including determination of paleo-meteoric water isotopic composition.

Temperature estimates from mineral pairs using oxygen isotope geothermometry were unsuccessful (SS002 148m – co-existing quartz and dickite; Table 5-4; Fig. 5-11). The results ended up with an invalid calculation (attempting to square root a negative value). This shows that one or more of the assumptions required for this process were not valid. Either the quartz or dickite within the quartz-pyrite-dickite vein were not co-deposited at the same temperature from the same fluid, or the isotopic value for one or both of these mineral pairs had been re-set by subsequent re-equilibration or alteration.

5.4.4 Interpretation of the oxygen and hydrogen isotope data

5.4.4.1 A brief comment on the isotopic composition of exsolved fluids

Examination of the isotopic fractionation of fluid in a melt exsolving into aqueous fluid shows that 'primary magmatic water' as defined by Taylor (1974) is more appropriately called 'residual magmatic water' (Hedenquist et al., 1998). This is explained in the following.

Magmatic water that discharges at surface is referred to as 'high-T volcanic vapours' (Fig. 5-11) and has relatively heavy δD isotopic compositions of about -20±10‰ (Giggenbach, 1992). Water initially dissolved in non-degassed felsic magmas is referred to as 'felsic magmas' (Fig. 5-11) and has a δD isotopic composition between -20 to -45‰ (Taylor, 1992). Therefore, if the typical aqueous fluid-melt fractionation factor ($\Delta D_{fluid\text{-}melt}$ = 20‰; Suzuki & Epstein, 1976) holds true, then an isotopically δD depleted fluid remains in the crystallising magma (Taylor, 1986). The 'residual magmatic water' field in Figure 5-11 down to the dashed line represents the 'primary magmatic water' field, as defined by Taylor (1974). Continued magma degassing in an open system could continue to fractionate the residual magmatic fluid to greatly δD depleted compositions (Taylor, 1988), particularly so in volcanic rocks due to eruptive open-system degassing (Hedenquist et al., 1998). This is represented by the field below the dashed line in 'residual magmatic waters' (Fig. 5-11). This effect has been documented in a number of deposits, e.g. Butte, Montana, U.S.A. (δD ca. -115 to -180‰; Taylor, 1997) and Mount Skukum, Canada (δD -175‰; Love et al., 1998) (see also: Fig. 18 in Hedenquist et al., 1998).

5.4.4.2 Hydrological evolution based on calculated fluid-rock isotopic exchange

Isotopic modelling of both a paleo-meteoric water and a paleo-magmatic water interacting with hypothetical fresh dacite/granodiorite has been undertaken in order to make inferences about the meteoric and/or magmatic inputs and water to rock ratios during alteration development.

Determining the isotopic composition of a paleo-meteoric water

As shown within Figure 5-11, the Cretaceous-Korean meteoric water range is -81 to -143‰ for δD (Shelton et al., 1988). A better constrained value for a paleo-meteoric water was determined

by So & Yun (1996) for an epithermal Au-Ag mineralised district located ca. 100km to the north of the Seongsan district by directly analysing fluid inclusions for δD within late-stage calcite veins. The δD of these fluid inclusions was assumed to represent the paleo-meteoric water at the time of entrapment. As this district is located only ca. 100km to the north, and the age of mineralisation was inferred to be around 76Ma, which is within ca. 2Ma of the waning hydrothermal system of the Seongsan district (So & Yun, 1996; compare with Chapter 4), this allows use of this value as a paleo-meteoric water isotopic composition. However, knowledge of the following assumptions are critical: that the paleo-meteoric water isotopic composition is based solely on δD values plotted on the modern-day meteoric water line, therefore does not take into account possible $\delta^{18}O$ shift which can be expected for paleo-meteoric waters, in the order of ±5‰ in $\delta^{18}O$ (Ohmoto, 1986). It also assumes that there has been no diffusion of hydrogen through the calcite crystal lattice, which would result in a change in the δD isotopic value. If these assumptions hold true, then the paleo-meteoric water would have an isotopic composition of δD = -110‰ and $\delta^{18}O$ = -15‰. A more negative paleo-meteoric water isotopic composition than the modern-Korean meteoric water isotopic compositional range is expected as the Korean peninsula was at higher latitudes during the Mesozoic (Shelton et al., 1988).

Determining the isotopic composition of a hypothetical fresh dacite/granodiorite

The igneous rocks within the broader Chollanam Province belong to a high-K calc-alkaline series formed in a continental margin volcanic arc above an active subduction zone, and show an enrichment in crustal components such as K, La, Ce, Sm, Nd and B, with high (La/Yb)cn ratios (ca. 22.67:1), and high initial $^{87}Sr/^{86}Sr$ ratios of 0.708 to 0.712 (Koh et al., 2000) (Chapter 1). This suggests that the rhyolites were predominantly I-type with a subordinate component of more evolved crustal material contaminating the melts. An I-type isotopic composition of δD = -65‰ and $\delta^{18}O$ = +8‰ (Criss & Taylor, 1986) is assumed but also acknowledging the possibility that the δD and $\delta^{18}O$ values of unaltered rocks at Seongsan may have been changed, reflecting the presence of some S-type material in the melt.

Calculating fluid-rock isotopic exchange pathways

The change in $\delta^{18}O$ and δD values of water by isotopic exchange with country rock depends on: the initial isotopic composition of the fluid and rock; the ratio of exchangeable oxygen (or hydrogen) atoms in the fluid to those in the rock; temperature, which determines the equilibrium isotopic fractionation factor between the fluid and rock; and the degree of isotopic equilibration (Ohmoto & Rye, 1974). When the fluid and the rock become isotopically equilibrated at a given temperature, the final isotopic composition of the water can be expressed as follows:

$$\delta f_w = (\delta i_r - \Delta_{r\text{-}w} + (w/r)\,(\delta i_w)) / (1 + (w/r)) \quad (24)$$

where: f_w is the final water isotopic value
i_w is the initial water isotopic value
i_r is the initial rock value
$\Delta_{r\text{-}w}$ is the fractionation factor between rock and water, and
w/r is the water to rock molar ratio

Equation (24) from Ohmoto & Rye (1974).

Equation (24) can be simplified for calculations by converting from a water to rock molar ratio to a water to rock weight ratio. Hypothetical fresh dacite/granodiorite contains an average of 50wt% oxygen and about 0.112wt% hydrogen. Therefore, assuming 1wt% water content, the ratio of wt% oxygen in water (88.8%) to that in the rock (50%) equals 1.78; the ratio of wt% hydrogen in water (11.2%) to that in the rock (0.112%) equals 100. By using these molar coefficients and using a water to rock weight ratio (R), equation (24) simplifies for oxygen and hydrogen as:

$$\delta^{18}Of_w = (\delta^{18}Oi_r - \Delta_{r\text{-}w} + (1.78R)\,(\delta^{18}Oi_w)) / (1 + (1.78R)) \quad (25)$$

and

$$\delta Df_w = (\delta Di_r - \Delta_{r\text{-}w} + (100R)\,(\delta Di_w)) / (1 + (100R)) \quad (26)$$

where: R is the water to rock weight ratio

See also: Taylor (1977), Field & Fifarek (1985) and Criss & Taylor (1986) for similar calculations.

Using paleo-meteoric water (δD = -110‰, $\delta^{18}O$ = -15‰) and paleo-magmatic water at isotopic equilibrium with hypothetical fresh dacite/granodiorite (δD = -65‰, $\delta^{18}O$ = +8‰) and mineral-water fractionation equation (11) for oxygen (K-feldspar-water) and mineral-water fractionation equation (20) for hydrogen (muscovite-water), isotopic exchange pathways can be calculated over a range of fluid to rock weight ratios and temperatures using equations (25) and (26) (Table 5-5; Fig. 5-12). K-feldspar and muscovite fractionation equations were chosen as they would represent the dominant oxygen and hydrogen bearing minerals. The K-feldspar-water fractionation equation (11) also approximates to the anorthite-water fractionation equation of O'Neil & Taylor (1967).

		R = 0.001		R = 0.01		R = 0.1		R = 1		R = 10	
	T (ºC)	$\delta^{18}O$	δD	$\delta^{18}O$	δD	$\delta^{18}O$	δD	$\delta^{18}O$	δD	$\delta^{18}O$	δD
paleo-meteoric water	150	-4.86	26	-5.02	-35	-6.38	-96	-11.35	-109	-14.46	-110
	200	-1.61	3	-1.82	-48	-3.62	-99	-10.18	-109	-14.29	-110
	250	0.75	-13	0.50	-57	-1.61	-100	-9.32	-109	-14.16	-110
	300	2.52	-25	2.24	-63	-0.10	-102	-8.69	-109	-14.07	-110
	400	4.95	-42	4.64	-73	1.97	-103	-7.81	-109	-13.94	-110
paleo-magmatic water	200	-1.57	7	-1.42	-25	-0.14	-58	4.55	-64	7.49	-65
	250	0.79	-9	0.90	-34	1.87	-59	5.40	-64	7.62	-65
	300	2.56	-21	2.65	-41	3.37	-61	6.04	-65	7.71	-65
	400	4.99	-38	5.04	-50	5.44	-62	6.92	-65	7.84	-65

Table 5-5 Calculated $\delta^{18}O$ and δD values for a paleo-meteoric and paleo-magmatic fluid in isotopic equilibrium with a hypothetical fresh dacite (1wt% H_2O) over a range of fluid to rock weight ratios and temperatures. See main text for further detail.

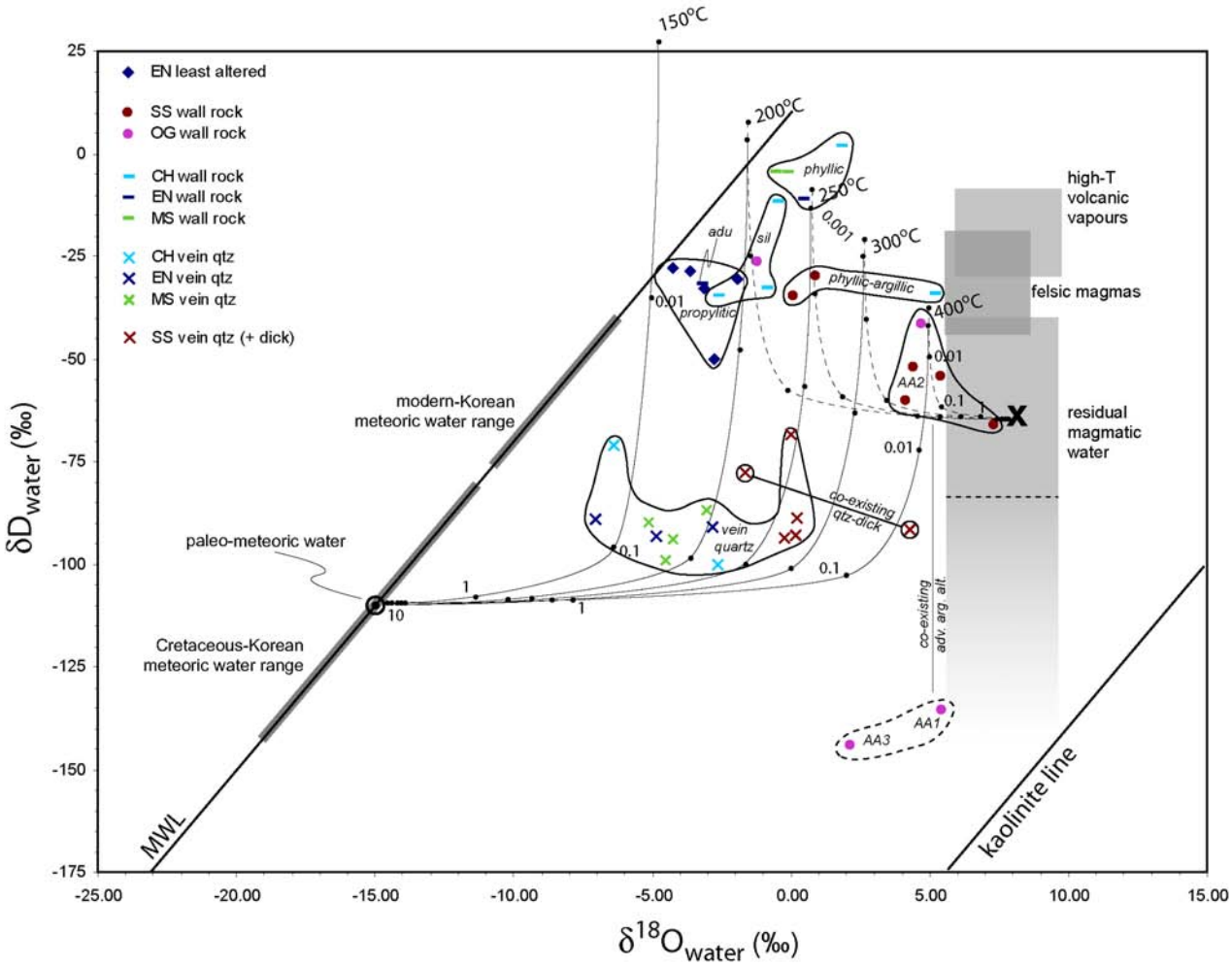

Fig. 5-12 $\delta^{18}O_{water}$ and δD_{water} plot as shown in Figure 5-11 (see Figure 5-11 for description) with calculated exchange pathways based on paleo-meteoric water (solid thin curves) and paleo-magmatic water (dashed thin curves) at equilibrium with hypothetical fresh dacite/granodiorite with 1wt% water content over a range of fluid to rock weight ratios (R = 10 to 0.001) and temperatures (150 to 400ºC). See main text for discussion and interpretation.

5.4.4.3 Interpretation of fluid-rock isotopic exchange at various temperatures and fluid to rock ratios

The isotopic character of calculated formation water for various alteration types and vein quartz from the Seongsan district shows several distinct clusters of $\delta^{18}O$ and δD isotopic compositions (Table 5-4; Fig. 5-11).

Hypothetical fresh dacite/granodiorite underwent district-wide propylitic alteration. Only limited samples within the district have preserved propylitic alteration without overprinting advanced argillic or phyllic alteration. Based on the isotopic exchange pathways within Figure 5-12, fluids at equilibrium with propylitic alteration (Eunsan least altered samples – blue diamonds, Fig. 5-12) could be either a cooling magmatic-derived fluid at 0.01 fluid to rock ratio, or a meteoric fluid at 0.01 fluid to rock ratio.

Following propylitic alteration, the district underwent advanced argillic alteration in localised zones at Seongsan, Ogmaesan and Chunsan (Table 3-3). Based on the isotopic exchange pathways (Fig. 5-12), fluids at equilibrium with advanced argillic alteration (Seongsan and Ogmaesan samples – maroon and pink dots, Fig. 5-12) could be either a cooling magmatic-derived fluid at 0.01 fluid to rock ratio, or a meteoric fluid at 0.001 fluid to rock ratio. The coarseness of the alunite implies advanced argillic alteration was a relatively high temperature hypogene process, rather than a lower temperature supergene process (Chapter 3, Section 3.2). The broader field of advanced argillic alteration is bounded by the isotopic exchange curves of magmatic water with dacite and relatively high fluid to rock ratios (Fig. 5-12). The intensity of the advanced argillic and associated silicic alteration and the loss of primary texture imply a relatively high fluid to rock ratio. Therefore, the relatively high δD values of advanced argillic alteration and textural evidence for higher fluid to rock ratios are more consistent with equilibrium at higher fluid to rock ratios with a magmatic-related fluid origin. If a meteoric-related fluid were responsible for such intense advanced argillic alteration, then the samples would be expected to plot at high fluid to rock ratios along the isotopic exchange curve for meteoric water and dacite (Fig. 5-12). Furthermore, samples of siliceous altered rock from Ogmaesan and Chunsan (represented by the 'sil' field in Fig. 5-12) have a distinctly different range of isotopic compositions compared to low-sulfidation vein quartz samples. The quartz sampled in Ogmaesan and Chunsan is paragenetically related to siliceous alteration developed during advanced argillic alteration, whereas the vein quartz samples are related to later phyllic-adularia alteration (see below). Ogmaesan and Chunsan siliceous altered rocks are inferred to have formed from magmatic-derived fluids as it is paragenetically synchronous with development of significant acid-sulfate alteration that has been shown to be magmatic-related. Two samples from Ogmaesan show depleted δD isotopic compositions (ca. -140 to -150‰) and

are inferred to have formed during degassing (see previous discussion on isotopic composition of exsolved fluids pg. 5-25).

After advanced argillic and associated siliceous alteration, isolated areas of the district underwent phyllic-adularia-siliceous alteration (Table 3-3). This alteration includes core zones of siliceous alteration grading outwards through adularia alteration and phyllic alteration to relic propylitic assemblages on the margins of the low-sulfidation systems (see Section 3.4.1). Siliceous altered zones during this paragenetic stage are represented by vein quartz samples from Eunsan, Moisan, Chunsan and Seongsan (vein quartz samples – cyan, blue and green cross; Fig. 5-12). Based on the isotopic exchange pathways within Figure 5-12, fluids at equilibrium with these vein quartz samples appear to have had a meteoric origin at ca. 0.1 fluid to rock ratio. The $\delta^{18}O$ shift between Eunsan, Moisan and Chunsan vein quartz (ca. -7 to -3‰) and Seongsan vein quartz (0 to 1‰) could possibly reflect vein development at Seongsan occurring at greater depths (ca. 290m) than that at Eunsan, Moisan and Chunsan (ca. 0 to 200m), rather than a temperature difference. These vein systems have formed at very high fluid to rock ratios, thereby minimising any isotopic exchange with wall rocks or pre-existing alteration. The isotopic composition of these vein quartz samples are dominated by meteoric-derived fluids.

Paragenetically distinct siliceous altered rocks at Ogmaesan and Chunsan and vein quartz associated with phyllic-adularia alteration (see: Table 3-3) have distinctly different isotopic compositions.

Based on the isotopic exchange pathways in Figure 5-12, fluids at equilibrium with phyllic alteration (Eunsan, Moisan and Chunsan rock samples – cyan, blue and green dash; Fig. 5-12) could be either a cooling magmatic-derived fluid at 0.1 to 0.01 fluid to rock ratio, or meteoric fluid at 0.01 to 0.001 fluid to rock ratio. Primary textures are preserved in phyllic altered rocks implying a low fluid to rock ratio during alteration. The phyllic altered samples represent earlier propylitic and/or advanced argillic altered rocks that have probably interacted with the same meteoric-derived fluids as that responsible for the low-sulfidation quartz-adularia veins.

However, the possibility of a component of magmatic-derived fluid during phyllic alteration cannot be entirely discounted. Magmatic-derived fluids are known to form phyllic alteration in the porphyry environment (Harris & Golding, 2002; Heinrich et al., 2004). Magmatic-derived fluids produced the advanced argillic alteration whereas quartz veins associated with phyllic-adularia-siliceous alteration were derived from meteoric fluids. The switch from advanced argillic to phyllic-adularia-siliceous alteration occurred within a ca. 2Ma period (Chapter 4). At

the onset of phyllic alteration, the broader rock mass may still have been infiltrated by residual magmatic-derived fluids. Phyllic alteration could have initially developed from fluids with a component of magmatic-derived fluids. However it is clear that meteoric-derived fluids produced the core phyllic-adularia-siliceous altered zones and associated veins.

The field in Figure 5-12 labelled 'phyllic-argillic' corresponds to samples from Seongsan and Chunsan that show earlier advanced argillic alteration partly overprinted by phyllic alteration (Table 3-3). These samples show a distinct isotopic compositional range between phyllic and advanced argillic samples. This is interpreted as comprising dominantly magmatic-derived values from the advanced argillic alteration of high fluid to rock ratio compared to the lower fluid to rock ratio of phyllic alteration.

5.5 SULFUR ISOTOPE CONSTRAINTS ON FLUID ORIGINS AND CHARACTERISTICS

Sulfur isotope studies have been undertaken to better understand the origin and history of the hydrothermal evolution of the prospects within the Seongsan district. Additionally, some mineral pairs have been sampled which are used to attempt temperature estimates.

5.5.1 Previous sulfur isotopic work in the Seongsan district

Koh & Chang (1997) undertook sulfur isotope work on the Seongsan clay-sulfate deposits and noted a marked difference in the isotopic composition of pyrite and alunite. They interpreted this to indicate that the acid sulfate alteration was of a primary hypogene origin.

5.5.2 Sulfur isotope methods

Samples were selected to represent sulfur species across the district and to complement the oxygen and hydrogen isotope samples. Pyrite and alunite were chosen as these were the main sulfur species present. Samples are grouped into two main categories, either 'high-sulfidation' or 'low-sulfidation', with a description of material type given in Table 5-6 (pg 5-43). Samples were off-cuts from diamond drill core and surface rock samples from Ogmaesan. Pyrite samples were gently crushed under a hydraulic press and then hand sorted under a binocular microscope. Alunite samples were scraped from pure alunite vein material with the purity being confirmed by thin section petrography, XRD and electron microprobe analysis.

K. Harris of the Central Science Laboratory (CSL), University of Tasmania, conducted all final sample preparation and sulfur isotope analysis, and has provided details of final sample preparation and analytical methodology used.

Sulfur isotope analysis for sulfides

Sulfide mineral separates (up to 25mg) were ground with 150mg of Cu_2O, cuprous oxide in an agate mortar and then placed in a pre-ignited mullite ceramic boat. The Cu_2O serves as the oxidant for the subsequent ignition of the sulfide sample at 950ºC in vacuo (Robinson & Kusakabe, 1975). The use of excess Cu_2O in this method ensures the low pO_2 favourable for SO_2 production with negligible SO_3 being produced. Contaminant gases are removed as follows: H_2O is frozen out at the freezing point of acetone (-95ºC), and CO_2 is then removed from the condensed SO_2 at the freezing point of n-pentane (-131ºC).

All sulfur isotope data are reported in δ notation in per mil units, (‰), where:

$$\delta^{34}S = (R_{sample}/R_{standard} - 1) \times 1000 \quad (27)$$

where: R is the isotopic $^{34}S/^{32}S$ ratio.

The standard is the Canyon Diablo Troilite (CDT). Isotopic analysis of the extracted SO_2 is performed with a VG SIRA Series 2 triple-collector mass spectrometer, using reference gas SO_2 calibrated against NBS 123 Sphalerite (+17.1 per mil versus CDT), IAEA-S-1 (-0.30 per mil versus CDT), Broken Hill Galena (+3.0 per mil versus CDT) and Rosebery Galena (+12.4 per mil versus CDT) as working standards to establish a calibration curve. All isotopic data are reported in per mil relative to CDT, with analytical uncertainties better than ± 0.3 per mil CDT for homogeneous mineral separates.

Sulfur isotope analysis for sulfates

The analysis of alunite for $\delta^{34}S$ with respect to CDT requires reaction of the sulfate (15-20mg) with a mixture of excess silica (600mg) and cuprous oxide (200mg) in vacuo at 1120ºC to produce SO_3, which is then passed over pure Cu turnings at 600ºC to reduce the SO_3 to SO_2. Following removal of any H_2O and CO_2 contaminants is by the same technique described for sulfide analysis, the SO_2 is collected at liquid nitrogen temperature (-196ºC), then admitted to the sample gas inlet of a VG SIRA Series 2 mass spectrometer for mass 66/64 ratio measurement against the working reference gas. The SO_2 yields from the barium sulfate standard, NBS 127 ($\delta^{34}S$ with respect to CDT = +20.3 per mil) and the laboratory working standards (Madame Howard Mine barite, $\delta^{34}S$ with respect to CDT = +31.2 per mil, and TASUL $BaSO_4$, $\delta^{34}S$ = +20.9 per mil) are used to establish a calibration curve. The typical error for this type of determination is ±0.2 per mil (1 standard deviation).

Temperature estimates from mineral pairs using sulfur isotope geothermometry

The temperature dependence of the fractionation factor of 32S and 34S between co-precipitated sulfide and sulfate minerals can be used as a geothermometer. This is done by solving simultaneous fractionation factor equations for sulfide-sulfate mineral pairs. However, to use this method, several assumptions must hold true. The mineral pairs must have been co-deposited in equilibrium with each other, forming at the same temperature from the same fluid, and they must have retained their original isotopic composition with minimal later re-equilibration or alteration (Campbell & Larson, 1998).

Co-existing pyrite and alunite from quartz-alunite-pyrite alteration at Seongsan and Ogmaesan have been sampled and used for sulfur isotope geothermometry. Ohmoto & Lasaga (1982) determined rates of chemical reactions between aqueous sulfides and sulfates. Since these are essentially identical to sulfur isotopic exchange rates between sulfides and sulfates, they were able to formulate an equation to describe the temperature dependence of the isotopic fractionation factor between sulfates and sulfides:

$$1000\ ln\ \alpha_{\text{sulfate-sulfide}} = 6.463 \times (10^6 / T^2) + 0.56 \quad (28)$$

where: T is temperature in Kelvin (= ºC + 273.15)

Equation (28) from Ohmoto & Lasaga (1982), as used by Rye (2005).

which approximates as (see equation (12)):

$$\delta^{34}S_{\text{sulfate}} - \delta^{34}S_{\text{sulfide}} = 6.463 \times (10^6 / T^2) + 0.56 \quad (29)$$

where the following relationship is true (Campbell & Larson, 1998):

$$\delta^{34}S_{\text{sulfate}} - \delta^{34}S_{\text{sulfide}} = \Delta^{34}S_{\text{sulfate-sulfide}} \quad (30)$$

hence:

$$\Delta^{34}S_{\text{sulfate-sulfide}} = 6.463 \times (10^6 / T^2) + 0.56 \quad (31)$$

therefore, solving for T:

$$T = \sqrt{\ [\ (6.463 \times 10^6) / (\Delta^{34}S_{\text{sulfate-sulfide}} - 0.56)\ ]} \quad (32)$$

where: T is temperature in Kelvin (= ºC + 273.15)

5.5.3 Sulfur isotope results

A histogram showing all $\delta^{34}S$ isotope data is shown in Figure 5-13, with a scatter plot of $\delta^{34}S$ of all data shown in Figure 5-14. Sulfide-sulfate $\delta^{34}S$ isotope data are shown in a $\delta^{34}S_{\text{sulfate}}$-$\delta^{34}S_{\text{sulfide}}$ plot (Fig. 5-15). Results have been summarised within Table 5-6.

	sample	mineral paragenesis	sample description	sulfate ^{34}S (‰)	sulfide ^{34}S (‰)
High-sulfidation:	SS002 148m	AA3 (late AA2?)	vein pyrite		-8.41
	SS001 169m	AA3 (late AA2?)	vein pyrite		-1.31
	SS001 71m a	AA3	vein alunite	7.00	
	SS001 71m b	AA3	vein alunite	7.33	
	OG 16	AA3 (late AA2?)	vein pyrite		0.11
	OG 36.1	AA3 (late AA2?)	vein pyrite		-2.78
	OG 54.1	AA3	alunite	4.95	
	OG 59.1	AA3	alunite	5.08	
	CH006 180.5m	AA3 (late AA2?)	alteration pyrite		12.29
Low-sulfidation:	CH003 115m	adu-sil	vein pyrite		3.87
	CH003 147m	adu-sil	vein pyrite		1.78
	EN006 81m	adu-sil	vein pyrite		5.50
	EN010 171m	adu-sil	vein pyrite		1.92
	MS007 76m	adu-sil	vein pyrite		-1.67
	MS001 109m	adu-sil	vein pyrite		-0.85

Table 5-6 $\delta^{34}S$ isotope data for pyrite and alunite mineral separates from the Seongsan district.

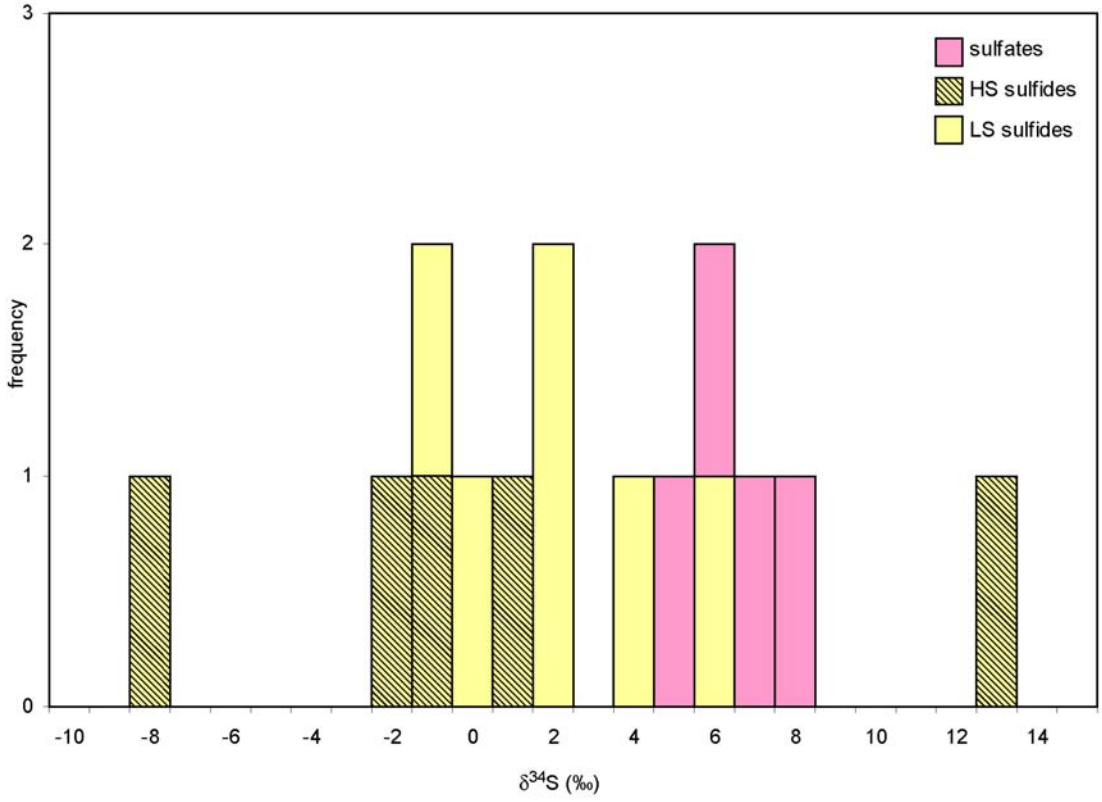

Fig. 5-13 A histogram showing the distribution of $\delta^{34}S$ isotopic compositions for sulfate (alunite) and sulfide (pyrite) minerals analysed from the Seongsan district. Alunites tend to have heavier isotopic compositions while associated pyrites in the high-sulfidation systems have particularly light isotopic compositions. Pyrites from the low-sulfidation systems tend to have an intermediate isotopic composition.

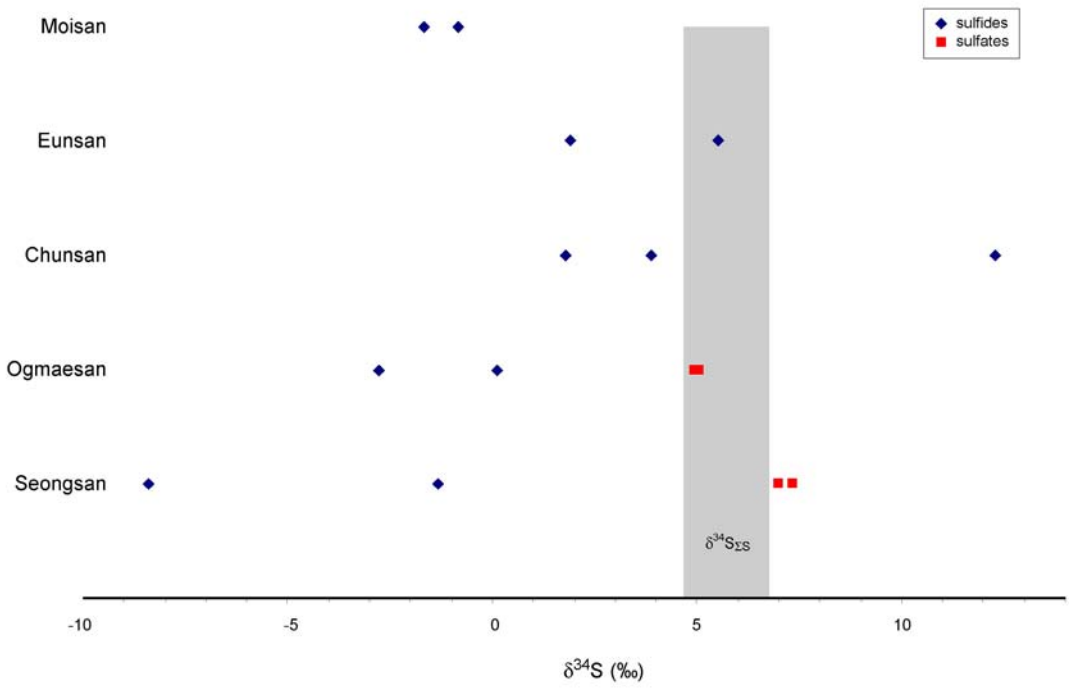

Fig. 5-14 Summary of $\delta^{34}S$ isotopic compositions for alunite and pyrite from the Seongsan district. The grey shaded area represents the range for calculated $\delta^{34}S_{\Sigma S}$ as determined from Figure 5-15. This figure highlights the disproportionate relationship between sulfur isotopic compositions in co-existing alunite and pyrite in the Seongsan and Ogmaesan systems.

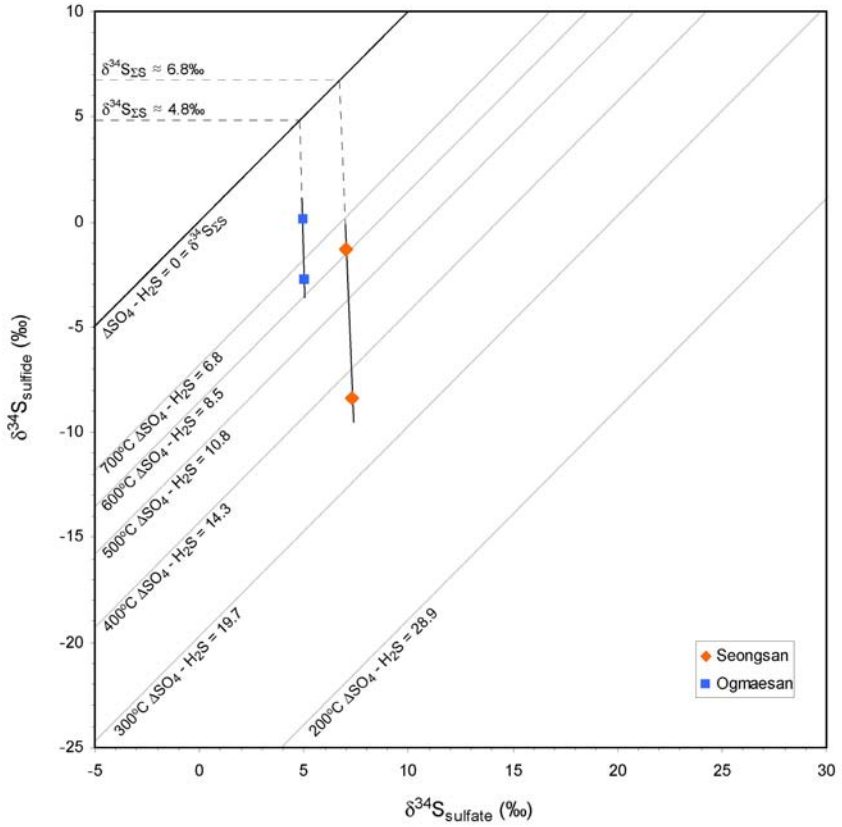

Fig. 5-15 $\delta^{34}S_{sulfate}$ - $\delta^{34}S_{sulfide}$ plot of alunite and pyrite mineral separates from Seongsan and Ogmaesan. Despite extensive examination, no directly co-existing sulfate-sulfide mineral pairs were identified. However, these alunite and pyrite samples formed during the same paragenetic stage and hence would probably have formed from the same fluid of fixed $\delta^{34}S_{\Sigma S}$. As no sulfate minerals were identified within the low-sulfidation prospects only data from Seongsan and Ogmaesan can be plotted on this figure. This figure highlights that the sulfate and sulfide minerals at Seongsan and Ogmaesan formed under strongly oxidised, SO_4-dominant conditions. See main text for further description and interpretation of this figure.

Temperature estimates from alunite-pyrite pairs using sulfur isotope geothermometry were calculated using equation (32). Alunite-pyrite pairs from Ogmaesan gave temperatures in the range 955.69ºC to 667.78ºC whereas those from Seongsan gave temperatures in the range 640.00ºC to 379.35ºC. These results are unrealistically high for both the Seongsan and Ogmaesan systems when compared with temperatures determined from phase relationships previously (Section 5.3). This shows that one or more of the assumptions required for this calculation are invalid. Ohmoto & Lasaga (1982) demonstrated that aqueous sulfate and sulfide components are not likely to be in equilibrium below 300ºC, commonly resulting in unrealistically high calculated temperatures.

5.5.4 Interpretation of sulfur isotope data

Marked fractionation of sulfur isotopes between sulfide and sulfate minerals is a characteristic of magmatic hydrothermal acid sulfate systems (Rye et al., 1992). Figures 5-13 and 5-14 show that alunite and pyrite from the Seongsan and Ogmaesan systems have distinctly different sulfur isotopic compositions. Pyrite and alunite sulfur isotopic compositions from Seongsan and Ogmaesan are consistent with their being derived from the disproportionation of SO_2 to H_2SO_4 and H_2S during condensation of a magmatic vapour plume (Ohmoto & Rye, 1979; Rye et al., 1992; Ohmoto & Goldhaber, 1997; Rye, 2005) from an original source sulfur isotopic composition ($\delta^{34}S_{\Sigma S}$) between the extremes represented by the alunite and pyrite values (Table 5-6; Figs. 5-13 to 5-14).

$\delta^{34}S$ values for vein pyrite from Eunsan, Chunsan and Moisan in the range -1.67 to 5.50‰ $\delta^{34}S$ (Figs. 5-13 & 5-14) are comparable with values in sulfides derived from magmatic fluids (ca. 0 to +5‰; Ohmoto & Goldhaber, 1997). The situation of magmatic sulfur isotopic values for sulfides and meteoric oxygen and hydrogen isotopic values for the fluids at equilibrium with vein formation is not unexpected and is explored in Section 5.7. Furthermore, the relatively small range of sulfur isotopic values for pyrite from Eunsan, Moisan and Chunsan suggests that H_2S was the dominant sulfur species in the fluids that formed these systems (Rye, 2005). Vein pyrite from Eunsan and Chunsan show a similar range for $\delta^{34}S$ between 1.78 and 5.50‰. However, vein pyrite from Moisan has a lighter $\delta^{34}S$ isotopic composition, similar to the $\delta^{34}S$ isotopic composition of pyrite from Seongsan and Ogmaesan. This implies that Moisan pyrites formed from a fluid that had undergone marked isotopic disproportionation with respect to sulfur before infiltrating the Moisan Fault Zone, whereas pyrite from Eunsan and Chunsan formed from fluids in which sulfur has not undergone as marked disproportionation.

One pyrite sample for Chunsan has 12.29‰ $\delta^{34}S$. This value is interpreted to represent isotopic exchange with oceanic sulfate which would have undergone inorganic reduction of sulfate to

sulfide. This process is cited for a number of deposits as a mechanism to explain high $\delta^{34}S$ values of sulfides (Ohmoto & Goldhaber, 1997). A sub-aqueous setting is implied from sedimentary structures for many rocks in the Seongsan district, so this is a geologically valid process, particularly for this sample which shows water-re-working of tuffaceous material and contains numerous carbonaceous flecks. This value is not characteristic of a magmatic sulfur signature (ca. 0 to 5‰) and if this sample were formed by isotopic exchange with sedimentary sulfur, a value in the order of -25‰ would be expected (Ohmoto & Goldhaber, 1997).

The use of $\delta^{34}S_{sulfate}$ - $\delta^{34}S_{sulfide}$ plots, like that in Figure 5-15, to interpret sulfate-sulfide sulfur isotopic exchange is a recent development (Fifarek & Rye, 2005). Modelling indicates that on a $\delta^{34}S_{sulfate}$ - $\delta^{34}S_{sulfide}$ plot, a straight line of negative slope represents a covariation in $\delta^{34}S_{SO4}$ and $\delta^{34}S_{H2S}$ values generated through SO_4^{2-} - H_2S isotopic exchange over a range of temperatures provided that the following assumptions remain true: the SO_4/H_2S ratio remained constant; the $\delta^{34}S_{\Sigma S}$ value remained constant; and isotopic equilibrium in a two-phase closed system was attained or closely approached. The absolute value of the slope of the straight line is equivalent to R, the SO_4/H_2S molar ratio. Isotherms plot as straight lines of +1 slope and can be easily calculated based on fractionation factors (see equation (31)). A theoretical upper temperature limit is reached where $\Delta_{sulfate\text{-}sulfide} = 0$. This isotherm represents $\delta^{34}S_{\Sigma S}$.

Therefore by plotting sulfide-sulfate mineral pair data on a $\delta^{34}S_{sulfate}$ - $\delta^{34}S_{sulfide}$ plot, the linear trendlines through the data can show whether a system was SO_4-dominant ($R = \infty$; subvertical trend), H_2S-dominant ($R = 0$; horizontal trend) or mixed ($R = 1$; perpendicular to isotherms), with the slope of the line giving an absolute SO_4/H_2S ratio. These trendlines, when projected back to the $\Delta_{sulfate\text{-}sulfide} = 0 = \delta^{34}S_{\Sigma S}$ line and projected back to an axis, estimate the $\delta^{34}S_{\Sigma S}$. Additionally, calculated temperature ranges or unique values can be graphically estimated based on the location of data in relation to isotherms.

Figure 5-15 shows that alunite and pyrite in Seongsan and Ogmaesan formed from a SO_4-dominant hydrothermal fluid. The slope of the trendline through $\delta^{34}S_{sulfate}$ - $\delta^{34}S_{sulfide}$ data = -22 in both systems. Projections of these trendlines back up to the line where $\Delta_{sulfate\text{-}sulfide} = 0$ gives an estimate of $\delta^{34}S_{\Sigma S}$, where values of 6.8‰ for Seongsan and 4.8‰ for Ogmaesan are obtained. As no sulfates were found within Eunsan, Moisan or Chunsan, plotting of data on a $\delta^{34}S_{sulfate}$ - $\delta^{34}S_{sulfide}$ plot to determine the exact ratio of SO_4/H_2S is not possible for these three systems. However, the narrow range for $\delta^{34}S$ indicates H_2S-dominant conditions in these three systems during pyrite deposition (see previous). This is in marked contrast to the SO_4-dominant conditions at Seongsan and Ogmaesan, and this implies two fundamentally different fluids were

responsible for high- and low-sulfidation hydrothermal activity in the Seongsan district, consistent with oxygen and hydrogen isotope data.

Although the temperatures for Seongsan and Ogmaesan (both calculated and graphically determined) are unrealistic and hence show that the sulfate-sulfide minerals formed out of isotopic equilibrium, the data trends from Figure 5-15 are still quite useful (Fifarek & Rye, 2005; Rye, 2005). One key point is that the Seongsan and Ogmaesan systems formed from hydrothermal fluids that were SO_4-dominant. However, high-sulfidation systems that are richly mineralised with respect to Au-Ag±Cu generally form from hydrothermal fluids that are H_2S-dominant or at least have a slope of between 0 and 1 indicating hydrothermal fluids are H_2S-dominant to equally SO_4/H_2S mixed. This will be explored in further detail later in the thesis (Chapter 6).

Figure 5-15 shows calculated $\delta^{34}S_{\Sigma S}$ values of 6.8‰ for Seongsan and 4.8‰ for Ogmaesan, which correlate well with calculated values for sulfur of 4.8‰ $\delta^{34}S$ for the Korean peninsula during the Cretaceous (Ishihara et al., 2000).

The combined sulfur, oxygen and hydrogen isotopic compositions and geological field relationships suggest that the advanced argillic alteration in the Seongsan district formed in a magmatic-steam environment (Rye et al., 1992). Documented occurrences of alunite forming in a magmatic-steam environment are rare, but include Marysvale in Utah (Cunningham et al., 1984) and Tambo in Chile (Deyell et al., 2005). Magmatic-steam processes remain poorly understood (Rye, 2005; Deyell et al., 2005).

5.6 TRACE METAL DATA: LOOKING FOR A GEOCHEMICAL SIGNATURE

Early work on the distribution of elements within the earths crust by Goldschmidt (1937, 1954) recognised that elements form general associations, based on similar geochemical affinity, rather than concentrations of a single element, as:

1. siderophile – shows an affinity for iron, concentrated in the earths core
2. chalcophile – shows an affinity for sulfur, concentrated in sulfides
3. lithophile – shows an affinity for silicates, concentrated in the earths crust
4. atmophile – as gases in the atmosphere, and
5. biophile – concentrated in living matter; essentially C, H, O, N, S, and P.

Element associations and indicators more specific than the associations from Goldschmidt's classification are known predominantly from empirical data on ore systems (Levinson, 1974, 1980; Eggo, 1997). For this study, selected chalcophile elements were compared to background values for similar rocks to highlight features of interest. These trace elements serve as indicators of the trace metal signature for each system and can give insights into fluid origins, sulfidation-states and hence fluid evolution. The trace metal signature also provides another way to compare and contrast the high- and low-sulfidation systems in the Seongsan district.

5.6.1 Methodology

Assay data from 1m sample intervals of diamond drill core and surface whole rock assay data were collected. Surface whole rock samples were used at Ogmaesan as diamond drill core was not available. Whole rock samples were selected and collected by the author. Surface samples from Ogmaesan were assayed for Au, Ag, Cu, Pb, Zn, As, Hg and Sb as these were the only elements available for analysis. Au was assayed by fire-assay on 30gm sample. Cu, Pb, Zn and Ag concentrations were measured by AAS following concentrated HCl acid digest and an $HCl/HNO_3/HClO_4$ leach in latter stages on 1gm samples. As and Sb were analysed by vapour generation and AAS from acid leach. Hg was analysed by flameless AAS.

Most diamond drill core samples were assayed for Au and Ag only (methodology as previous). If base-metal mineralisation was thought to be present, sample intervals were also assayed for Cu, Pb and Zn using the same methodology as previously described. If initial assays returned high-grade results, original sample pulp splits were re-assayed by ICPMS for either 5 or 39 additional elements.

For Seongsan, Eunsan, Moisan and Chunsan, a total of 11,318 Au-Ag-only assays of diamond drill core were conducted with an additional 2,142 assays for Au, Ag, Cu, Pb and Zn (Moisan only). For Ogmaesan, a total of 45 Au, Ag, Cu, Pb, Zn, As, Hg and Sb whole rock assays were conducted. For Seongsan, Eunsan, Moisan and Chunsan, only 20 39-element and 143 5-element (Seongsan only: Au, Ag, Cu, As, Sb) ICPMS assays were conducted at the discretion of Ivanhoe Mines Ltd.

From the available assay and ICPMS multi-element data, the following elements were selected for comparison: Au, Ag, Cu, Pb, Zn, As, Hg, Sb, Mo, Bi and Th. This element suite was chosen because it characterises precious (Au and Ag) and base metal (Cu, Pb and Zn) mineralisation. Empirical data (Levinson, 1974, 1980) shows that the remaining elements (As, Hg, Sb, Mo, Bi and Th) can characterise certain environments of formation. Mo, Bi and Th imply affinities with magmatic-porphyry settings and high-sulfidation systems; As, Hg and Sb suggest links to low-sulfidation systems generally dominated by meteoric fluids (Hedenquist et al., 2000; Sillitoe & Hedenquist, 2003; Table 1-2).

More specifically, Molybdenum (Mo) is chalcophile and associated with Cu, Au, Ag and Zn; a positive Mo anomaly is generally regarded as an indicator of porphyry/magmatic settings (Levinson, 1980). Bismuth (Bi) is chalcophile and associated with Mo, Sn, W, Cu, Pb, Au and Ag in metallic deposits (Levinson, 1980). A positive Bi anomaly can highlight an association to proximal reduced granitic intrusions (Thompson et al., 1999; Thompson & Newberry, 2000). Thorium (Th) is lithophile and associated with K and U. A positive Th anomaly may indicate a magmatic setting (Levinson, 1980). Arsenic (As) is chalcophile and associated with Au and Ag in vein settings, ore halos and numerous other elements in various sulfide ores (Levinson, 1980). Arsenic (As) is commonly used as an indicator for precious metal mineralisation (Eggo, 1997), but occurs in many different Au deposit forming environments. Mercury (Hg) is chalcophile and associated with Sb, As, Au and Ag in vein settings (Levinson, 1980). Antimony (Sb) is chalcophile and associated with As, Bi, Pb, Ag and Cu in a variety of precious metal vein settings and ore halos (Levinson, 1980).

5.6.2 Trace metal data: Seongsan and Ogmaesan compare and contrast

Seongsan is more richly mineralised with respect to Au-Ag than Ogmaesan, although absolute values at Seongsan are still low, generally <1ppm Au and <10ppm Ag. Assays show that there are variable Ag-rich, Au-Ag-rich and Au-rich zones, with Ag to Au ratios averaging 18:1 (Ag and Au correlation = 0.306; n=817; Fig. 5-16). The variable Au-Ag mineralisation could be explained by a shift in the redox state of the system affecting the stability of metal complexes, i.e. Cl^- complexes shifting to HS^- complexes (e.g. Lepanto; Hedenquist et al., 1998). Ag-rich

samples comprise argentite/acanthite Ag_2S. Au-rich samples comprise electrum as inclusions in pyrite, resulting in Ag-rich, and Au-rich zones with occasional co-existing Au-Ag rich zones. Additional sulfides identified at Seongsan include Fe-poor sphalerite and galena. Paragenetically, these samples represent sulfide±Au±Ag mineralisation associated with advanced argillic 2 alteration (Table 3-3).

Of the 817 drill core samples, only 1 interval (0.36m; Fig. 3-15) represents cross cutting low-sulfidation style vein development and only Au and Ag assay data is available (0.13ppm Au, 1.3ppm Ag).

Assays show that Ogmaesan is essentially barren with respect to Au and Ag (n=45; Fig. 5-16). Almost all Ag assays were below or at detection limits of 0.5ppm. No sulfides other than pyrite have been identified within the Ogmaesan system.

Both Seongsan and Ogmaesan show elevated levels of As and Sb, and both are depleted in Cu. The later reflects intense leaching during advanced argillic alteration and a lack of Cu-sulfides in advanced argillic veins.

Samples at Seongsan that are enriched with Hg correspond to a <5m wide zone of illite-altered phreatomagmatic breccia that cross cuts earlier advanced argillic altered rock. These samples comprise pyrite, Ag-sulfosalts (pyrargyrite/pearceite) and acanthite/argentite. They are located within the Sangbong Pit, ca. 2km northeast of the main Seongsan system and within 500m of the Chunsan system (1 to 4ppm Au; up to 300ppm Ag; Fig. 5-16; Appendix 5). This style of mineralisation is associated with adularia-phyllic mineralisation development at Chunsan, evident from the presence of illite alteration and associated low-sulfidation mineralisation within the phreatomagmatic breccia. Although similar alteration and mineralisation is found at Chunsan (and Eunsan), similar styles of mineralisation are not. The phreatomagmatic breccia does not characterise the advanced argillic alteration and associated mineralisation as seen elsewhere at Seongsan.

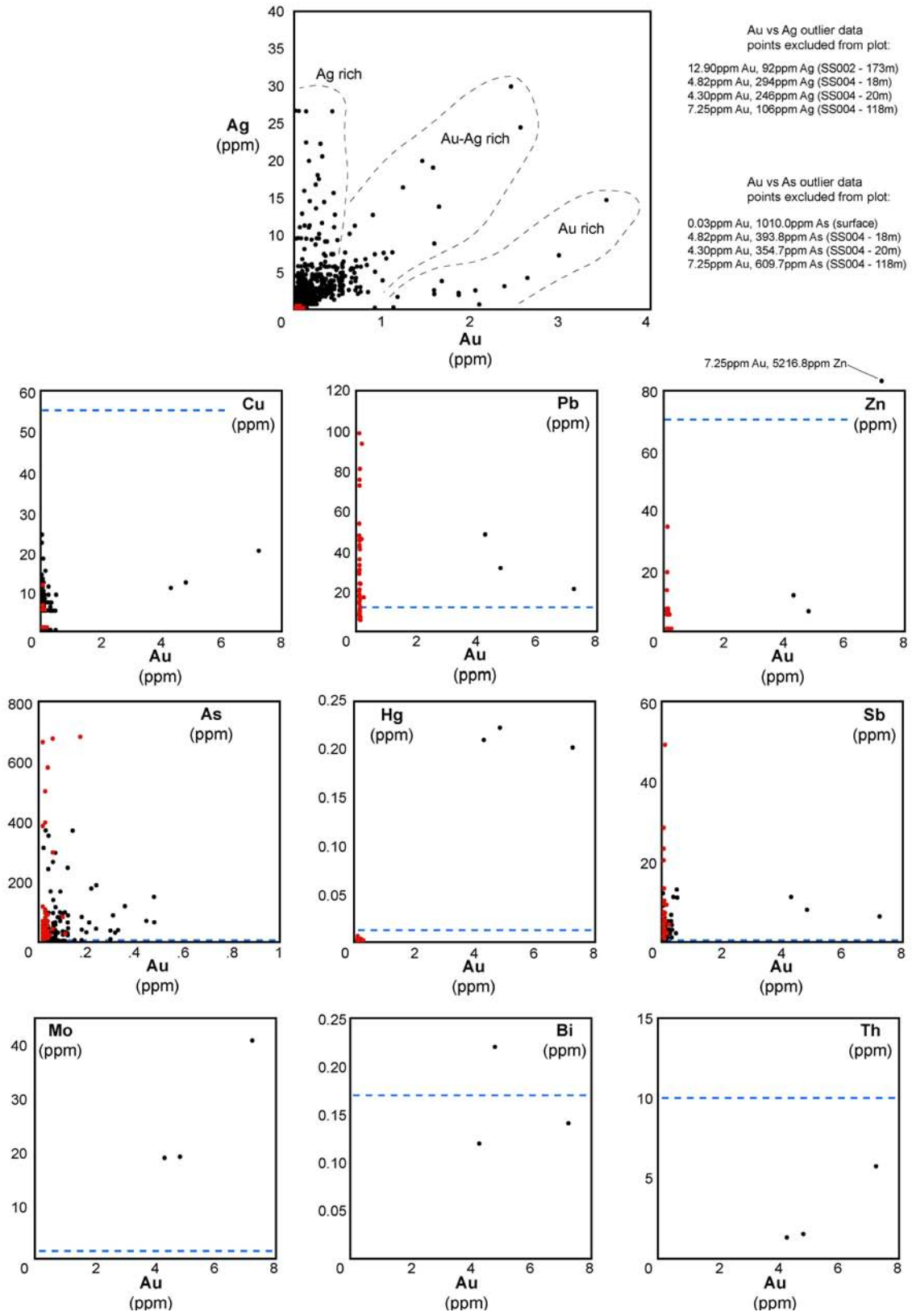

Fig. 5-16 Multi-element versus Au diagrams showing data from Seongsan (black dot) and Ogmaesan (red dot). See main text for discussion and interpretation of results. Dashed blue line represents average crustal abundances: 0.004ppm Au; 0.07ppm Ag; 55ppm Cu; 12.5ppm Pb; 70ppm Zn; 1.8ppm As; 0.08ppm Hg; 0.2ppm Sb; 1.5ppm Mo; 0.17ppm Bi; and 10ppm Th (Levinson, 1974).

5.6.3 Trace metal data: Eunsan, Moisan and Chunsan compare and contrast

A comparison of trace metal data shows distinct differences between the Eunsan, Moisan and Chunsan systems (Fig. 5-17). Moisan contains the highest levels of Au, Cu, Pb, Zn, As, Hg, Sb and Bi compared to Eunsan and Chunsan. Chunsan contains the highest levels of Mo and Th, while Eunsan contains the highest levels of Ag. Of the most significance are a positive Mo anomaly at Chunsan and a positive Bi anomaly at Moisan, which both suggest some affinity to magmatic activity.

Eunsan Ag and Au assays (n=6214; Fig. 5-17) can be divided into: 1. Ag-rich, Au-poor (Ag:Au ca. 100:1); 2. Au-Ag-rich (Ag:Au ca. 10:1); and 3. Au-rich, Ag-poor (Ag:Au ca. 1:1). Ag-rich, Au-poor zones generally occur above the base of oxidation (ca. minus 30mRL), and are inferred to be related to supergene processes (Section 3.4.2.2). Primary Au-Ag-rich zones comprise pyrite (FeS_2), Ag-sulfides (acanthite/argentite Ag_2S), Ag-sulfo-salts (prousite/pyrargyrite ($Ag_3[As,Sb]S_3$) and pearcite/polybasite ($(Ag,Cu)_{16}Sb_2S_{11}$)), native Ag and variably Au/Ag-rich electrum. Au-rich zones comprise fine Ag-poor electrum, typically directly associated with adularia. Eunsan shows no significant enrichment or depletion in base metals against background values (n=5; Fig. 5-17) implying that Fe-poor sphalerite ([Zn,Fe]S), galena (PbS), chalcopyrite ($CuFeS_2$) and tennantite/tetrahedrite ($Cu[As,Sb]_4S_{13}$) may have been derived from minor remobilisation of Cu, Pg and Zn locally. Eunsan is depleted in Th and Bi (n=5; Fig. 5-17), and enriched in Au, Ag, As, Hg, Sb and Mo (n=5; Fig. 5-17).

Moisan is rich in both Au and Ag but there is no clear correlation between these two elements. Au-rich mineralisation is present, but not as common as Ag-rich mineralisation (n=4432; Fig. 5-17). Surface samples have bonanza grades typically enriched in Ag and are inferred to be related to supergene processes. Primary Au-Ag-rich zones comprise pyrite (FeS_2), Au-Ag-rich tellurides (hessite Ag_2Te, empresite AgTe, krennerite $Au,AgTe_4$), native Te, Ag±Au substituted (for Cu) in the series goldfieldite ($Cu_3[Te,Sb]S_4$) to tennantite/tetrahedrite ($Cu[As,Sb]_4S_{13}$), Ag-sulfides (acanthite/argentite Ag_2S) and electrum. Moisan has significant base metal mineralisation containing up to ca. 1.8% Pb and Zn and ca. 0.3% Cu with Fe-poor sphalerite ([Zn,Fe]S) ± galena (PbS) ± chalcopyrite ($CuFeS_2$) ± the series goldfieldite ($Cu_3[Te,Sb]S_4$) ± tennantite/tetrahedrite ($Cu[As,Sb]_4S_{13}$) being the main base-metal bearing sulfides (Cu, Pb, Zn; n=2142; Fig. 5-17). Moisan shows elevated levels of all elements analysed except for Th which shows minor depletion (Au vs Cu, Pb & Zn n=2142; Au vs remaining n=5; Fig. 5-17). Of particular note are the three high Bi values, up to ca. 1200ppm.

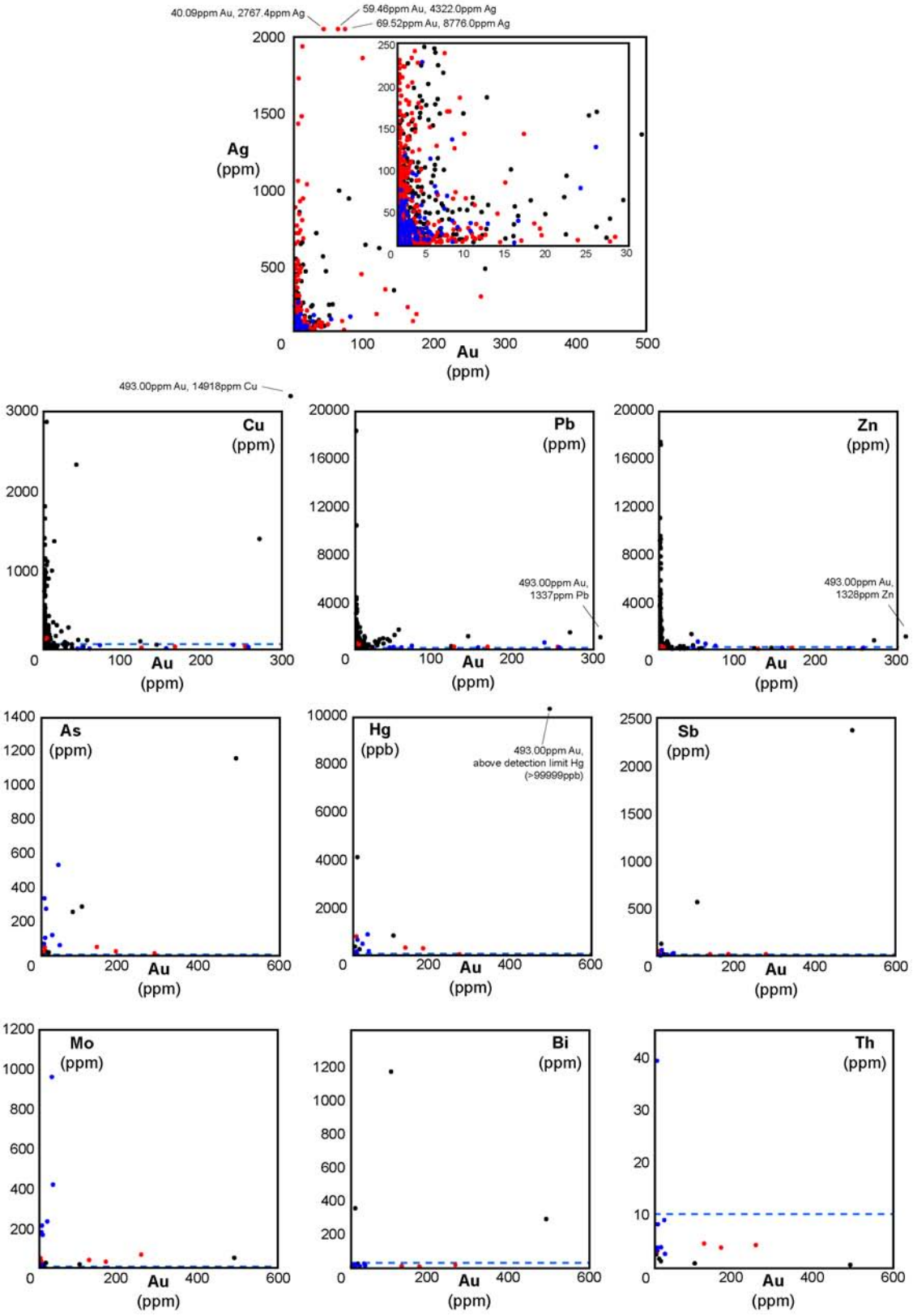

Fig. 5-17 Multi-element versus Au diagrams showing data from Moisan (black dot), Eunsan (red dot) and Chunsan (blue dot). See main text for discussion and interpretation of results. Dashed blue line represents average crustal abundances: 0.004ppm Au; 0.07ppm Ag; 55ppm Cu; 12.5ppm Pb; 70ppm Zn; 1.8ppm As; 0.08ppm Hg; 0.2ppm Sb; 1.5ppm Mo; 0.17ppm Bi; and 10ppm Th (Levinson, 1974).

Chunsan also hosts Ag-rich and Ag-Au mineralisation (n=1997; Fig. 5-17). Au-rich mineralisation is not as common as Ag-rich mineralisation. Primary Au-Ag rich zones comprise pyrite (FeS_2), electrum as inclusions in pyrite and tennantite/tetrahedrite ($Cu[As,Sb]_4S_{13}$) with Au±Ag substitution. Chunsan is depleted in Cu (n=5; Fig. 5-17). Pb and Zn show no significant enrichment or depletion (n=5; Fig. 5-17). Base metal mineralisation at Chunsan comprises rare chalcopyrite ($CuFeS_2$) and tennantite/tetrahedrite ($Cu[As,Sb]_4S_{13}$). Chunsan shows show no significant enrichment or depletion in Bi or Th (n=5; Fig. 5-17). Chunsan is enriched in Au, Ag, As, Hg, Sb, with significant enrichment of Mo (n=5; Fig. 5-17).

5.7 SUMMARY OF RESULTS FOR THIS CHAPTER

This Chapter documents the results of numerous geochemical analyses performed on paragenetically well-constrained samples in an attempt to characterise the epithermal systems of the district and gain an insight into their genesis and relationships with each other.

Fluid inclusions were examined in order to provide some constraints on the temperature, pressure and chemical composition of fluids that formed each system. Unfortunately, no suitable primary fluid inclusions were found. Secondary fluid inclusions from Eunsan and Chunsan comprise low salinity fluids (ca. <2 wt% NaCl equiv.). Secondary fluid inclusions from Moisan comprise CO_2-bearing medium salinity fluids (ca. 8 to 13 wt% NaCl equiv.).

Geochemical conditions of formation during alteration were then examined using phase relationships of alteration minerals and sulfide mineral assemblages. This showed that the advanced argillic altered Seongsan and Ogmaesan systems formed under oxidised, acidic, SO_4-dominant conditions, whereas the phyllic-adularia altered Eunsan, Moisan and Chunsan systems formed under reduced, near-neutral pH, H_2S-dominant conditions. Additionally, the sulfidation-state of ore forming fluids was examined. It was determined that the advanced argillic alteration at Seongsan and Ogmaesan formed under high-sulfidation conditions, with sub-economic Au-Ag bearing sulfides at Seongsan characterised by intermediate-sulfidation states. Sulfides associated with Au-Ag mineralisation within the phyllic-adularia altered systems at Eunsan, Moisan and Chunsan formed predominantly under intermediate- to low-sulfidation conditions.

Isotope analyses were undertaken to help elucidate further the origins of the hydrothermal fluids. Combined analyses of oxygen and hydrogen isotopes showed that there were essentially two isotopically distinct fluids, a magmatic-derived fluid that formed the advanced argillic systems, and a meteoric-derived fluid that formed the phyllic-adularia Au-Ag vein systems. Sulfur isotope data combined with the previous oxygen and hydrogen isotope data and geological field relationships imply a SO_4-dominant, magmatic-steam origin for the fluids that formed the advanced argillic alteration at Seongsan and Ogmaesan. The phyllic-argillic alteration and Au-Ag mineralisation at Eunsan, Moisan and Chunsan formed from fluids in which H_2S was the dominant sulfur species.

Oxygen and hydrogen isotope data from the low-sulfidation systems suggests formation by meteoric-derived fluids, whereas the sulfur isotope data suggests magmatic-derived sulfur. Two possible scenarios are provided to explain this. Pulses of magmatic-derived sulfur contributed to the vein sulfide material, but due to the dominant influx of meteoric-derived fluid compared

to the magmatic-derived sulfur, the overall oxygen and hydrogen isotopic value of the quartz material appears meteoric-derived. Alternatively, during the influx of meteoric-derived fluids, minimal sulfur species would have been present in that fluid except for those scavenged from the surrounding host rocks, which would have had a magmatic-derived sulfur isotopic value.

Chapter 6:
A comparison of the epithermal systems in the Seongsan district with epithermal systems elsewhere

6.1 INTRODUCTION

The primary objective of this project was to investigate the geological setting and the spatial and temporal links between the distinctly different epithermal systems in the Seongsan district of South Korea. Several subsidiary aims (1 to 5; pg 1-17) focussed the research, including documenting the local geology and structural setting of the epithermal systems, documenting the mineral assemblages and paragenesis of each epithermal system, dating the low-sulfidation systems of the district and documenting the fluid inclusion, oxygen, hydrogen and sulfur isotopic characteristics of each epithermal system.

Results of this work are presented in Chapters 2 to 5 and showed that in the Seongsan district, kaolinite, dickite and alunite-rich advanced argillic alteration resulted from an influx of magmatic-derived hydrothermal fluids along sinistral strike-slip wrench faults and hydrothermal breccias between 82.4 and 79.7Ma. Gold-silver bearing adularia-quartz-illite veining and alteration resulted from an influx of dominantly meteoric-derived fluid during a phase of normal dip-slip faulting that partially reactivated the earlier wrench fault network between 78.4 and 76.9Ma, at least 1.3Ma after advanced argillic alteration. Data from the Seongsan district therefore shows a coupled change in both structural setting and hydrothermal fluid characteristics between 79.7 and 78.4Ma, resulting in the development of two distinctly different groups of epithermal-style hydrothermal systems in the same general area.

To what extent the high- and low-sulfidation systems in the Seongsan district are related parts of a single event or two separate unrelated events has been debated since the latter were first recognised by Kirwin et al. (1999). Results outlined in Chapters 4 and 5 imply that they are unrelated events at least 1.3Ma apart. These results are discussed further below as part of a broader analysis of the relationships between high-, intermediate- and low-sulfidation hydrothermal systems. This topic addresses the first of three comparative aims of the thesis (aim 6; pg 1-17).

Mineralised high-sulfidation systems are commonly thought of as metal-bearing systems. However, in addition to metals, clay and sulfate are extracted in commercial quantities from some high-sulfidation systems like those in the Seongsan district. Individual high-sulfidation systems generally only contain clay-sulfate or metal-bearing ore suggesting the different commodities are mutually exclusive. Known high-sulfidation systems with metal or clay-sulfate resources are compared below to gain a clearer understanding of the features which control whether metal or clay resources develop in high-sulfidation systems. This topic addresses the second comparative aim of the thesis (aim 7; pg 1-17).

The understanding of ore controls in the Seongsan district developed here provides an opportunity to develop exploration targeting criteria for clay-sulfate and metal-bearing epithermal systems within adjacent parts of southwest Korea. Some general criteria, which may aid exploration for similar deposits in other terranes, are also highlighted below. This topic addresses the final comparative aim of the thesis (aim 8; pg 1-17).

6.2 RELATIONSHIPS BETWEEN HIGH-, INTERMEDIATE- AND LOW-SULFIDATION EPITHERMAL SYSTEMS

6.2.1 Definitions and setting the scene

Hedenquist et al. (2000) suggested the subdivision of low-sulfidation systems into intermediate-sulfidation and end-member low-sulfidation systems (see also Table 1-1 and Figs. 1-3 to 1-7). The key distinction between low-, intermediate and high-sulfidation systems as used by Hedenquist et al. (2000) is the sulfidation-state of ore-bearing sulfides. Principal field-oriented characteristics that can be used to distinguish these epithermal types have been listed previously in Table 1-2 (Chapter 1, pg 1-9). Key sulfide species that characterise high-sulfidation systems include enargite, luzonite and covellite. Intermediate-sulfidation systems are characterised by sphalerite, galena, tetrahedrite-tennantite and chalcopyrite. Low-sulfidation systems are characterised by minor to very minor arsenopyrite± pyrrhotite; minor sphalerite, galena and chalcopyrite. Some alteration assemblages and textures are also indicative of the type of system in which they developed.

The classification proposed by Hedenquist et al. (2000) also suggests that intermediate-sulfidation and end-member low-sulfidation deposits form in different tectonic and magmatic settings; based on their interpretation of the characteristics of epithermal deposits in the northern Great Basin, western United States (John, 1999; John et al., 1999).

Hedenquist et al. (2000) suggest that end-member low-sulfidation systems are characterised by near-neutral pH, low-salinity, gas-rich and reduced meteoric-dominated fluids that are equilibrated with the altered host rocks (e.g. Broadlands-Ohaaki, New Zealand). In contrast, high-sulfidation systems are characterised by acidic, saline, magmatic-dominated fluids that are far from being in equilibrium with host rocks (e.g. White Island, New Zealand). Intermediate-sulfidation systems are interpreted as being genetically related to high-sulfidation systems, having higher salinity fluids than low-sulfidation deposits, and fluids that are not fully equilibrated with the host rock, possibly suggesting a magmatic affinity.

John (2001) noted that the low-sulfidation deposits in the northern Great Basin separate into two groups that have spatial and temporal associations with different compositions and styles of magmatism, that formed in different tectonic settings and which have consistent mineralogical differences and different Au-Ag ratios. However, John (2001) also states that the sulfidation states of most of these deposits have not been rigorously evaluated and therefore the inferred genetic relationship of the two groups of epithermal systems forming under different sulfidation-states is untested. John (2001) also goes into detail for several deposits that show exceptions to the generalised grouping. Finally, John (2001) comments that if the classification of epithermal deposits proposed by Hedenquist et al. (2000) is to be widely adopted, detailed studies of other deposits in other regions that formed in various tectonic settings and associated with different types of magmatism should be conducted to see if there are consistent relationships between these features and sulfidation-state.

6.2.2 Relationships between different styles of epithermal systems in the Seongsan district

Alteration within Seongsan and Ogmaesan comprises core zones of siliceous and silicic (vuggy silica) altered rock surrounded by extensive haloes of kaolinite, dickite and alunite bearing advanced argillic alteration (Table 3-3) comparable to some acid-sulfate altered high-sulfidation epithermal systems (Hayba et al., 1985; Heald et al., 1987; Hedenquist et al., 2000). Sulfide and trace metal assemblages (Chapter 5) indicate that sub-economic Au-Ag mineralisation at Seongsan comprises sulfides with sulfidation states indicative of high- to intermediate-sulfidation conditions. No Au-Ag mineralisation was observed at Ogmaesan.

Alteration within Eunsan and Moisan comprises core zones of siliceous altered rock, with halos of adularia, phyllic and propylitic alteration (Table 3-3) comparable to adularia-sericite altered low-sulfidation epithermal systems (Hayba et al., 1985; Heald et al., 1987; Hedenquist et al., 2000). Sulfide and trace metal assemblages (Chapter 5) indicate that Au-Ag mineralisation at Eunsan and Moisan comprises sulfides with sulfidation states indicative of low- to intermediate-sulfidation-state conditions.

Alteration within Chunsan comprises an early stage of advanced argillic alteration in which core zones of siliceous and silicic (vuggy silica) altered rock are surrounded by haloes of kaolinite, dickite and minor alunite bearing advanced argillic alteration (Table 3-3) comparable to the Seongsan and Ogmaesan high-sulfidation systems. Overprinting this is a stage of alteration comparable to the Eunsan and Moisan low-sulfidation systems, in which core zones of siliceous altered rock are surrounded by halos of adularia, phyllic and propylitic alteration (Table 3-3). This overprinting low-sulfidation stage is also evident at Seongsan (Chapter 3, Section 3.4.2), although to a much lesser degree. Sulfide and trace metal assemblages (Chapter 5) indicate that

Au-Ag mineralisation at Chunsan associated with the adularia-sericite alteration comprises sulfides with sulfidation states indicative of low- to intermediate-sulfidation-state conditions.

Advanced argillic alteration at Seongsan is focussed by a network of sinistral strike-slip faults, implying that this phase of hydrothermal activity developed in a wrench-type tectonic setting. Quartz-adularia veins and associated alteration at Eunsan, Moisan and Chunsan developed during normal movement on faults, implying that this phase of hydrothermal activity developed in an extensional tectonic setting. Changes in the paragenetic character of the epithermal systems therefore also coincide with changes in the structural setting of the district.

Detailed examination of the geochemical and isotopic characteristics of the hydrothermal fluids responsible for the high- and low-sulfidation systems show marked differences between them. Magmatic-dominated, acid, oxidised, SO_4-dominant fluids formed the advanced argillic alteration and associated clay-sulfate mineralisation in the high-sulfidation systems. Meteoric-dominated, near-neutral pH, reduced, H_2S-dominant fluids formed the adularia-sericite alteration and associated Au-Ag mineralisation in the low-sulfidation systems.

Published age data for the clay-sulfate deposits of the district and new age data for the Au-Ag low-sulfidation systems (this study) show that these two distinct styles of hydrothermal activity occurred at least 1.3Ma apart, with the acid-sulfate high-sulfidation systems forming first. When the age data are integrated with the paragenetic, geochemical and structural data, they highlight a coupled change in the structural setting and hydrothermal fluid characteristics midway through the Late Cretaceous hydrothermal evolution of the Seongsan district.

Overall, the two styles of epithermal systems in the Seongsan district could be considered two distinct parts of a broader long-lived cycle of crustal convergence, subduction, volcanism and associated hydrothermal activity.

6.2.3 Comparison of the Seongsan and other districts that host high-, intermediate- and low-sulfidation epithermal systems

Comparison of the Seongsan district with other districts that host high-, intermediate- and low-sulfidation epithermal systems within the same general area may highlight similar relationships between these different types of epithermal systems across many districts. Alternatively, the relationships between different styles of epithermal systems may be different in each case.

Districts that contain high-, intermediate- and low-sulfidation systems within the same general area are not common, but include the Mankayan district in the Philippines (Hedenquist et al.,

1998; Claveria et al., 1999; Garcia Jr, 2004); the Comstock district in Nevada (Vikre et al., 1988; John, 2001; Hudson, 2003; Berger et al., 2003 and others); southern Kyushu in Japan (Hedenquist et al., 1994; Faure et al., 2002; Watanabe, 2004, 2005; Garwin et al., 2005); Mt Skukum in Canada (Love et al., 1998); and Masupa Ria in Indonesia (Thompson et al., 1994). The Comstock district appears to show many similarities to the Seongsan district and has been subject to a large number of detailed studies that have investigated the alteration, mineralisation and structural controls on the epithermal deposits. Detailed comparison with the Seongsan district is therefore possible.

6.2.3.1 Seongsan and Comstock

Previous workers in the Comstock district (Vikre et al., 1988; John, 2001; Hudson, 2003; Berger et al., 2003 and many others) have described early advanced argillic alteration that comprises quartz±alunite±pyrophyllite±diaspore±kaolinite/nacrite/dickite±pyrite zoned outwards from fractures that propagate away from co-genetic andesitic intrusions. Blanket-like cristobalite± kaolinite±alunite alteration is developed in the periphery of the district. Approximately 1 to 2Ma later, two related stages of low-sulfidation quartz veins, quartz-adularia stockworks and associated peripheral quartz±chlorite±illite±muscovite alteration formed in and around steep to moderately dipping faults. Early stage veins in this later low-sulfidation event only contain sub-ore-grade Au and Ag, but later low-sulfidation veins contain the main Au-Ag ore-bearing paragenetic phase in the Comstock district. This superimposition of low- on high-sulfidation systems mimics the relationship in the Seongsan district.

The structural setting during advanced argillic alteration in the Comstock district has not been reported. The tectonic setting during emplacement of the closely related host rocks was transpressional (John, 2001). However, the zonation of advanced argillic alteration around individual intrusives that form radial dyke sets and around faults that show minimal displacement suggests development under low differential stress. No known precious- or base-metal mineralisation is associated with advanced argillic alteration in the Comstock district although, high-sulfidation Au±Cu mineralised systems do occur in the broader surrounding area (e.g. Goldfield, Nevada). Low-sulfidation veins within the Comstock district formed in an extensional setting related to basin opening. Berger et al. (2003) propose that a transient period of transpressional stress deformed the early stage sub-ore-grade quartz-vein networks, which resulted in the formation of spatially restricted compartments of high vertical and low lateral permeability and hydraulic connectivity. Renewed extension during the later ore grade episode of low-sulfidation hydrothermal activity then focused fluid flow through these restricted zones of high permeability and hydraulic connectivity, resulting in formation of bonanza ore-bodies.

Both the Seongsan and Comstock districts share many similar geological, structural, spatial and temporal relationships. They both formed in similar tectonic and magmatic settings related to subduction along an active continental margin arc with high-K calc-alkaline series host rocks. Both include an early stage of high-sulfidation advanced argillic alteration that is essentially barren with respect to metal mineralisation, which is overprinted by low-sulfidation Au-Ag-Cu-Pb-Zn-bearing veins and associated alteration. The structural setting of the high- and low-sulfidation events are also similar, with compressional (Seongsan) and compressional to low differential stress-states (Comstock) during advanced argillic alteration and extensional stress-states (Seongsan and Comstock) during later low-sulfidation Au-Ag-bearing veining and associated alteration. Both districts show a coupled change in structural setting and hydrothermal fluid characteristics over a period of ca. 1 to 2Ma.

6.2.3.2 Seongsan and Mt Skukum

Similar geological relationships as at Seongsan and Comstock also characterise the Mt Skukum area, although there are few detailed reports available. Love et al. (1998) described early advanced argillic alteration that comprises quartz±alunite±pyrophyllite±kaolinite zones centred on small rhyolitic stocks that are essentially barren with respect to metal mineralisation. These are overprinted by economic Au-bearing quartz-calcite-adularia veins and associated adularia-sericite type alteration. These distinct epithermal systems formed ca. 1.5Ma apart, but both formed during ongoing magmatism in the Mt Skukum Volcanic Complex. Again, the superimposition of low- on high-sulfidation style alteration is a feature of this area like the Seongsan and Comstock districts.

6.2.3.3 Seongsan and Kyushu

Southern Kyushu in Japan also hosts high-, intermediate- and low-sulfidation deposits that have been studied extensively (e.g. Hedenquist et al., 1994; Faure et al., 2002; Watanabe, 2004, 2005 and many others). High-, intermediate- and low-sulfidation epithermal systems in southern Kyushu are located within 5km of each other in areas such as the Nansatsu district and Kago where high-sulfidation Cu-Au deposits occur with minor occurrences of low-sulfidation veins <5km away. Larger examples of each are located over a distance of ca. 50 to 80km (e.g. Nansatsu district high-sulfidation Cu-Au deposits, the Kushikino intermediate-sulfidation Au-Ag deposit and the Hishikari low-sulfidation Au-Ag deposits).

Southern Kyushu is a Cretaceous to Paleogene magmatic arc / accretionary prism comprising basement granodiorite material overlain by sandstone and shale, intruded by Miocene granitic rocks, and later overlain by Miocene to Pleistocene volcanic rocks (Hosono & Nakano, 2004). At Nansatsu, high-sulfidation Cu-Au±Ag mineralisation (4.5 to 3.7Ma) is generally associated

with enargite±luzonite-pyrite±covellite and is hosted within core zones of vuggy silica, which are surrounded by halos of advanced argillic (alunite±dickite/kaolinite± pyrophyllite), argillic (illite to illite/smectite) and propylitic alteration (Izawa & Cunningham, 1989; Hedenquist et al., 1994). At Kushikino, intermediate-sulfidation Au-Ag mineralisation (3.63 to 3.35Ma) is associated with quartz-electrum-argentite-naumannite-polybasite-pyrargyrite and minor adularia (Matsuhisa et al., 1985). At Hishikari, low-sulfidation Au-Ag mineralisation (1.11 to 0.73Ma) is generally associated with steeply-dipping crustiform-colloform banded quartz-adularia-pyrite-electrum-argentite veins with illitic alteration haloes and vein deformation indicators suggesting veins formed in an extensional stress environment (Izawa et al., 1990; Faure et al., 2002; Hosono & Nakano, 2004).

The change from high- to intermediate- to low-sulfidation deposits in southern Kyushu is ascribed to a change in the stress state of the arc from low differential stress during development of high- and intermediate-sulfidation deposits to extension during development of low-sulfidation deposits. The change in the stress state of the arc has been attributed to the onset of slab rollback of the subducting Philippine Plate at ca. 2Ma, driven by the change from young to old slab material, separated by the Kyushu-Palau ridge (Watanabe, 2004, 2005).

These observations suggest that there was a similar coupled evolution of tectonic setting and epithermal system development within the Seongsan district and southern Kyushu. Both districts show a change in the stress state of the arc from compressional or low differential stress during high- and intermediate-sulfidation development to extensional during low-sulfidation development, related to hinge retreat of the associated subducting slab. Indeed, the timing of the change from high- to low-sulfidation epithermal systems in the Seongsan district may help to further constrain the timing of this change in the larger scale tectonic stress state/setting of southern Korea.

Furthermore, Hosono & Nakano (2004) suggested that the Pb-Sr isotopic composition of the Hishikari system may provide constraints on the contribution of deep crustal fluids to mineralisation. They report that the metals in the veins were essentially derived from a mixture of magmatic fluid and deep crustal fluid. The release of the deep crustal fluid was triggered by rhyodacitic intrusions during a period of extension, which enabled the fluid and metals to ascend into the brittle upper crust along faults that developed during extension. This suggests that hinge retreat triggered extension, which in turn developed fault networks and enabled the emplacement of magma, which focussed and drove the metal-bearing fluid ascent.

6.3 CONTROLS ON THE DEVELOPMENT OF HIGH-SULFIDATION CLAY/ SULFATE OR GOLD-SILVER±COPPER DEPOSITS

Previous sections highlighted that some high-sulfidation epithermal systems appear to form clay deposits (e.g. the Seongsan district), others metal deposits (e.g. the Nansatsu district) and some a sub-economic mix of both (e.g. quartz±alunite±pyrite alteration within the Comstock district). Possible controls on whether high-sulfidation systems form either clay or metal deposits are explored within this section.

6.3.1 Clay deposits: key characteristics

The primary ore at the Seongsan and Ogmaesan clay deposits is dickite/kaolinite, which is utilised in the production of many industrial and domestic products, including ceramics, paints, plastics, paper and glass fibre. Clay ore lacks significant sulfide or other Fe-bearing minerals.

Many clay deposits occur in South America, Asia and Europe. However these deposits commonly formed by supergene processes (e.g. Simeone et al., 2005). Only a limited number of clay deposits formed in epithermal systems. Hypogene epithermal systems that have been mined for clay predominantly occur in southeast China, South Korea and southwest Japan (Kitagawa et al., 1999). Similar material also occurs in the Budawang rift in southeast New South Wales, Australia (Glaser, 1988).

Clay deposits in Japan are known as ‘Roseki’ deposits. These Roseki deposits generally occur in Cretaceous volcanic rocks in southwest Japan and are commonly exploited for commercial grade clay (Watanabe et al., 1998; Kitagawa et al., 1999; Hongu et al., 2000). The Late Cretaceous in Japan was characterised by extensive continental-arc ilmenite- and magnetite-series magmatism and associated subaerial acidic pyroclastic volcanic rocks (Watanabe et al., 1998). Age data for Roseki deposits appear to show a temporal and spatial association with the ilmenite-series magmatism (Watanabe et al., 1998; Kitagawa et al., 1999). However, the clay deposits are generally hosted within volcanic rocks that are associated with magnetite-series magmatism, suggesting formation of the clay deposits from magnetite-series magmatism rather than ilmenite-series (Watanabe et al., 1998; Kitagawa et al., 1999). Most form as massive stratabound clay deposits or less commonly as clay-bearing vein systems (Watanabe et al., 1998; Hongu et al., 2000). Ishihara & Imaoka (1999) suggest that one of the largest Roseki deposits formed after a local caldera, ca. 15km by 15km in size, collapsed and hydrothermal fluids ascended through the caldera walls and spread into permeable horizons.

Comparison of the Comstock and Seongsan districts highlights that they share several key geological similarities (Section 6.2.4.1; Table 6-1 and references within). However, high-sulfidation fluids in the Seongsan district formed economic clay mines, whereas clay-rich alteration in the Comstock district includes significant sulfide and is not a suitable source of clay ore for mining. One key geological characteristic that is not shared between the districts is the composition of the local host rocks. The Seongsan district is hosted by rhyodacitic rocks, whereas the Comstock district is hosted by andesitic rocks. Typical analyses of andesite contain 8.1wt% total Fe (as combined FeO and Fe_2O_3) whereas dacite and rhyolite contain only 3.0 and 2.3wt% total Fe respectively (Philpotts, 1990). Alteration of andesite results in significant pyrite being present, whereas alteration of dacite and rhyolite results in minimal pyrite due to less overall Fe in the host rock. This suggests that host rock composition must have played a key role in the development of the economic clay deposits at Seongsan and the formation of sulfide within the advanced argillic alteration at Comstock.

However, host rock composition can not be the only controlling factor on whether or not a high-sulfidation system will form an economic clay deposit or not. The Goldfield system is hosted by rhyolite and contains significant advanced argillic alteration and metalliferous mineralisation. This suggests that significant Fe was introduced and deposited within the Goldfield system during mineralisation. Figure 5-8 highlights that only especially oxidised, low-pH fluids promote alunite formation, hence at the Goldfield system, Fe must have been introduced under H_2S-dominant conditions to form pyrite rather than alunite (Fig. 5-8). Southern Kyushu also hosts significant advanced argillic alteration within andesitic host rocks. However, the deposits are strongly mineralised with Au-Cu and have not formed clay deposits.

Comparison of the Seongsan and Comstock districts highlights that a felsic host rock composition is a critical controlling factor in the development of clay deposits. However, examination of the Goldfield system shows that a felsic host rock does not guarantee a clay deposit. The features explored above suggest that the Seongsan clay deposits, the Roseki clay deposits and analogous systems throughout East Asia formed from oxidised hydrothermal fluids associated with contemporaneous magmatism and volcanism in a continental ensialic backarc tectonic setting. The common features to all these clay/sulfate deposits in East Asia suggest that a continental backarc tectonic setting (as opposed to forearc/island-arc setting), strongly oxidised, low-pH, SO_4-dominant hydrothermal fluids (as opposed to more reduced H_2S-dominant fluids) have played important roles in the formation of commercial grade clay/sulfate deposits.

deposit	tectonic setting	magmatic and igneous association	host rocks	structural setting	age (Ma)	main ore	surface extent of mineralisation (km^2)	orebody form	alteration assemblages	ore mineral assemblages	ore-related textures	pH of hydrothermal alteration fluids	sulfidation state of ore forming fluids	relative oxidation state of system	magmatic / meteoric signature (O,H isotopes)	H_2S / SO_4 dominant (S isotopes)	ore forming processes	key 'mixed' characteristics	temp (°C)	salinity (wt %)	references
Known epithermal systems and districts																					
White Island, TVZ, New Zealand	active island-arc volcano	magnetite-series calk-alkaline	andesite -dacite	extensional (graben) ± dextral shear	0.01 to now	embryonic Cu±Au	unknown	unknown	cristobalite, alunite, anhydrite, pyrite, Al-rich chlorite	unknown	unknown	acid (3 to 4)	HS	oxidised	magmatic / mixed with local seawater	SO_4	inferred cooling, or cooling from mixing		380	?	Giggenbach, 1987; Cole, 1990; Hedenquist et al., 1993; Cooke & Simmons 2000; Rapien et al., 2003; Giggenbach et al., 2003
Broadlands-Ohaaki, TVZ, New Zealand	active geothermal system in back-arc basin	magnetite-series calk-alkaline	rhyolite-dacite	extensional and dextral shear	0.3(?) to now	embryonic Au, Ag ± base-metals	Ohaaki pools, 13.5kg Au over 800m^2	sinter + artificially generated infill in wells	quartz, illite, adularia, albite, chlorite, calcite, pyrite, smectite, siderite	chalcopyrite, galena, sphalerite, magnetite, pyrite, electrum	sinter, colloform-crustiform banded, disseminated base metals	neutral (6 to 8)	LS	reduced	meteoric	H_2S	boiling		250	?	Cole, 1990; Simmons & Browne, 2000; Cooke & Simmons, 2000
Nansatsu district, southern Kyushu, Japan	magmatic arc / accretionary prism	magnetite-series calk-alkaline	andesite	compres-sional to near neutral	4.5 to 3.7	Au, Cu	15 (Kasuga) 2 (Iwato) <1 (Akeshi)	massive	vuggy silica, alunite, dickite, kaolinite, pyrophyllite, illite, illite/smectite	enargite, pyrite, luzonite, native Au, electrum, covellite	vug filling, disseminated	acid	HS	oxidised	magmatic mixed with meteoric	H_2S:SO_4 3:1 ore fluid	cooling from mixing		160 to 230	<2	Izawa & Cunningham, 1989; Hedenquist et al., 1994; Watanabe, 2004
Kushikino, southern Kyushu, Japan	magmatic arc / accretionary prism	magnetite-series calk-alkaline	andesite	near neutral	3.63 to 3.35	Au, Ag	20	veins	quartz, adularia, sericite, chlorite, carbonate	electrum, argentite, naumannite, polybasite, pyrargyrite	crustiform, vein breccias, lattice	neutral	IS	undeter-mined (probably reduced)	undetermined (probably meteoric mixed with deep source)	undeter-mined (probably H_2S)	boiling		170 to 250	?	Matsuhisa et al., 1985
Hishikari, southern Kyushu, Japan	magmatic arc / accretionary prism	magnetite-series calk-alkaline	andesite	extensional	1.11 to 0.73	Au, Ag	3	veins	chlorite-illite, inter-stratified clays, quartz-illite, cristobalite-smectite; adularia as infill in veins	pyrite, chalcopyrite, argentite, electrum and naumannite-aguilarite	crustiform-colloform, lattice	neutral	LS to IS	reduced	meteoric; possible deep source of metals (Pb-Sr)	H_2S	boiling	? possible active geothermal overprint as alteration zon-ation is discor-dant to veins	180 to 250	0 to 0.12	Izawa et al., 1990; Hedenquist et al., 1994; Faure et al., 2002; Hosono & Nakano, 2004; Garwin et al., 2005
'Roseki' clay deposits, Japan	magmatic arc / back-arc	ilmenite-series calk-alkaline	rhyolite	trans-pressional	ca. 87 to 63 and ca. 15	clay	undetermined	massive strata-bound	kaolinite/dickite± pyrophyllite±illite	kaolinite/dickite± pyrophyllite	replacement, rarely as veins	acid	no sulfide: HS by correlation	oxidised	undetermined (probably magmatic)	SO_4	hydrothermal alteration		?	?	Watanabe et al., 1998; Kitagawa et al.., 1999; Ishihara & Imaoka, 1999; Hongu et al., 2000
Zijinshan, Fujian Province, China	continental margin volcanic arc	magnetite-series high-K calk-alkaline	dacite	?extension	ca. 105 to 100	Cu, Au	60	breccias, veins	alunite-qtz-py; dickite-qtz-py-zunyite-sericite; sericite-qtz-py	digenite, enargite, covellite, gold	vug filling, disseminated	acid	HS to IS	undeter-mined (probably oxidised to reduced)	undetermined (probably magmatic)	undeter-mined (probably SO_4 early H_2S late)	mixing, cooling	region hosts metalliferous HS & LS epithermal & porphyry Cu-Au systems	100 to 320	0 to 22	So et al., 1998; Zhang et al., 2003
Summitville, Colorado, USA	magmatic arc	calc-alkaline	quartz latite	extensional	22.4	Au, Ag, Cu, Pb	2	massive	vuggy silica, alunite, kaolinite, pyrite, illite, smectite	enargite, luzonite, pyrite, covellite, native Au, sphalerite, galena	disseminated, breccias	acid	HS to IS	reduced to ox. to reduced	magmatic	H_2S early to SO_4 to H_2S late	boiling, mixing, oxidation		170 to 320	0 to 25 & 32 to 42	Stoffregen, 1987; Rye et al., 1992; Gray & Coolbaugh, 1994; Arribas Jr., 1995; Bethke et al., 2005
Goldfield, Nevada, USA	continental margin volcanic arc	magnetite-series high-K calk-alkaline	rhyolite	?trans-pressional	21 to 20	Au, Ag, Cu	1.5	massive	vuggy quartz, alunite, kaolinite, pyrite, barite	enargite, goldfieldite, luzonite, pyrite, bismuthinite	disseminated, breccia pipes, ledges	acid	HS to IS	undeter-mined (probably oxidised to reduced)	undetermined (probably magmatic)	H_2S:SO_4 1:1	boiling		220 to 290	0.2 to 8	Ashley & Silberman 1976; Vikre 1989
Comstock district, Nevada, USA	continental margin volcanic arc	magnetite-series high-K calk-alkaline	andesite	transpres-sional to trans-tensional	16 to 13	Au, Ag ± Cu, Pb, Zn	25	massive quartz veins and stockworks	mixed: rare K-silicate; acid-sulfate-pyrite; & adularia-sericite associated with Au-Ag	sph, cpy, gal, pyrite, electrum ± Ag-sulfides and Ag-sulfosalts	massive, crustiform-colloform, breccia	mixed: early acid to neutral during Au-Ag	IS	variable: oxidised to reduced	? meteoric	SO_4 early H_2S late	boiling, cooling	early acid-sulfate alteration overprinted by Au-Ag-bearing adularia-sericite altered IS veins	220 to 300	0.4 to 6.1	Vikre et al., 1988; John, 2001; Hudson, 2003; Berger et al., 2003; Simmons et al., 2005
Mt Skukum, Canada	magmatic arc	calc-alkaline	andesite and rhyolite	undeter-mined	55.7 & 54.1	Au	500m by 500m	veins	mixed: early acid-sulfate (no pyrite) ; to adularia-sericite-carbonate associated with Au-Ag	quartz, calcite, adularia, sulfides, electrum	crustiform banded veins, bladed carbonate and vein breccias	mixed: early acid to neutral during Au-Ag	?LS to ?IS (inferred from alt., sulfides not reported)	undeter-mined (probably oxidised to reduced)	magmatic mixed with meteoric for acid-sulfate meteoric for Au-Ag veins	undeter-mined (probably SO_4 early H_2S late)	undetermined, (probably boiling)	early acid-sulfate alteration overprinted by Au-Ag-bearing adularia-sericite altered IS veins	?	?	Love et al., 1998

deposit	tectonic setting	magmatic and igneous association	host rocks	structural setting	age (Ma)	main ore	surface extent of mineralisation (km^2)	orebody form	alteration assemblages	ore mineral assemblages	ore-related textures	pH of hydrothermal alteration fluids	sulfidation state of ore forming fluids	oxidation state of system	magmatic / meteoric signature (O,H isotopes)	H_2S / SO_4 dominant (S isotopes)	ore forming processes	key 'mixed' characteristics	temp (°C)	salinity (wt %)	references
Seongsan district epithermal systems																					
Seongsan	continental margin volcanic back-arc	magnetite-series high-K calk-alkaline	rhyo-dacite	trans-pressional wrenching	80.9 (±1.2) to 78.1 (±1.1)	clay / sulfate	ca. 1	massive replacement	kaolinite/dickite ± sulfide, alunite, siliceous ± silicic	kaolinite/dickite, alunite	replacement	acid	HS to IS	oxidised	magmatic	SO_4	hydrothermal alteration	overprinting adularia-phyllic alteration and LS-style veins	< 280	3.9	Kim & Nagao, 1992 (age data only) Koh, 1996 (fluid inclusion salinity data only)
Ogmaesan	continental margin volcanic back-arc	magnetite-series high-K calk-alkaline	rhyo-dacite	trans-pressional wrenching	81.4 (±1.0) to 79.0 (±1.2)	clay / sulfate	ca. 1	massive replacement	kaolinite/dickite ± sulfide, alunite, siliceous ± silicic	kaolinite/dickite, alunite	replacement	acid	no Au-Ag: HS by correlation with alteration	oxidised	magmatic	SO_4	hydrothermal alteration		<250?	?	Kim & Nagao, 1992 (age data only)
Eunsan	continental margin volcanic back-arc	magnetite-series high-K calk-alkaline	rhyo-dacite	trans-tensional extension	77.9 ^ (±0.3)	Au, Ag	ca. 500m by 50m	veins	albite-carbonate, illite, adularia, siliceous	pyrite, acan/argen, Ag-sulfo-salts, Ag, electrum, ±(sp, gal, cpy, t/t) *	colloform-crustiform, cockade, vein breccias	early incipient acid to neutral	LS to IS	reduced	meteoric (?mixed)	H_2S	boiling	minor incipient early adv. arg. alteration	230	*0.5 to 1.2	
Moisan	continental margin volcanic back-arc	magnetite-series high-K calk-alkaline	rhyo-dacite	trans-tensional extension	77.4 ^ (±0.5)	Au, Ag ± Cu, Pb & Zn	ca. 500m by 100m	veins	albite-carbonate, illite, adularia, siliceous, adv. arg. overprint	pyrite, Ag-Au-rich tellurides, native Te, acan/argen, sp, gal, cpy, goldf-t/t	crustiform-colloform, crystalline, vein breccias	early incipient acid to neutral	LS to IS	reduced	meteoric (?mixed)	H_2S	boiling	LS/IS veins but trace metal data suggests significant magmatic input	230	*8.1 to 13.7	
Chunsan	continental margin volcanic back-arc	magnetite-series high-K calk-alkaline	rhyo-dacite	trans-tensional extension	78.1 ^ (±0.3)	Au, Ag	ca. 500m by 100m	stratabound	albite-carbonate, illite, adularia, siliceous ± silicic	pyrite, electrum, t/t, cpy	replacement / infill of earlier leached material	early acid to neutral	LS to IS	reduced	meteoric (?mixed)	H_2S	boiling	early adv. arg. alteration overprinted by adularia-phyllic alteration and adu-Au IS/LS mineralisation	230	*0.7 to 2.6	

Table 6-1 Selected geological characteristics of some epithermal systems and those of the Seongsan district (…continued from previous page). HS, IS, LS = high-, intermediate- and low-sulfidation. adv. arg. = advanced argillic; alt. = alteration. ^ = age data done this study. qtz = quartz, py = pyrite, adu = adularia, en = enargite, lz = luzonite, t/t = tennantite/tetrahedrite, cpy = chalcopyrite, sph = sphalerite, gal = galena, acan/argen = acanthite/argentite, goldf = goldfieldite (Cu variably substituted by Ag-Au in the series to tennantite/tetrahedrite). TVZ = Taupo Volcanic Zone.

6.3.2 Au-Ag±Cu high-sulfidation deposits: key characteristics

Current literature suggests that Au±Cu-rich high-sulfidation systems often require a separate, later, intermediate- to low-sulfidation fluid phase after high-sulfidation alteration to make an orebody (Arribas Jr, 1995; Allibone et al., 1995; Cooke & Simmons, 2000; Hedenquist et al., 2000; Einaudi et al., 2003; Sillitoe & Hedenquist, 2003).

To clarify when metal and clay mineralisation develop in high-sulfidation systems, key geological and paragenetic characteristics of high-sulfidation epithermal systems have been listed within Table 6-1. Key characteristics of some intermediate- and low-sulfidation systems have also been listed in Table 6-1 to further compare the evolution of the Seongsan district with other known epithermal systems.

The advanced argillic alteration within the Comstock district does not host any clay or metalliferous mineralisation, whereas, the Goldfield high-sulfidation system is Au-Ag mineralised. Goldfield is hosted within the same 'western andesite assemblage' (John, 2001) as Comstock and shares similar tectonic, magmatic and igneous associations. Goldfield and Comstock both show early stages of advanced argillic alteration development. Detailed examination of the Goldfield system (Table 6-1 and references therein) shows that the Au-Cu±Ag mineralisation at Goldfield occurs as disseminated, replacement and breccia-hosted stages of ore-bearing sulfide whose deposition post-dates the advanced argillic alteration. This paragenetic stage has not been described at Comstock though.

Examination of Table 6-1 shows that metalliferous high-sulfidation systems include a later high-grade, ore-bearing paragenetic stage that post-dates the main stage of advanced argillic alteration. High-sulfidation systems that lack significant metalliferous ore, some of which contain economic clay ore, such as the Seongsan and Ogmaesan systems, do not include a later high-grade, metalliferous ore-bearing paragenetic stage.

Examination of Table 6-1 also highlights that the oxidation state of the system and whether or not H_2S or SO_4 is the dominant sulfur species are key criteria in determining whether clay or metalliferous mineralisation develop in high-sulfidation systems. High-sulfidation systems must be oxidised and SO_4-dominant to form advanced argillic alteration. However, to evolve into metalliferous mineralised systems, hydrothermal fluids must at least be on the SO_4/H_2S buffer or H_2S-dominant to allow sulfide and metal transportation and precipitation. Conversely, for high-sulfidation systems to develop as a clay deposit, strongly oxidised, low-pH, SO_4-dominant conditions must prevail throughout the paragenesis.

6.3.3 Thoughts on why some high-sulfidation systems develop an intermediate- to low-sulfidation mineralising stage and others do not…?

As highlighted previously, current literature suggests that the main metalliferous mineralising stage within high-sulfidation systems is later than the advanced argillic alteration. This later stage is commonly thought to form from hydrothermal fluids that are of an intermediate- to low-sulfidation-state (Arribas Jr, 1995; Allibone et al., 1995; Cooke & Simmons, 2000; Hedenquist et al., 2000; Einaudi et al., 2003; Sillitoe & Hedenquist, 2003). However, some systems like Nansatsu, show high-sulfidation-state mineralisation (Hedenquist et al., 1994). Others are cut by later discordant low-sulfidation-state mineralised veins (e.g. the Seongsan and Comstock systems), and others do not develop a mineralising stage at all (e.g. the Ogmaesan system).

It is generally regarded that it is the additive combination and optimisation of relatively common tectonic, magmatic, hydrothermal and structural processes that is required for the formation of ore deposits rather than one unique process (Richards, 2003). This section briefly speculates on processes that could result in the formation of mineralised intermediate- to low-sulfidation fluids that are observed in some high-sulfidation systems. The processes that control their emplacement will depend on favourable tectonic, magmatic, hydrothermal and structural settings; these topics are not discussed here.

Fluids that evolve from magmas can be initially rich in either SO_2 or H_2S, depending on the oxidation state of the magma (Ohmoto, 1986). The SO_2/H_2S ratio of the evolved magmatic fluid depends on the oxidation state of the magma, temperature, pressure and the rapidity with which the fluids are released (Rye, 2005). High pressure favours H_2S and low pressure favours SO_2 (Rye, 2005), thus if the evolved magmatic fluid is suddenly released into the epithermal environment, it will partition into a SO_2-rich vapour-phase and a dense H_2S-rich fluid-phase (Henley & McNabb, 1978; Fournier, 1987; Giggenbach, 1992; Rye, 1993; Fournier, 1999; Rye, 2005). Magmatic fluids/vapours that rise slowly will react with Fe-bearing minerals, thus resulting in the disproportionation of SO_2 into H_2SO_4 and H_2S (Ohmoto & Rye, 1979; Rye, 1993; Giggenbach, 1997; Rye, 2005). However, under rapid ascent, SO_2-rich fluids/vapours will not react with host rocks and will remain SO_2-rich. Upon reaching the epithermal environment, these SO_2-rich fluids/vapours disproportionate and develop large amounts of H_2SO_4, forming advanced argillic alteration. These combined processes can overwhelm the rock buffer, resulting in further H_2SO_4 generation, which further propagates advanced argillic alteration (Giggenbach, 1997; Rye, 2005). The H_2S that is derived either directly from the magma or via the disproportionation of SO_2 will react with Fe-bearing minerals in the wall rock to produce pyrite, or will be oxidised in the steam-heated environment, or will vent to the surface (Rye, 2005). The partitioned, dense fluid will be H_2S-rich and may pond over time, thus

further reducing the sulfidation-state of the fluid via reaction with Fe-bearing minerals in crystalline igneous rocks (Ohmoto & Rye, 1979; Rye, 1993; Giggenbach, 1997; Fournier, 1999; Rye, 2005) or by reaction with an influx of magma of differing composition, although probably more mafic (Hattori & Keith, 2001), or by continued magmatic disproportionation (Rye, 2005).

These processes suggest that for high-sulfidation systems like Goldfield and Summitville that have an intermediate-sulfidation-state mineralisation stage, deep fluids may not have been tapped until sometime after the development of the advanced argillic alteration. Depending on the length of time between initial partitioning and fluid ascent, the deep fluid may have reduced over time to an intermediate- or even low-sulfidation-state, by the processes outlined above. In rarer cases, high-sulfidation systems like Nansatsu, which have high-sulfidation-state minerals associated with Au-Cu mineralisation, deep fluids may have been tapped only shortly after advanced argillic alteration while they were still in a high-sulfidation-state. Alternatively, the metals may have been partitioned into the initial magmatic vapour phase. These processes may also explain why, in districts that host both high- and low-sulfidation systems, the low-sulfidation systems tend to form at least 1 to 2Ma after high-sulfidation hydrothermal activity; as this may be the minimum time required to reduce a high-sulfidation-state hydrothermal fluid into a low-sulfidation-state.

In high-sulfidation systems, Au is thought to be transported either as chloride complexes (e.g. $AuCl_2^-$) in acidic brines of magmatic origin, or hydrosulfide complexes (e.g. $AuHS_{(aq)}$) and/or vapour phases (e.g. $AuS_{(g)}$, $CuS_{(g)}$, or $CuCl_{(g)}$) in reduced, low-salinity, acidic fluids and/or gases formed from condensation of magmatic gases into groundwater (Cooke & Simmons, 2000; Fig. 1-4). Chloride complexes will precipitate Au from solution by dilution, cooling and/or pH increases, possibly from mixing with ground waters, whereas hydrosulfide complexes and/or vapour phases will deposit Au from solution in response to boiling or to mixing-induced oxidation, but not to temperature, dilution, salinity or pH changes.

This suggests that for Goldfield and similar high-sulfidation systems that include an intermediate-sulfidation-state mineralisation stage, Au was transported as a hydrosulfide complex and was precipitated from solution by boiling and/or mixing-induced oxidation. Less commonly, for Nansatsu and similar high-sulfidation systems that comprise a high-sulfidation-state mineralisation stage, Au was transported as a chloride complex that was probably partitioned into the early magmatic vapour phase and precipitated Au from solution by cooling.

6.3.4 Implications for the hydrothermal fluid evolution in the Seongsan district

The variation in $\delta^{34}S$ of sulfur species from the various epithermal systems within the Seongsan district could have formed from either or a combination of: 1. magmatic disproportionation of a single parent fluid, 2. by influx of multiple magmatic fluids with variable oxidation states, 3. through reduction of sulfur from lithostratigraphic buffering, and 4. influx of reduced meteoric waters (Ohmoto & Goldhaber, 1997).

The oxygen and hydrogen isotopic ratios in the high- and low-sulfidation fluids in the Seongsan district are distinctly different. This suggests that rock buffering of an early high-sulfidation fluid to a low-sulfidation fluid was not a dominant process in the generation of the later low-sulfidation fluids. If it were, then a broader range of oxygen and hydrogen isotopic compositions would be expected rather than the discrete groupings observed. Furthermore, it is unlikely that the local stratigraphic pile was responsible for any significant reduction of SO_4-dominant fluids to H_2S-dominant fluids by buffering reactions of ascending hydrothermal fluids, as there is a distinct lack of significant Fe-bearing minerals in the lithological sequence. The migration of hydrothermal fluid through this lithological sequence is unlikely to have significantly re-set any geochemical characteristics as they are predominantly similar to the assumed felsic parent magma.

Oxygen and hydrogen isotope data from the low-sulfidation systems suggests formation by meteoric-derived fluids, whereas the sulfur isotope data suggests magmatic-derived sulfur. Two possible scenarios are provided to explain this. Pulses of magmatic-derived sulfur contributed to the vein sulfide material, but due to the dominant influx of meteoric-derived fluid compared to the magmatic-derived sulfur, the overall oxygen and hydrogen isotopic value of the quartz material appears meteoric-derived. Alternatively, during the influx of meteoric-derived fluids, minimal sulfur species would have been present in that fluid except for those scavenged from the surrounding host rocks, which would have had a magmatic-derived sulfur isotopic value.

It is inferred for the Seongsan district that a rapidly ascending highly oxidised SO_2-rich magmatic-steam phase disproportionated near surface and formed large amounts of H_2SO_4. This sulfuric acid formed the advanced argillic alteration within the Seongsan district. A deep, H_2S-dominant, metal-bearing, residual fluid developed as a result of the initial magmatic disproportionation and subsequent tapping of the SO_2-rich magmatic-steam phase. This H_2S-dominant, metal-bearing fluid was not tapped during advanced argillic alteration. At the onset of extension in the Seongsan district, deep-seated faults tapped relatively small volumes of the H_2S-dominant, metal-bearing fluid and allowed it to ascend and mix with large volumes of surficial meteoric waters that reduced it further. This later, H_2S-dominant, intermediate- to low-

sulfidation-state, metal-bearing hydrothermal fluid largely of meteoric origin formed the Au-Ag-bearing low-sulfidation epithermal systems of the Seongsan district and the Au-Ag-bearing intermediate-sulfidation-state assemblages found discordantly cross-cutting the advanced argillic alteration within the Seongsan system.

6.4 IDENTIFICATION OF HIGH-SULFIDATION EPITHERMAL SYSTEMS PROSPECTIVE FOR METAL AND/OR CLAY/SULFATE MINERALISATION

Alteration associated with high-sulfidation epithermal systems can be extensive and much of it barren with respect to metalliferous mineralisation. Significant mineralisation is often hosted by only a few percent of the overall volume of alteration (e.g. the Nena-Frieda River district, Morrison et al., 1999). In some rare cases, the advanced argillic zones are host to significant disseminated mineralisation that is part of the high-sulfidation paragenesis (e.g. Pueblo Viejo, Kesler et al., 1981; Muntean et al., 1990; Nelson, 2000; Kesler et al., 2005). Where mineralisation is confined to a relatively small part of the overall hydrothermal system, it can represent a formidable exploration target.

Examination of the epithermal systems within Sections 6.2 and 6.3 highlighted a number of geological criteria that could possibly be used as discriminators between barren, metalliferous- or clay/sulfate-mineralised high-sulfidation systems. These discriminators are: the composition of host rocks, their tectonic setting, whether H_2S or SO_4 is the dominant sulfur species in the hydrothermal system and chemical zonation within magmatic alunites. These are discussed here and incorporated together in the following Section in developing an exploration model.

6.4.1 Composition of host rocks

The composition of host rocks determines the potential of a high-sulfidation system to form an economic clay deposit or not. Metalliferous high-sulfidation systems are hosted within both rhyolite and andesite host rocks, however, andesitic examples are much more common, whereas clay-sulfate deposits are confined to rhyolitic-dacitic host rocks (Table 6-1). Andesitic rocks are significantly enriched in Fe-bearing minerals compared to rhyodacitic rocks. Under advanced argillic alteration, andesite forms clay±silica with significant sulfide contamination generated by reduction of the hydrothermal fluid by reaction with Fe-bearing minerals in the host rock. This destabilises the aqueous sulfide species and results in sulfide precipitation. Extensive rhyolitic to dacitic host rocks is thus an essential component for the development of clay deposits.

6.4.2 A fore-arc versus back-arc tectonic setting

Kyushu in Japan is located right at the fore-arc and hosts high-sulfidation Au-Cu±Ag, intermediate-sulfidation Au-Ag and low-sulfidation Au-Ag mineralisation. This region is particularly metalliferous-rich and hosts a variety of epithermal deposit styles. However, mainland southern Japan is located in a back-arc setting and is host to a significant number of 'Roseki' clay deposits. This distinct difference in metallogeny is probably coupled with the fact that rhyolitic rocks, which are prerequisite host rocks for clay deposits, are dominant in the back-arc setting whereas andesite dominates in the fore-arc. A back-arc tectonic setting in a continental margin or evolved arc situation is more conducive to rhyolitic volcanism. Such terranes are therefore more prospective for potential high-sulfidation clay deposits. Fore-arc settings are more conducive to andesitic volcanism and therefore more prospective for potential metalliferous-mineralised high-sulfidation systems.

6.4.3 The H_2S:SO_4 composition of a system

Examination of a number of known high-sulfidation systems shows that metalliferous mineralised systems are derived from at least equally H_2S/SO_4-mixed to H_2S-dominant hydrothermal fluids (e.g. Lepanto, Nansatsu and Rodalquilar, Arribas Jr, 1995; Summitville, Bethke et al., 2005; Julcani, El Salvador, Gaspé and Frieda, Rye, 2005; Pierina, Fifarek & Rye, 2005). In contrast, the metalliferous-barren high-sulfidation systems of the Seongsan district are derived from SO_4-dominant hydrothermal fluids (see also Rye, 2005). The Au-Ag-bearing low-sulfidation epithermal systems in the Seongsan district show evidence for H_2S-dominant hydrothermal fluid conditions during mineralisation.

By utilising sulfur isotopic compositions of sulfide and sulfate species in $\delta^{34}S_{sulfate}$ - $\delta^{34}S_{sulfide}$ plots, such as Figure 5-15 (Fifarek & Rye, 2005; Rye, 2005), it can be determined if the sulfur-bearing species formed under mixed, H_2S- or SO_4-dominant conditions. The use of $\delta^{34}S_{sulfate}$ - $\delta^{34}S_{sulfide}$ plots is a recent development and they may not have been utilised as an exploration tool to discriminate between mineralised and barren high-sulfidation systems as yet. Caution must therefore be used, as the geochemical signature of sulfates and sulfides from different paragenetic stages from within an individual system can show different isotopic signatures (e.g. Tambo in Chile, Deyell et al., 2005). If predominantly SO_4-dominant conditions exist, then the prospectivity for high-sulfidation-style metalliferous mineralisation is limited, and conversely the prospectivity of potential high-sulfidation style clay deposits is significantly increased. However, if mixed, or predominantly H_2S-dominant conditions exist during alteration, then the prospectivity for potential high-sulfidation style metalliferous mineralisation is significantly increased, and conversely the prospectivity for potential clay deposits is significantly reduced.

6.4.4 Chemical zonation within magmatic alunites

Isotopic studies on alunite are used extensively to allow us to determine likely fluid sources and environments of formation, such as whether magmatic or supergene processes were responsible for alunite formation (Rye, 2005). However, in addition to isotopic studies, a relatively small number of empirical studies on chemical zonation, or the distinct lack of it, within alunite ($KAl_3(SO_4)_2(OH)_6$) provides useful information on changing fluid compositions over time (Aoki, 1991; Hedenquist et al., 1994; Deyell et al., 2005). A wide range of substitutions in alunite are possible. The substitution of Na for K defines the alunite-natroalunite solid solution. Other substitutions for K may include: Ca, Ba, Sr, REE, Pb, Ag, H_3O and NH_4. The substitution of Fe^{3+} for Al^{3+} defines the alunite-jarosite solid solution. The substitution of $(PO_4)^{3-}$ for $(SO_4)^{2-}$ forms the APS (aluminium-phosphate-sulfate) group of minerals.

Examination of published accounts on the chemical variation in alunite shows some variation between systems, indicating that host rock composition and local hydrothermal conditions control alunite compositions. In fact, Deyell & Dipple (2005) go as far as to say that the quantitative use of alunite K-Na compositions as a guide to mineral exploration should be treated with caution. Broader trends that are evident from the limited data suggest that the most varied mineralogical and chemical zonation occurs in hypogene magmatic alunite (e.g. Nansatsu in Japan, Hedenquist et al., 1994; Temora in Australia, Allibone et al., 1995). Magmatic-steam or steam-heated alunites show much less to no chemical variation, with natroalunite favoured by higher temperatures and alunite is more common at lower temperature shallow levels (Aoki, 1991; Hedenquist et al., 1994). Examination of the chemical zonation, or lack of it, in magmatic alunites should be able to further indicate the environment of formation and whether that is more or less prospective for either metalliferous or clay mineralisation.

6.4.5 Background Au values in early stage high-sulfidation style alteration

Metals selectively partition into either the dense residual fluid phase or the vapour phase with Au and Cu favouring the SO_2-rich vapour phase whereas remaining base metals favour the residual dense H_2S-rich fluid phase (Heinrich et al., 1992; Heinrich et al., 1999; Heinrich et al., 2004; Davidson et al., 2005). This suggests that background Au values within paragenetically early high-sulfidation style alteration may give an indication of whether Au was in the system or not. Metalliferous mineralised high-sulfidation systems tend to have 0.1 to 1.0ppm Au within this stage (e.g. Temora, Allibone et al., 1995), whereas the Ogmaesan system is particularly barren with respect to Au and Ag (ca. <0.1ppm). This could be used in conjunction with SO_4:H_2S ratios to indicate an increase in prospectivity for a later ore-bearing stage of metalliferous mineralisation.

6.4.6 So, what is the key thing to look out for…?

It appears that not one particular geological criterion or one particular analysis can provide 'the' answer as to whether or not a high-sulfidation system contains metalliferous mineralisation, other that seeing the mineralised paragenetic stage itself, just as no unique geological process appears to be required for their formation (e.g. Richards, 2003). It will be the recognition of a number of key geological criteria occurring together that will lead to the discovery of mineralised high-sulfidation systems. Alternatively, the recognition of a distinct lack of key geological criteria should highlight high-sulfidation systems that are barren, or least prospective. An examination of host rocks and the H_2S:SO_4 composition of a system should provide a fairly rapid assessment of the prospectivity for potential clay/sulfate mineralisation.

A key factor in the development of a metalliferous mineralised high-sulfidation system is an ore-bearing paragenetic stage that is later than the advanced argillic alteration, which is commonly thought to form from hydrothermal fluids that are of an intermediate- to low-sulfidation-state (Section 6.3.3; Arribas Jr, 1995; Allibone et al., 1995; Cooke & Simmons, 2000; Hedenquist et al., 2000; Einaudi et al., 2003; Sillitoe & Hedenquist, 2003). Recognition of a paragenetically late, ore-bearing stage, or the distinct lack of it, will be critical for success in the discovery of metalliferous mineralised high-sulfidation systems, and recognition of barren systems.

6.5 EXPLORATION MODELS FOR EPITHERMAL CLAY/SULFATE AND GOLD-SILVER DEPOSITS IN SOUTH KOREA

This section presents an exploration model for clay/sulfate and Au-Ag epithermal deposits that may be used to find similar deposits to those in the Seongsan district in similar terranes in South Korea.

6.5.1 Possible evidence of a caldera setting for the Seongsan district…?

Many previous workers (Chapter 1) have suggested that the clay-sulfate deposits of the broader region are localised around and are genetically related to a caldera setting. The possibility of a caldera setting for the Seongsan district is thus explored here in order to determine whether the Seongsan district is localised in a caldera and if this is a useful exploration targeting feature.

Calderas are collapse features resulting from the evacuation and eruption of magma from a subsurface reservoir. They generally range in size from less than 1 up to 10s of kms in diameter. Ignimbrite eruptions resulting from caldera collapse can be less than $1km^3$ but large-scale individual ignimbrite eruptions are those greater than $100km^3$ but also can be in the order

of up to 1,000km^3 or more. Cumulatively, within a caldera, ignimbrite deposits can be several 100s of m thick up to a few km thick, and outside the caldera can be up to 100s of m thick extending over 10,000 to 1,000,000km^2 (Cas & Wright, 1987; Elston, 1994). Calderas are typically localised along regionally important fault zones that are intermittently active before and after the caldera cycle (Rytuba, 1994). In mineralised calderas, the ore deposits are typically controlled by structures developed during caldera formation and by regional faults that intersect and reactivate the caldera-related structures (Rytuba, 1994). In areas of transtension, the main caldera faults may not be circular, but instead form a series of connecting linear or arcuate structures (Stix et al., 2003). Caldera systems can show multiple stages of magma resurgence or withdrawal and can have multiple zones of ring fractures and ring domes. This results in calderas that are not centred or symmetrical but which show complex overprinting collapse events (Elston, 1994; e.g. Rotorua caldera, New Zealand, Milner et al., 2002; Fig. 6-1). Caldera development can show a continuum from intrusions that never reach the surface, to clusters of domes, to a climax in which shallow batholiths leak and form a tumescent dome, to bursting along ring fractures as their cupolas approach the surface (Elston, 1994).

Flow dome complexes similar to the $Ic_{1\text{-}3}$ intrusions at Seongsan, form in a variety of volcanic environments and structures. In strato-volcanoes, dacitic domes may occupy the summit calderas (e.g. Mt St Helens, Washington) or adventive sites on the margins (e.g. Santiaguito, Guatemala). In resurgent calderas, rhyolitic domes typically occupy the core or marginal ring fractures (e.g. Lake Taupo, New Zealand). Elsewhere domes or groups of domes may be isolated from other volcanic features or not clearly controlled by pre-existing volcanic structures (e.g. Lipari, Italy) (Morrison, 1992). Therefore, flow dome complexes such as Ic_1, Ic_2 and Ic_3 have no particular unequivocal relationship to calderas.

There are about twelve documented occurrences of calderas in South Korea. These are generally confined to the Yuchon Group, typically in the southeastern part of the Kyongsang Basin (Cha, 1985; Yun, 1993; Hwang, 1995; Hwang, 2002; Fig. 6-1B). These calderas are of variable size but generally have diameters in the range of 8 to 12km but can be up to 30km or more. Most are inferred from interpreted circular volcanic structures recognised in Landsat images rather than detailed mapping on the ground. There appears to be two main ages for caldera development in South Korea at around 100 to 85Ma and 70 to 60Ma, with the best-developed calderas related to the latter phase. Some calderas show complete ring fracture zones and at least one with tuffs partially infilling ring fractures. Two have elliptical vents infilled with densely welded tuff. Downsag and piecemeal collapse types have been recognised. Most data is published in Korean. This summary of calderas in South Korea was provided through personal communication with Dr Reedman (June 2004). Cha & Yun (1987) identified a caldera

occurring within the Yeongdong-Kwangju 'depression', which is ca. 50 to 100km east-northeast of the Seongsan district.

The 'Haenam caldera' in the Seongsan area was proposed on the basis of geographical rather than geological features (Cha & Yun, 1988). Clay-silica deposits are located around an inferred circular feature ca. 30 to 40km in diameter, centred on the Sani granite with a symmetry to the surrounding geological units (Fig. 1-17). The Sani granite was presumed to be Cretaceous in age and hence thought to be the resurgent magma that drove caldera formation. It was subsequently dated and determined to be Jurassic in age. Therefore, the Sani granite 'dome' is an unrelated feature and not evidence of a caldera.

The Seongsan district contains many rocks that would be found in a caldera setting, such as lava flows and porphyritic rocks from domes and subvolcanic intrusives, pyroclastic flow, surge and fall deposits, volcaniclastic debris flow breccias, and alluvial-fan, fluvial and lacustrine sedimentary rocks. Despite this, key geological factors that indicate a caldera setting for these rocks are still missing and they could also develop outside of a caldera within an active volcanic field. Distinctive caldera features, such as significant vent, collapse and caldera floor breccias, post eruption talus breccias, possible evidence of caldera margin walls, moat deposits, caldera fill ignimbrites of significant thickness, subsided and stoped/rafted blocks of regional host rocks, ring fractures, ring domes, and radial faults and dikes, significant margin faulting and accommodation structures are not observed within the Seongsan district, and are not reported to occur in the broader Haenam area. Therefore, it is unlikely that the Haenam caldera (Fig. 1-17) is a real feature, but rather an artefact of the interpretation of several coincident geographical features.

Furthermore, during what would have been the time of development of the 'Haenam caldera', the stress-regime was strike-slip under a transpressional to transtensional setting. Under this stress-regime, a caldera would likely form as a series of connecting linear or arcuate structures (Stix et al., 2003), not as a circular feature like the inferred 'Haenam caldera'. In addition, the distinctive 'Hwangsan Tuff' (HVf) ignimbrite it is coarser to the east, indicating the probable source for this deposit was further east (Reedman, pers. comm. Nov. 2003). Therefore, any source caldera margin would lie to the east and this does not fit with the inferred location of the 'Haenam caldera' (Fig. 1-17). If the volcaniclastic debris flow breccia (AVdb) unit represents a caldera flow/breccia, then based on its location and extent, it would seem unlikely that this unit was deposited from an inferred 'Haenam caldera'. Therefore, if a caldera were responsible for the HVf or AVdb units, then neither caldera would fit in size or location with the inferred 'Haenam caldera'. Field evidence for a caldera in the Seongsan district is lacking.

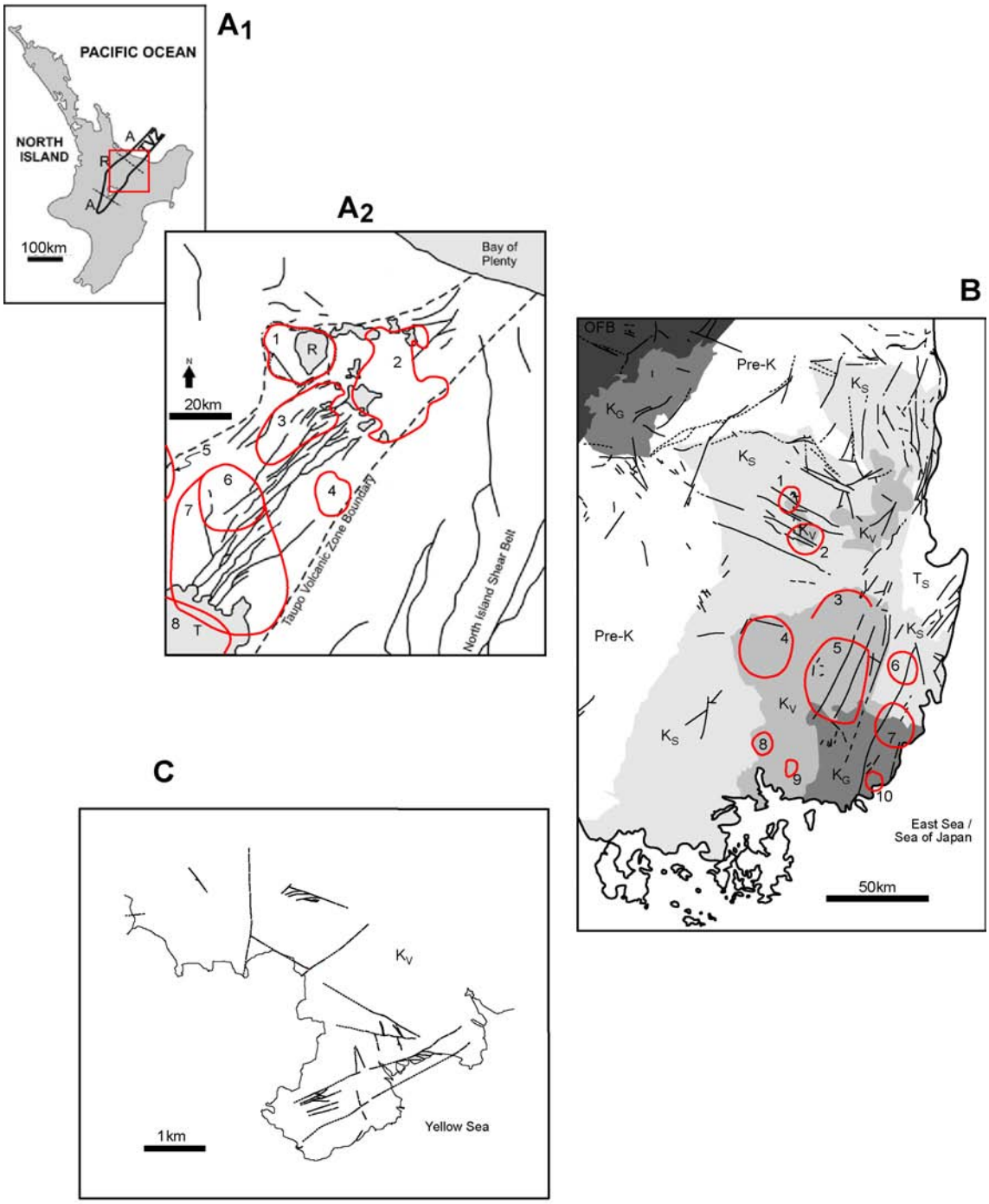

Fig. 6-1 **A_1**: North Island of New Zealand showing the location of the Taupo Volcanic Zone (TVZ). A = andesite dominated, R = rhyolite dominated. **A_2**: The broad structural framework of the main calderas (numbered) within the TVZ. Grey areas within A_2 are lakes or sea. T = Lake Taupo, R = Lake Rotorua. Calderas: 1 = Rotorua, 2 = Haroharo (in Okataina Volcanic centre), 3= Kapenga, 4 = Reporoa, 5 Mangakino, 6 = Maroa, 7 = Whakamaru and 8 = Taupo (modified from Rowland & Sibson, 2001 and Milner et al., 2002; after Houghton et al., 1995). **B**: The broad structural framework for the main calderas (numbered) within southeast Korea. OFB = Okchon Fold Belt, Pre-K = pre-Cretaceous Formations, K_S = Cretaceous sedimentary Formations, K_V = Cretaceous volcanic Formations, K_G = Cretaceous granites, T_S = Tertiary Formations. Calderas: 1 = Geumseogsan, 2 = Hwasan, 3 = Choijeongsan, 4 = ?, 5 = Unmunsa, 6 = Chisulryeongsan, 7 = Daeunsan, 8 = Jangsan, 9 = Jinrye and 10 = Palryeongsan (modified from Koh et al., 2002 and pers. comm. Reedman, July 2004). **C**: The broad structural framework of the Seongsan district (surface exposures of 'Kv' – nomenclature from B – Cretaceous volcanic rocks).

Note: K_S, K_V and K_G are components that make up the Kyongsang Basin.

6.5.2 Deep-seated roots: faults and/or intrusives

In order for deep, metal-rich hydrothermal fluids to ascend and develop mineralisation at shallow levels, deep-seated faults and/or intrusives must develop to enable these fluids to ascend and transport their metals to shallow, structurally favourable sites for deposition. Similar conclusions have been reached for other systems, such as the high-sulfidation Nansatsu system, where Hosono & Nakano (2004) used Pb-Sr isotopic evidence to highlight the contribution and importance of deep crustal fluids to the mineralisation at Hishikari. They suggested that the metals were derived largely from magmatic fluid and deep crustal fluid and that these were tapped during intrusion of magma that occurred synchronous with mineralisation.

The Rodalquilar caldera complex and its neighbour, the Los Frailes caldera in Spain also clearly highlight the need for deep-seated intrusives and fault networks in the development of epithermal mineralisation (Cunningham et al., 1990; Rytuba et al., 1990; Sänger-von Oepen et al., 1990). The Rodalquilar caldera is host to high-sulfidation Au deposits that show a close spatial and temporal association with intrusives that post-date the caldera. These intrusives are absent from the nearby (ca. <5km) Los Frailes caldera, which is unmineralised. This further highlights that a caldera setting is not a prerequisite for mineralisation.

Also of particular note is the work of Baker et al. (2005) at Pajingo, where significant Au-Ag-bearing low-sulfidation epithermal mineralisation occurs. A mineralised lode was compared to a non-mineralised area, and their key conclusion was that deep-seated structures were absent from the non-mineralised lode, thereby not enabling deep, mineralised fluids to ascend during favourable conditions and develop mineralisation in structurally favourable sites.

6.5.3 Implications for the Seongsan district and similar terranes: exploration targeting criteria for clay/sulfate and Au-Ag epithermal deposits

The examination of possible discriminators in previous sections has highlighted a number of geological criteria that are important to recognise when exploring for potential systems in similar terranes. Some of the key geological criteria to focus on are listed below. These have been discussed in detail throughout the text of this Chapter.

Regional fundamentals

- be in the right terrane:
  - fore-arc more prospective for low-sulfidation style Au-Ag deposits + high-sulfidation metalliferous deposits
  - back-arc more prospective for high-sulfidation style clay/sulfate deposits

Local fundamentals

- have the right host rocks:
  - andesite more prospective for low-sulfidation style Au-Ag deposits + high-sulfidation metalliferous deposits
  - rhyodacitic more prospective for high-sulfidation style clay/sulfate deposits
- knowledge of regional- to local-scale stress regimes:
  - extensional more prospective for low-sulfidation style Au-Ag deposits
  - wrenching more prospective for high-sulfidation style clay/sulfate deposits
- recognition of deep-seated structures and/or intrusives locally:
  - these can tap potentially mineralised fluids and allow ascent and precipitation
- be aware of cover that post-dates hydrothermal activity (e.g. AVdb):
  - the age range of hydrothermal activity in the Seongsan district is between ca. 82 to 77Ma, therefore any unit younger than 77Ma could be covering potential high-sulfidation clay and/or low-sulfidation Au-Ag mineralisation
- a caldera setting is not required:
  - strike-slip wrench faults host the high-sulfidation style clay/sulfate deposits
  - extensional normal faults host the low-sulfidation style Au-Ag deposits

Geochemical fundamentals

- H_2S/SO_4 composition:
  - H_2S-dominant more prospective for metalliferous mineralisation
  - SO_4-dominant more prospective for clay/sulfate
- chemical zonation within magmatic alunites:
  - no chemical zonation increases the prospectivity for potential clay/sulfate deposits
  - chemical zonation increases the prospectivity for potential metalliferous deposits
- background Au values in paragenetically early high-sulfidation alteration:
  - ca. 0.1 to 1.0ppm Au and H_2S-dominant indicates potential for overprinting metalliferous ore-stage
  - ca. <0.1ppm Au and SO_4-dominant indicates potential for clay/sulfate deposit

6.6 TARGETTING EPITHERMAL CLAY/SULFATE AND GOLD-SILVER DEPOSITS AT THE CONTINENTAL SCALE IN EAST ASIA

6.6.1 Comparison of southern Korea to similar terranes in China, Japan and Russia

The Cretaceous to Early Tertiary tectonic settings of southeastern China, southern Korea, southwestern Japan and far eastern Russia were similar. Similar continental margin volcanic arc terranes developed in all locations during this time (Fig. 6-2). These volcanic terranes developed from the convergence of the Farallon-Izanagi and Kula-Pacific Plates with the Asian continent (Fig. 1-10). Magmatic activity in the region during the Cretaceous first initiated in southeastern China, and migrated northeastward through the southern parts of Korea and subsequently into southwestern Japan and some parts of far eastern Russia (Weng & Huang, 1983; Kinoshita, 1995; Watanabe et al., 1998; Kitagawa et al., 1999; Lee, 1999; Chough et al., 2000; Li, 2000; Okada, 2000; Zhou & Li, 2000).

This migration is evident in the age of mineral deposits that are associated with magmatism and volcanism, such as 'pyrophyllite' deposits that are distributed throughout Cretaceous volcanic rocks of East Asia. The age of 'pyrophyllite' deposits range from 99 to 91Ma in southeastern China, 92 to 51Ma in Korea (age-range includes 'pyrophyllite' provinces in Korea which occur in the southeast, Fig. 1-15, younging to the east) and 87 to 63Ma in inner southwestern Japan (Kitagawa et al., 1999). Analysis within southwestern Japan of a variety of mineral deposits that are directly associated with magmatism and volcanism confirms the generally northeastward migration of magmatic and volcanic activity (Watanabe et al., 1998).

In addition to pyrophyllite deposits, the Cretaceous Fujian Belt of volcanic rocks of southeastern China host significant porphyry-epithermal systems. Within the Zijinshan region of the Fujian Belt, low-sulfidation Ag-Au deposits, high-sulfidation Cu-Au deposits, porphyry Cu±Mo deposits and Cu±Au deposits transitional between epithermal and porphyry styles (So et al., 1998; Zhang et al., 2003) have been identified. The Zijinshan mine was the first recognised high-sulfidation epithermal Cu±Au system of Cretaceous age in mainland China (So et al., 1998). In addition to the Zijinshan district, there are other epithermal deposits widespread along most of the coastal region of the Guangdong, Fujian and Zhejiang Volcanic Belts, although many are not well developed nor described (Kerrich et al., 2000). These epithermal deposits are located south of an area of economically important Cu-Fe-Au-Mo porphyry and skarn systems (Pan & Dong, 1999; Kerrich et al., 2000). The epithermal deposits are associated with 146 to 87Ma potassic, calc-alkaline igneous rocks that appear to be products of post-collisional crustal extension within Neoproterozoic and younger rocks (Kerrich et al., 2000; Li, 2000).

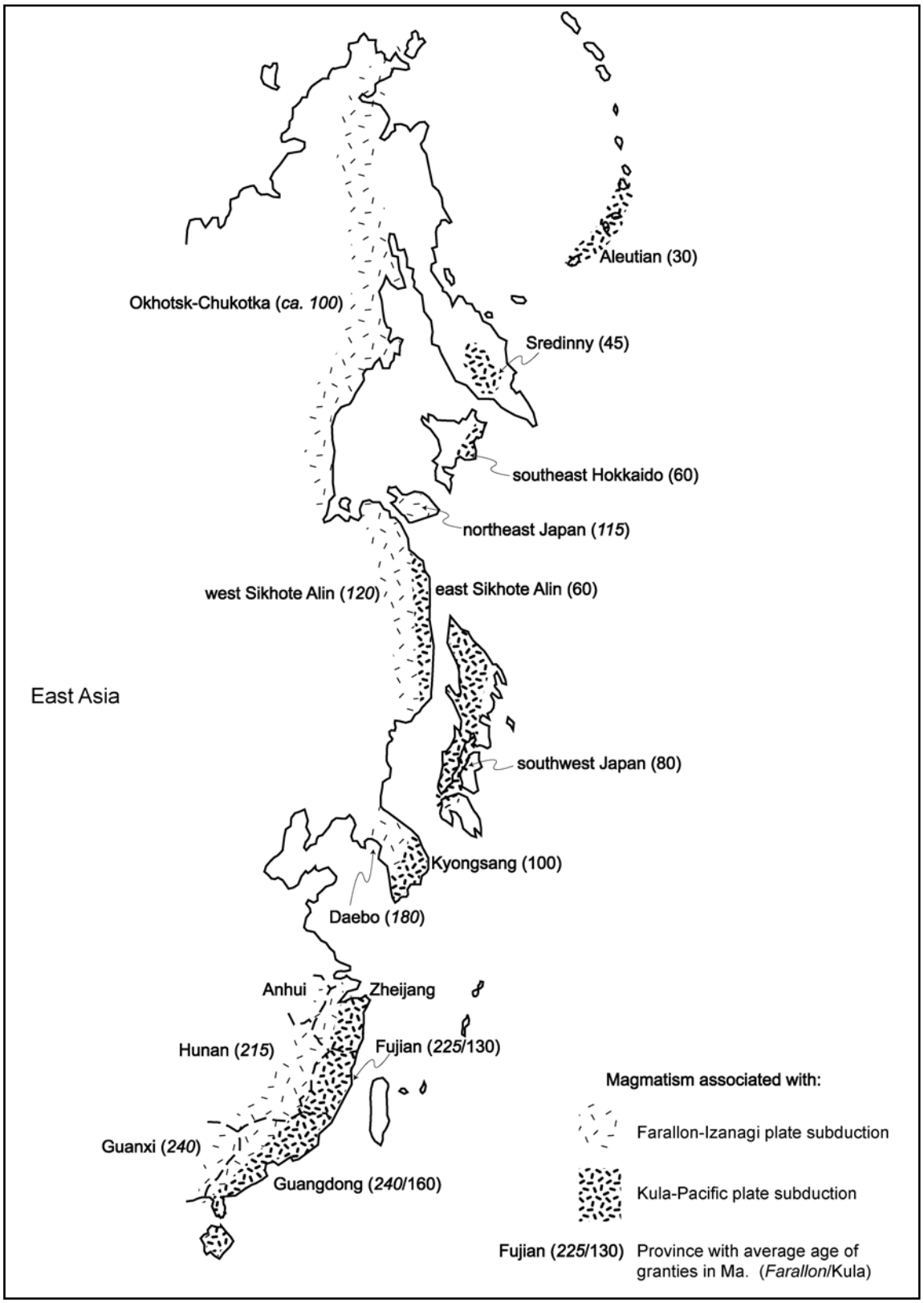

Fig. 6-2 Magmatic belts of East Asia, distinguished by the dominant plate subduction causing the magmatism (by either the Farallon-Izanagi or Kula-Pacific as indicated by hatching; see: Fig. 1-10). Modern day Japan has been split and rotated back to its approximate position during magmatism, although note that paleo Japan would be a different outline to modern day Japan due to post Cretaceous volcanic activity and accretion. Figure after Kinoshita (1995).

The Cretaceous volcanic rocks of inner southwestern Japan also host numerous deposit types related to extensive continental-arc magmatism (volcanic and plutonic), resulting in the formation of various mineral deposit types, related mainly to ilmenite series (Late Cretaceous) or magnetite series (Palaeogene) granitic rocks (Watanabe et al., 1998). These deposit types include tungsten (102 to 82Ma), mesothermal base- and precious-metal mineralisation (89 to 77Ma and ca. 70Ma), pyrophyllite ('Roseki') deposits and veins (87 to 63Ma), Mo (< ca. 71Ma) and polymetallic (Cu-Pb-Zn-Sn±W) skarns (ca. 89 to 62Ma) (Watanabe et al., 1998). Other more commonly-known epithermal Au-Ag deposits in Japan are associated with Plio-Pleistocene volcanic rocks within outer southwestern Japan (Watanabe et al., 1998).

The Cretaceous Okhotsk-Chukotka volcanic belt in far northeastern Russia hosts epithermal Au-Ag deposits (Konstantinov et al., 1993; Kerrich et al., 2000). Au-Ag deposits within this region occur in a variety of geological environments; those hosted in volcanic intrusive domes consisting of Early Cretaceous acid volcanic rocks share a similar geological setting to the epithermal Au-Ag systems within the Seongsan district. $^{40}K/^{40}Ar$ dating of quartz-chlorite-adularia veins indicates an age range of 94 to 80Ma, whereas quartz-rhodonite-rhodochrosite veins indicate an age range of 91 to 77Ma (Konstantinov et al., 1993). Ore formation seems to show a close temporal association with shallow level arc-related magmatism and they appear to post-date the main period of collisional tectonism (Kerrich et al., 2000).

Au-Ag deposits hosted by the Cretaceous Sikhote-Alin volcanic belt in far eastern Russia have features similar to epithermal deposits (Yushmanov, 1997; Ivanov et al., 1998; Vasilenko & Strizhkova, 1998; Yushmanov, 1999; Tomson et al., 2002). Low- and high-sulfidation precious-metal epithermal deposits have been recognised within the western and eastern Sikhote-Alin Belt of Cretaceous intermediate to acidic volcanic rocks. Limited published data in English on this area leads to interpretive observations by the author that these deposits were formed in the Late Cretaceous to Paleogene and are hosted on the periphery of intrusive domes under conditions of sinistral strike-slip movement along regional northeasterly faults.

This brief examination of mineral deposits that occur within the Cretaceous to Early Tertiary volcanic rocks of East Asia shows that Au-Ag mineralisation is common, but is generally associated with a forearc setting, albeit in an inboard location, but not associated with backarc volcanic chains where multiple volcanic chains have developed. This similar conclusion was also reached when discussing tectonic settings in Section 6.4.2.

6.7 THESIS SUMMARY

6.7.1 Synthesis of results: main conclusions and outcomes of the research

The primary objective of this project was to investigate the geological setting and the spatial and temporal relationships between the distinctly different epithermal systems in the Seongsan district of South Korea. The primary objective and subsequent detailed aims of the research have been successfully addressed.

The Seongsan district hosts high-sulfidation style clay-sulfate-silica deposits that are exploited as commercial sources of kaolinite and dickite. The district also hosts several low-sulfidation Au-Ag mineralised epithermal systems that have only been recognised recently. Host rocks of the district comprise a sequence of extensive pyroclastic ignimbrite flow deposits and their associated subplinian to plinian to phreatoplinian fall and surge deposits. Sub-volcanic intrusives, including domes and flows, and associated proximal to distal pyroclastic and volcaniclastic deposits formed during later stages in the magmatic history. These are all intercalated with various epiclastic deposits including fluvial, alluvial fan, and lacustrine sediments. These unconformably overlie Mesozoic granites and basement Precambrian metamorphic rocks of the Okchon Fold Belt.

The district is cut by numerous faults that are characterised by steeply-dipping brittle fractured rock and range from minor planar features to zones 100's of metres wide. Fault zone asymmetry, stratigraphic offset across faults and slickenlines developed on fault planes constrained the sense and direction of offset. Faults have several preferred orientations and can be traced up to several kilometres along strike. The structural framework of the Seongsan district was determined to have developed under two distinctly different stress regimes, characterised initially by wrenching (district-scale stress regime 1) followed by extension (district-scale stress regime 2).

Detailed paragenetic studies led to the recognition of two distinct hydrothermal events in the district: one similar to acid-sulfate / high-sulfidation systems and the other similar to adularia-sericite / low-sulfidation epithermal systems. Cross-cutting paragenetic relationships show that the low-sulfidation systems overprint the high-sulfidation systems. The high-sulfidation systems are focussed within sinistral strike-slip fault zones and breccias that developed from wrenching during transpression (district-scale stress regime 1). The low-sulfidation systems are localised on normal faults that developed from later extension (district-scale stress regime 2). No evidence of a caldera setting was seen in the Seongsan district despite previous workers assumptions to the contrary.

$^{40}Ar/^{39}Ar$ stepwise heating age data derived from adularia in the low-sulfidation systems coupled with published age data on the high-sulfidation deposits shows that the change from advanced argillic alunite-bearing alteration to adularia-phyllic alteration occurred between 1.3Ma and 5.5Ma apart. This suggests that the epithermal systems of the district formed during two discrete hydrothermal events rather than one evolving hydrothermal event that would be expected to last less than 0.5Ma. However, the two styles of epithermal systems in the Seongsan district could be considered two distinct parts of a broader long-lived cycle of crustal convergence, subduction, volcanism and associated hydrothermal activity in southwest Korea.

Phase relationships of hydrothermal mineral assemblages show that the high-sulfidation systems formed under oxidised, acidic, SO_4-dominant conditions, whereas the low-sulfidation systems formed under reduced, near-neutral pH, H_2S-dominant conditions. Fluids associated with the Au-Ag-bearing paragenetic stages were of intermediate- to low-sulfidation-state, regardless of which epithermal system they formed in. Oxygen and hydrogen isotopic ratios show that two isotopically distinct fluids formed the high- and low-sulfidation systems. A meteoric-derived fluid formed the low-sulfidation Au-Ag vein systems, whereas a magmatic fluid formed the high-sulfidation systems. Sulfur isotopic ratios of pyrite and alunite from the high-sulfidation systems show marked fractionation. Coupled with oxygen and hydrogen isotope data, the sulfur isotopic ratio values and the relatively narrow range of $\delta^{34}S_{sulfate}$ compared to $\delta^{34}S_{sulfide}$ implies a SO_4-dominant, magmatic-steam origin for fluids that formed the advanced argillic alteration in the high-sulfidation deposits. The relatively narrow range of $\delta^{34}S_{sulfide}$ from the low-sulfidation systems implies that the veining and associated phyllic-argillic alteration formed from fluids in which H_2S was the dominant sulfur species.

Comparison of the Seongsan district with other district that host both high- and low-sulfidation systems highlighted that, although rare, these districts commonly show a superimposition of low- on high-sulfidation style alteration (±mineralisation) coupled to a change in structural setting, typically over a period of ca. 1 to 2Ma. This suggests that these districts share a common structural and hydrothermal evolution.

Controls on whether high-sulfidation systems form clay/sulfate or metalliferous mineralised systems were examined. This allowed development of exploration targeting criteria that discriminate between clay/sulfate, metalliferous mineralised and barren epithermal systems. Rhyolitic to dacitic host rocks and SO_4-dominant conditions play critical roles in the development of clay deposits. For metalliferous mineralised systems, sulfur speciation as H_2S-dominant plays a critical role, whereas host rock composition is less critical. Recognition of several key criteria occurring together will lead to the discovery of mineralised systems,

whereas the recognition of a lack of key criteria should highlight barren or least prospective systems.

The Seongsan district is possibly the first documented area in Korea, if not globally, that hosts both high- and low-sulfidation epithermal systems that produce economic clay/sulfate and Au-Ag from the same district.

6.7.2 Future recommendations: possible follow-on research themes

1. Determine in detail the geochemistry of mafic rocks within the district that were emplaced prior to mineralisation. This can be used to help further constrain the tectonic setting leading up to and during both clay/sulfate and Au-Ag mineralisation (cf. Collins, 2002).

2. Examine tectonic, magmatic, hydrothermal and structural settings in relation to mineral deposits with a focus on East Asia. This would utilise southern Korea as an example of a double volcanic-chain, back-arc, inboard location that typically hosts clay/sulfate mineralisation with rare occurrences of metalliferous-mineralisation. This topic would also utilise the data mentioned above. It still remains unclear why parts of southeastern China, southern Japan and parts of far northeastern Russia are so strongly metalliferous mineralised compared to southern Korea, as they all share a similar magmatic and tectonic evolution (cf. Kerrich, et al., 2000; Kay & Mpodozis, 2001; Tosdal & Richards, 2001; Richards, 2003; Garwin et al., 2005; Lallemand et al., 2005; Rosenbaum et al., 2005; Watanabe, 2005).

3. Conduct detailed $\delta^{34}S$, δD, $\delta^{18}O_{SO4}$, $\delta^{18}O_{OH}$ isotope analyses, major and REE geochemical analyses, fluid inclusion gas analyses and stepwise $^{40}Ar/^{39}Ar$ age data on alunite (and pyrite) from the Seongsan district, in particular the Seongsan system, in order to document in detail the formation of alunite within a magmatic-steam environment. This data could also be used to place further constraints on the H_2S/SO_4 evolution over time in the Seongsan district (cf. Rye, 2005; Deyell et al., 2005; Landis & Rye, 2005).

4. Attempt to improve and broaden the classification of epithermal systems to include barren and non-metalliferous systems. The Seongsan district highlights that metalliferous ore is not the only economic product of epithermal systems and that barren systems are difficult to classify under current sulfidation-state classification schemes (cf. Hayba et al., 1985; Heald et al., 1987; Hedenquist, 1987; Hedenquist, 2000; Sillitoe & Hedenquist, 2003; Cooke & Deyell, 2003; Simmons et al., 2005).

5. Examine mineralised high-sulfidation systems and see if there is a correlation in the age difference between the initial advanced argillic alteration and the later mineralisation stage with the sulfidation state of the mineralising stage, i.e. is there an increase in reduction of the sulfidation-state over time from residual buffering of the metal-bearing fluid (cf. Section 6.3.3).